AEDC-TR-72-66

ANALYSIS OF THE THREE-DIMENSIONAL COMPRESSIBLE TURBULENT BOUNDARY LAYER ON A SHARP CONE AT INCIDENCE IN SUPERSONIC AND HYPERSONIC FLOW

John C. Adams, Jr.

ARO, Inc.

June 1972

VON KÁRMÁN GAS DYNAMICS FACILITY
ARNOLD ENGINEERING DEVELOPMENT CENTER
AIR FORCE SYSTEMS COMMAND
ARNOLD AIR FORCE STATION, TENNESSEE

NOTICES

When U. S. Government drawings specifications, or other data are used for any purpose other than a definitely related Government procurement operation, the Government thereby incurs no responsibility nor any obligation whatsoever, and the fact that the Government may have formulated, furnished, or in any way supplied the said drawings, specifications, or other data, is not to be regarded by implication or otherwise, or in any manner licensing the holder or any other person or corporation, or conveying any rights or permission to manufacture, use, or sell any patented invention that may in any way be related thereto.

Qualified users may obtain copies of this report from the Defense Documentation Center.

References to named commercial products in this report are not to be considered in any sense as an endorsement of the product by the United States Air Force or the Government.

ANALYSIS OF THE THREE-DIMENSIONAL COMPRESSIBLE TURBULENT BOUNDARY LAYER ON A SHARP CONE AT INCIDENCE IN SUPERSONIC AND HYPERSONIC FLOW

John C. Adams, Jr.
ARO, Inc.

FOREWORD

The work reported herein was sponsored by Headquarters, Arnold Engineering Development Center (AEDC), Air Force Systems Command (AFSC), under Program Element 65802F.

The results of research presented were obtained by ARO, Inc. (a subsidiary of Sverdrup & Parcel and Associates, Inc.), contract operator of AEDC, AFSC, Arnold Air Force Station, Tennessee, under Contract F40600-72-C-0003. The research was conducted from July 1971 to February 1972 under ARO Project No. VW5206; and the manuscript was submitted for publication on April 11, 1972.

Appreciation and acknowledgement is extended to Dr. W. J. Rainbird, Chairman, Division of Aerothermodynamics, School of Engineering, Carleton University, Ottawa, Canada, and to Mr. A. Martellucci, Consultant, Aerothermodynamics Laboratory, Re-entry and Environmental Systems Division, General Electric Company, Philadelphia, Pennsylvania, for providing the author with detailed tabulations of their experimental data.

Portions of the supersonic (Mach 1.80) results in this report have been presented by the author in AIAA Paper No. 72-186, entitled "Finite-Difference Analysis of the Three-Dimensional Turbulent Boundary Layer on a Sharp Cone at Angle of Attack in a Supersonic Flow," given at the AIAA 10th Aerospace Sciences Meeting, San Diego, California, January 17-19, 1972.

This technical report has been reviewed and is approved.

MAURICE A. CLERMONT
Captain, CF
Research and Development Division
Directorate of Technology

ROBERT O. DIETZ
Acting Director
Directorate of Technology

ABSTRACT

An analytical approach toward numerical calculation of the three-dimensional turbulent boundary layer on a sharp cone at incidence under supersonic and hypersonic flow conditions is presented. The theoretical model is based on implicit finite-difference integration of the governing three-dimensional turbulent boundary-layer equations in conjunction with a three-dimensional scalar eddy-viscosity model of turbulence. Comparison of the present theory with detailed experimental measurements of the three-dimensional turbulent boundary-layer structure (velocity and temperature profiles), as well as surface streamline direction (obtained via an oil-flow technique) and surface heat-transfer rate, reveals good agreement. Effects of wall temperature on the three-dimensional turbulent boundary-layer profiles under hypersonic conditions are considered relative to interpretation of hot wall, hypersonic wind tunnel, force testing as it relates to cold wall, atmospheric re-entry. The calculated surface upwash angle is found to be fairly sensitive to wall temperature effects with the larger values of the angle occurring with the hotter wall.

CONTENTS

APPENDIXES

I. ILLUSTRATIONS

Figure

Figure | Page

NOMENCLATURE

A_*	van Driest damping constant, 26.0
C_{f_∞}	Local skin-friction coefficient based on free-stream conditions, $2\tau_w/\rho_\infty U_\infty^2$
C_p	Constant pressure specific heat for air, 6006 ft^2/sec^2-°R
D	van Driest wall damping term
$\overline{G}$	Scalar velocity function
H'	Fluctuating total enthalpy
$\overline{H}$	Mean total enthalpy
h'	Fluctuating static enthalpy
$\overline{h}$	Mean static enthalpy
k	Laminar (molecular) thermal conductivity
k_*	Inner law mixing length constant, 0.435
L	Slant length of sharp cone

ℓ_*	Mixing length
M_∞	Free-stream Mach number
P_o	Stagnation pressure
Pr	Laminar Prandtl number for air, 0.71
Pr_t	Turbulent Prandtl number, 0.90
$\bar{p}$	Static pressure
p_∞	Free-stream static pressure
$\dot{q}$	Heat flux
$\dot{q}_w$	Wall heat flux
R	Specific gas constant for air, 1716 ft^2/sec^2-°R
$Re_{\infty,L}$	Free-stream Reynolds number, $\rho_\infty U_\infty L/\mu_\infty$
$Re_{\infty,x}$	Free-stream Reynolds number, $\rho_\infty U_\infty x/\mu_\infty$
r	Body radius
St_∞	Local Stanton number based on free-stream conditions, $(\dot{q}_w)/[\rho_\infty U_\infty C_p(T_o - T_w)]$
$\overline{T}$	Mean static temperature
T_e	Static temperature at outer edge of boundary layer
T_o	Stagnation temperature
T_{ref}	Reference temperature
T_w	Wall temperature
T_∞	Free-stream static temperature
U_e	Streamwise velocity component at outer edge of boundary layer
U_∞	Free-stream velocity
u′	Fluctuating streamwise velocity component
$\bar{u}$	Mean streamwise velocity component
V	Combined normal velocity components according to Eq. (6)
v′	Fluctuating normal velocity component
$\bar{v}$	Mean normal velocity component
W_e	Crossflow velocity component at outer edge of boundary layer

w'	Fluctuating crossflow velocity component
$\bar{w}$	Mean crossflow velocity component
x	Coordinate along body surface
y	Coordinate normal to body surface
y_ℓ	Characteristic thickness of boundary layer in Eq. (30)
α	Angle of attack
γ	Specific heat ratio for air, 1.40
δ	Boundary-layer thickness
δ_ℓ	Laminar boundary-layer thickness
δ_t	Turbulent boundary-layer thickness
δ_v	Sharp cone semivertex angle
$\delta^*_{2\text{-D}}$	Two-dimensional displacement thickness, $\int_0^\infty [1-(\bar{\rho}\bar{u}/\rho_e U_e)]\, dy$
ϵ	Eddy viscosity
ϵ_i	Eddy viscosity in inner region
ϵ_o	Eddy viscosity in outer region
κ	Eddy thermal conductivity
λ	Outer law mixing-length constant, 0.090
μ	Laminar (molecular) viscosity
μ_∞	Free-stream laminar (molecular) viscosity
ξ, η, ζ	Transformed coordinates defined by Eqs. (44), (45), and (46)
ρ'	Fluctuating mass density
$\bar{\rho}$	Mean mass density
ρ_e	Mass density at outer edge of boundary layer
ρ_∞	Free-stream mass density
τ	Shear stress
τ_w	Wall shear stress
ϕ	Circumferential coordinate
ω	Streamline direction, $\tan^{-1}(\bar{w}/\bar{u})$

ω_e	Streamline direction at outer edge of boundary layer, $\tan^{-1}(W_e/U_e)$
ω_s	Streamline direction at body surface, $\tan^{-1}(\tau_{w,\phi}/\tau_{w,x})$

SUBSCRIPTS

e	Outer edge of boundary layer
o	Stagnation or total
ref	Reference value
s	Surface
sep	Separation
turb	Turbulent
w	Wall
x	x-direction
ϕ	ϕ-direction
∞	Free-stream

SUPERSCRIPTS

'	Fluctuating quantity
—	Averaged quantity with respect to time

SECTION I
INTRODUCTION

Only within the last decade, with the advent of large, high-speed digital computers, has the problem of numerical integration of the two-dimensional compressible turbulent boundary-layer equations using a two-layer (inner-outer) eddy-viscosity model to describe turbulence become feasible. The works of Smith and Cebeci (Ref. 1), Patankar and Spalding (Ref. 2), and Herring and Mellor (Ref. 3), as well as the Langley Compressible Turbulent Boundary Layer Symposium (Ref. 4), are representative examples of the current state-of-the-art in numerical calculation techniques for compressible two-dimensional turbulent boundary-layer flows. In general, the two-layer (inner-outer) eddy-viscosity law, coupled with the so-called van Driest damping for the near-wall region, appears to be entirely satisfactory and accurate for two-dimensional turbulent boundary-layer flows in the subsonic and supersonic regime. More recent works (Refs. 5-9) indicate that the same two-layer eddy-viscosity law is applicable even in the hypersonic regime.

With regard to the three-dimensional compressible turbulent boundary-layer problem, little work has been done to present. The three-dimensional compressible turbulent boundary-layer equations have been derived by Braun (Ref. 10) and Vaglio-Laurin (Ref. 11). Several attempts to solve these equations using integral techniques in conjunction with the so-called small crossflow assumption (which uncouples the streamwise momentum equation from the crossflow momentum equation) have been made by Cooke (Ref. 12), Smith (Ref. 13), and Bradley (Ref. 14), as well as Braun and Vaglio-Laurin cited previously. These integral approaches were not entirely satisfactory because of the difficulties in adequately representing the crossflow velocity profile. However, the recent work of Shanebrook and Hatch (Ref. 15) employing hodograph models for the crossflow velocity component appears promising toward removal of the above-mentioned difficulty. It should be mentioned in this connection that Zakkay and Calarese (Ref. 16) have successfully applied an integral analysis for the compressible turbulent boundary layer undergoing both adverse pressure gradient and crossflow along a plane of symmetry.

The paper by Hunt, Bushnell, and Beckwith (Ref. 17) is the first, to the author's knowledge, to apply marching finite-difference integration to the three-dimensional compressible turbulent boundary-layer equations for swept infinite cylinders under hypersonic conditions. In this work three different approaches to the formulation of eddy-viscosity

models for three-dimensional turbulent boundary layers were considered with two of the formulations being used in the numerical solutions and one being completely rejected (the independence principle approach). Of the two acceptable eddy-viscosity models, the most plausible formalism (in the opinion of the present author) is the invariant turbulence approach which is based on the concept that the three-dimensional eddy viscosity should depend only on the properties of the turbulence and a local eddy scale. The application of this concept to a mixing-length model suggests that the eddy viscosity should be a scalar function independent of the coordinate direction. Implicit in this approach is the requirement that the directions of the three-dimensional turbulent shear stress components are the same as the directions of the corresponding mean velocity gradients. As shown by Bradshaw (Ref. 18) through a three-dimensional kinetic-energy-of-turbulence approach, the directions of the shear stress components are not, in general, exactly the same as the directions of the corresponding mean velocity components. However, in the near-wall region, Bradshaw's shear stress equations reduce to the scalar eddy viscosity-mixing length model discussed above.

Recent analyses by Nash (Ref. 19) and Cooper (Ref. 20) concerning three-dimensional turbulent boundary layers in an incompressible flow indicate that use of the above-discussed invariant turbulence concept will lead to acceptable results when coupled to an accurate integration technique for numerical solution of the three-dimensional turbulent boundary-layer equations. Nash uses an empirically modified kinetic-energy-of-turbulence equation in conjunction with the assumption that the turbulent shear stress acts in the direction of the mean rate of strain of the mean motion to compute the magnitude of the turbulent shear stress. The work by Cooper applies the scalar eddy viscosity-mixing length model to the problem of three-dimensional incompressible laminar and turbulent boundary-layer flow associated with a rotating disk in an infinite fluid otherwise at rest. Cooper reports excellent agreement between theory and experimental data for radial and circumferential velocity profiles, displacement thickness, shape factor, and drag attributable to skin friction for both laminar and turbulent three-dimensional boundary layers. It should be noted here that Cooper applied a modified version of the Cebeci and Smith (Ref. 21) linearized implicit finite-difference method, whereas Nash used an explicit finite-difference scheme which has recently been updated and improved (see Ref. 22 for clarification). The method of Nash has also recently been modified to include the effects of centrifugal and Coriolis forces for application to calculation of the incompressible three-dimensional turbulent boundary layer on a helicopter rotor as reported in Refs. 23 and 24.

The present document reports on an analytical investigation and development of a finite-difference calculation technique for the analysis of the three-dimensional compressible turbulent boundary layer on a sharp cone at angle of attack in a supersonic or hypersonic flow. The sharp cone geometry at angle of attack is of obvious importance to aerodynamic and propulsion engine applications. Specifically, the governing three-dimensional turbulent boundary-layer equations for a compressible flow are simplified by the conical nature of the sharp cone flow field and numerically integrated on a digital computer utilizing a marching implicit finite-difference technique. Three-dimensional turbulence is accounted for using the three-dimensional eddy-viscosity invariant turbulence approach discussed above in conjunction with an inner-outer mixing-length formalism from two-dimensional flows carried over to the three-dimensional flow of present interest. The inviscid conical flow field about the sharp cone at incidence is determined using a prior documented digital computer code which, in turn, furnishes the outer-edge conditions for input to the present boundary-layer analysis. To assess the accuracy and applicability of the present theory, comparisons of the calculated three-dimensional turbulent boundary-layer profiles (velocities and temperature) are made with detailed experimental flow-field surveys of the three-dimensional turbulent boundary-layer structure at various circumferential locations around a sharp cone at incidence under supersonic flow conditions. Comparisons between the present theory and experimental measurements of surface heat transfer under hypersonic flow conditions are also given for a sharp cone at various angles of incidence. Detailed, hypersonic, three-dimensional, turbulent boundary-layer profiles around a sharp cone at incidence are presented (although there are no experimental profiles for comparison). Effects of wall temperature on the three-dimensional turbulent boundary layer under hypersonic conditions are examined in some detail relative to interpretation of hot wall, hypersonic wind tunnel force testing as it relates to cold wall, atmospheric re-entry.

SECTION II
ANALYTICAL ANALYSIS

The present analytical investigation employs a three-dimensional turbulent boundary-layer analysis coupled with a three-dimensional inviscid conical flow analysis for a sharp cone at incidence in a supersonic or hypersonic stream. Development of the boundary-layer analysis is presented below; the inviscid analysis utilizes a documented digital computer code which is described briefly.

2.1 GOVERNING THREE-DIMENSIONAL TURBULENT BOUNDARY-LAYER EQUATIONS

The present analysis employs the three-dimensional compressible turbulent boundary-layer equations in terms of time-averaged mean flow quantities as derived by Vaglio-Laurin (Ref. 11). The coordinate system is taken to consist of geodesics and geodesic parallels, following Moore (Ref. 25). In this coordinate system the body surface is defined by $y = 0$ and a point in space is defined by the distances, x, y, and $r(x)\phi$ where the length $r(x)\phi$ depends explicitly on the distance x and where r(x) has the dimensions of length. This coordinate system is especially useful in the analysis of flow about bodies for which a coordinate x can be defined such that body cross sections are similar for various values of x. The quantity r(x) then gives the variation of scale for these cross sections. For the sharp cone geometry under present consideration, the geodesic coordinates are taken to be the cone generators and the geodesic parallels are the circles swept by the meridional angle. The corresponding length function r(x) is the local radius of the body. See Fig. 1 for clarification of the sharp cone geometry, nomenclature, and coordinate system. The time-averaged mean velocity components are taken to be $\bar{u}$, $\bar{v}$, and $\bar{w}$ in the directions of x, y, and ϕ, respectively. The governing equations of motion are, following Vaglio-Laurin (Ref. 11):

CONTINUITY

$$\frac{\partial}{\partial x}(\bar{\rho}\bar{u}r) + \frac{\partial}{\partial y}(\bar{\rho}\bar{V}r) + \frac{\partial}{\partial \phi}(\bar{\rho}\bar{w}) = 0 \qquad (1)$$

STREAMWISE (x) MOMENTUM

$$\bar{\rho}\bar{u}\frac{\partial \bar{u}}{\partial x} + \bar{\rho}\bar{V}\frac{\partial \bar{u}}{\partial y} + \frac{\bar{\rho}\bar{w}}{r}\frac{\partial \bar{u}}{\partial \phi} - \frac{\bar{\rho}(\bar{w})^2}{r}\frac{\partial r}{\partial x} = -\cancel{\frac{\partial \bar{p}}{\partial x}}^{0} + \frac{\partial}{\partial y}\left[\mu\frac{\partial \bar{u}}{\partial y} - \bar{\rho}\,\overline{u'v'}\right] \qquad (2)$$

CIRCUMFERENTIAL (ϕ) MOMENTUM

$$\bar{\rho}\bar{u}\frac{\partial \bar{w}}{\partial x} - \bar{\rho}\bar{V}\frac{\partial \bar{w}}{\partial y} + \frac{\bar{\rho}\bar{w}}{r}\frac{\partial \bar{w}}{\partial \phi} + \frac{\bar{\rho}\bar{u}\bar{w}}{r}\frac{\partial r}{\partial x} = \frac{-1}{r}\frac{\partial \bar{p}}{\partial \phi} + \frac{\partial}{\partial y}\left[\mu\frac{\partial \bar{w}}{\partial y} - \bar{\rho}\,\overline{v'w'}\right] \qquad (3)$$

NORMAL (y) MOMENTUM

$$\frac{\partial \bar{p}}{\partial y} = 0 \qquad (4)$$

ENERGY

$$\bar{\rho}\bar{u}\frac{\partial \bar{H}}{\partial x} + \bar{\rho}V\frac{\partial \bar{H}}{\partial y} + \frac{\bar{\rho}\bar{w}}{r}\frac{\partial \bar{H}}{\partial \phi} = \frac{\partial}{\partial y}\left[\mu\left(\frac{\partial \bar{H}}{\partial y} + \frac{1-Pr}{Pr}\frac{\partial \bar{h}}{\partial y}\right) - \bar{\rho}\overline{v'H'}\right] \tag{5}$$

where

$$V = \bar{v} + \frac{\overline{\rho' v'}}{\bar{\rho}} \tag{6}$$

and the usual expressions for the mean and fluctuating parts of the dependent variables are used; e. g.,

$$\rho = \bar{\rho} + \rho' \tag{7}$$

Implicit in Vaglio-Laurin's derivation of the above equations are the following stipulations:

a. The rates of change of the mean flow properties in the x- and ϕ-directions $[\mathcal{O}(1)]$ are smaller than the rates of change in the y-direction $[\mathcal{O}(\delta^{-1})]$ by an order of magnitude.

b. Mean squares and products of the turbulent fluctuations are $\mathcal{O}(\delta)$; that is, the turbulent level is small. The terms involving mean squares of the velocity fluctuations are taken to be negligible, which is valid for high Reynolds number flows with a zero or favorable pressure gradient.

c. The time average molecular transports are approximated by those pertaining to the mean flow properties; indeed, even the latter are negligible, except very near the wall, compared with terms involving the turbulent transports.

Also implicit in the above equations is the requirement of an inviscid conical flow field which leads to the term $\partial \bar{p}/\partial x = 0$; a full discussion of the inviscid conical flow field about a sharp cone at incidence in a supersonic or hypersonic flow will be given later in this section.

The energy equation (5) is defined in terms of the mean stagnation enthalpy

$$\bar{H} = \bar{h} + \frac{\bar{u}^2 + \bar{w}^2}{2} \tag{8}$$

If the two momentum equations (2) and (3) are multiplied by $\bar{u}$ and $\bar{w}$, respectively, and added, one obtains an equation for $(\bar{u}^2 + \bar{w}^2)/2$ which is simplified by the fact that the curvature terms (those involving $\partial r/\partial x$)

vanish. If then this equation is combined with the energy equation (5), one obtains the following energy equation in terms of the mean static enthalpy:

ENERGY

$$\bar{\rho}\bar{u}\frac{\partial \bar{h}}{\partial x} + \bar{\rho}V\frac{\partial \bar{h}}{\partial y} + \frac{\bar{\rho}\bar{w}}{r}\frac{\partial \bar{h}}{\partial \phi} = \bar{u}\frac{\partial \bar{p}}{\partial x}^{0} + \frac{\bar{w}}{r}\frac{\partial \bar{p}}{\partial \phi} + \mu\left[\left(\frac{\partial \bar{u}}{\partial y}\right)^2 + \left(\frac{\partial \bar{w}}{\partial y}\right)^2\right] - \bar{\rho}\,\overline{u'v'}\frac{\partial \bar{u}}{\partial y} - \bar{\rho}\,\overline{v'w'}\frac{\partial \bar{w}}{\partial y} + \frac{\partial}{\partial y}\left[\frac{\mu}{Pr}\frac{\partial \bar{h}}{\partial y} - \bar{\rho}\,\overline{v'h'}\right] \tag{9}$$

This is the form of the energy equation used in the present analysis.

If subscript w denotes wall and subscript e denotes outer edge of the boundary layer, the associated boundary conditions on the above defined equations are

MOMENTUM

$$\begin{aligned} y = 0 &: \bar{u} = \bar{v} = \bar{w} = \overline{u'v'} = \overline{v'w'} = \overline{\rho'v'} = 0 \\ \lim y \to \infty &: \bar{u} \to U_e,\ \bar{w} \to W_e \\ &\quad \overline{u'v'} \to 0,\ \overline{v'w'} \to 0,\ \overline{\rho'v'} \to 0 \end{aligned} \tag{10}$$

ENERGY

$$\begin{aligned} y = 0 &: \bar{h} = h_w,\ \overline{v'h'} = 0 \\ \lim y \to \infty &: \bar{h} \to h_e,\ \overline{v'h'} \to 0 \end{aligned} \tag{11}$$

which reflect the requirements of no slip and no homogeneous mass injection (suction or blowing) at the wall as well as a prescribed constant wall enthalpy. The normal momentum equation (4) reveals that the static-pressure variation across the boundary layer is negligible, and hence the static pressure, $\bar{p}(\phi)$, is regarded as an external input to the boundary-layer analysis from a separate inviscid analysis. The outer-edge velocities, U_e and W_e, as well as the outer-edge static enthalpy, h_e, must be determined from the inviscid analysis consistent with the imposed static-pressure distribution.

The gas model adopted for the present study is thermally and calorically perfect air having a constant specific heat ratio $\gamma = 1.40$ and obeying the equation of state

$$\bar{p} = \bar{\rho}R\bar{T} \tag{12}$$

where R = 1716 ft^2/sec^2-°R. Hence, under this assumption,

$$\bar{h} = C_p \bar{T} \tag{13}$$

where C_p = 6006 ft^2/sec^2-°R. The laminar viscosity, μ, is taken to obey Sutherland's law

$$\frac{\mu}{\mu_{ref}} = \frac{T_{ref} + 198.6}{\bar{T} + 198.6} \left(\frac{\bar{T}}{T_{ref}} \right)^{3/2} \tag{14}$$

where $\bar{T}$ must have units of °R and subscript ref denotes a reference condition. The laminar Prandtl number, Pr, is taken to be a constant value of 0.71 across the entire boundary layer.

2.2 TURBULENT TRANSPORT LAWS

Before Eqs. (1), (2), (3), and (9) can be solved, expressions must be supplied for the Reynolds stress or turbulent shear terms in the momentum equations and the turbulent flux of static enthalpy in the energy equation. The approach used in the present analysis is to model these terms as functions of the mean-flow variables following the analysis by Hunt, Bushnell, and Beckwith (Ref. 17).

The concept that the Reynolds stress in turbulent flow is proportional to a momentum exchange coefficient times the mean-flow velocity gradient normal to the surface is well known and commonly used in turbulent boundary-layer analyses. This concept is based on an assumed analogy between the so-called eddy viscosity and the molecular viscosity. The total shear components in the streamwise (x) and circumferential (ϕ) directions are written as

$$\tau_x = \mu \frac{\partial \bar{u}}{\partial y} - \bar{\rho}\,\overline{u'v'} = \mu \frac{\partial \bar{u}}{\partial y} + \epsilon_x \frac{\partial \bar{u}}{\partial y} \tag{15}$$

$$\tau_\phi = \mu \frac{\partial \bar{w}}{\partial y} - \bar{\rho}\,\overline{v'w'} = \mu \frac{\partial \bar{w}}{\partial y} + \epsilon_\phi \frac{\partial \bar{w}}{\partial y} \tag{16}$$

where the eddy viscosities ϵ_x and ϵ_ϕ in the x- and ϕ-directions, respectively, might in general be different. Since the total resultant shear must be a vector quantity, its magnitude is written as

$$\tau = \left[\left(\tau_x \right)^2 + \left(\tau_\phi \right)^2 \right]^{1/2} = \left[\left(\mu + \epsilon_x \right)^2 \left(\frac{\partial \bar{u}}{\partial y} \right)^2 + \left(\mu + \epsilon_\phi \right)^2 \left(\frac{\partial \bar{w}}{\partial y} \right)^2 \right]^{1/2} \tag{17}$$

In a similar manner the total heat flux in the energy equation (9) becomes

$$\dot{q} = \frac{k}{C_p}\frac{\partial \bar{h}}{\partial y} - \bar{\rho}\,\overline{v'h'} \approx \frac{k}{C_p}\frac{\partial \bar{h}}{\partial y} + \frac{\kappa}{C_p}\frac{\partial \bar{h}}{\partial y} \tag{18}$$

where κ is the so-called eddy thermal conductivity.

2.3 EDDY-VISCOSITY MODEL

The simplest approach to the formulation of models for the Reynolds stress is based on Prandtl's mixing-length hypothesis. For two-dimensional flow, this hypothesis states that

$$\left.\begin{aligned} u' &\propto -\ell_* \frac{\partial \bar{u}}{\partial y} \\ v' &\propto \ell_* \left|\frac{\partial \bar{u}}{\partial y}\right| \end{aligned}\right\} \tag{19}$$

The turbulent shear and eddy viscosity are then

$$\tau_{turb} \equiv -\bar{\rho}\,\overline{u'v'} = \epsilon\frac{\partial \bar{u}}{\partial y} = \bar{\rho}\ell_*^2\left|\frac{\partial \bar{u}}{\partial y}\right|\frac{\partial \bar{u}}{\partial y} \tag{20}$$

from whence

$$\epsilon = \bar{\rho}\ell_*^2\left|\frac{\partial \bar{u}}{\partial y}\right| \tag{21}$$

The quantity ℓ_* is termed the mixing length and is some characteristic length related to the size or scales of eddies responsible for the flux of momentum in the y-direction. Although the details of such a transfer mechanism are not well understood, the basic concept gives satisfactory results even at hypersonic Mach numbers in the presence of heat-transfer and pressure gradients as mentioned in the review of turbulent boundary-layer literature given in Section I.

The turbulent boundary-layer studies by Prandtl (Ref. 26) and Glushko (Ref. 27) are based on the concept that the eddy viscosity should depend only on the properties of the turbulence and a local eddy scale. Extending this concept to the three-dimensional case of present interest suggests that the eddy viscosity should be a scalar function independent of the coordinate direction. Accordingly, the components of the Reynolds stress are written as

$$\tau_{turb,\,x} \equiv -\bar{\rho}\,\overline{u'v'} = \bar{\rho}\ell_*^2\frac{\partial \bar{G}}{\partial y}\frac{\partial \bar{u}}{\partial y} \tag{22}$$

$$\tau_{turb,\,\phi} \equiv -\bar{\rho}\,\overline{v'w'} = \bar{\rho}\ell_*^2\frac{\partial \bar{G}}{\partial y}\frac{\partial \bar{w}}{\partial y} \tag{23}$$

so that the eddy viscosity is

$$\epsilon = \epsilon_x = \epsilon_\phi = \bar{\rho} \ell_*^2 \frac{\partial \bar{G}}{\partial y} \tag{24}$$

To determine the scalar function $\bar{G}$, Eq. (24) is substituted into Eq. (17) with the result that the magnitude of the total resultant shear becomes

$$\tau = \left(\mu + \bar{\rho} \ell_*^2 \frac{\partial \bar{G}}{\partial y} \right) \left[\left(\frac{\partial \bar{u}}{\partial y} \right)^2 + \left(\frac{\partial \bar{w}}{\partial y} \right)^2 \right]^{1/2} \tag{25}$$

Now, by analogy with Eqs. (20) and (21) where the velocity-gradient function for the turbulent shear component is repeated in the eddy-viscosity expression, the relationship for the determination of the $\bar{G}$ function becomes

$$\frac{\partial \bar{G}}{\partial y} = \left[\left(\frac{\partial \bar{u}}{\partial y} \right)^2 + \left(\frac{\partial \bar{w}}{\partial y} \right)^2 \right]^{1/2} \tag{26}$$

which results in the final form of the eddy viscosity

$$\epsilon = \bar{\rho} \ell_*^2 \left[\left(\frac{\partial \bar{u}}{\partial y} \right)^2 + \left(\frac{\partial \bar{w}}{\partial y} \right)^2 \right]^{1/2} \tag{27}$$

Hunt, Bushnell, and Beckwith (Ref. 17) call the above representation of the Reynolds stress the invariant turbulence model. The key assumption in this model is that the eddy viscosity is a scalar function independent of coordinate direction. In a recent analysis of three-dimensional incompressible turbulent boundary-layer flows using the kinetic-energy-of-turbulence approach, Nash (Ref. 19) has advanced arguments that the turbulent shear stress is likely to act in the mean rate of strain direction, defined by the components of the mean velocity gradient vector, so that his closure equation is simply, in the nomenclature of the present analysis,

$$\frac{\tau_{\text{turb, x}}}{\dfrac{\partial \bar{u}}{\partial y}} = \frac{\tau_{\text{turb, }\phi}}{\dfrac{\partial \bar{w}}{\partial y}} \tag{28}$$

The same equation results from the scalar eddy-viscosity model presented by Eqs. (22) and (23) above. On the other hand, Bradshaw (Ref. 18) has derived a set of differential equations for the two components of the turbulent shear stress based again on the kinetic-energy-of-turbulence approach but permitting the turbulent shear stress vector

to deviate from the mean rate of strain direction. However, in the near-wall region, Bradshaw's turbulent shear stress equation reduces to the form, again in the nomenclature of the present analysis,

$$\tau_{turb} = \bar{\rho}\ell_*^2\left[\left(\frac{\partial \bar{u}}{\partial y}\right)^2 + \left(\frac{\partial \bar{w}}{\partial y}\right)^2\right] \tag{29}$$

which is identical with the results of Eqs. (25) and (26) derived above for the turbulent shear contributions. Arguments for the preference of either variance or invariance of the turbulent shear stress vector relative to the mean rate of strain direction are currently based on slender evidence. The analytical studies by Nash (Ref. 19) and Cooper (Ref. 20) concerning three-dimensional incompressible turbulent boundary layers indicate that the above-defined invariant model of turbulence results in very acceptable calculated boundary-layer parameters relative to experiment. Much more work, especially carefully controlled experiments involving three-dimensional compressible turbulent boundary layers, remains to be done before the question of variance or invariance can be completely resolved. Until such time, the above invariant turbulence model appears plausible for studying three-dimensional turbulent boundary-layer flow.

2.4 MIXING-LENGTH MODEL

The turbulent shear stress in a three-dimensional turbulent boundary layer as governed by Eqs. (25) and (26) is treated herein by the use of a two-layer inner-outer model using Prandtl's mixing-length hypothesis and a modification of van Driest's analysis for the near-wall region. This results in a continuous distribution of the shear stress from the laminar value at the wall, through the fully turbulent region, reaching zero at the outer edge of the boundary layer. The energy transport in a turbulent boundary layer is treated in this work through the incorporation of the eddy conductivity, κ, into a turbulent Prandtl number, Pr_t. Exactly the same empirical functions are used as in the two-dimensional flow reported by Adams (Ref. 8). This is justified by noting that the scalar properties of a turbulence field are unlikely to be affected by moderate three-dimensionality because turbulence is inherently three-dimensional in nature for even so-called two-dimensional flows.

After Escudier (Ref. 28), Patankar and Spalding (Ref. 2) recommend the following variation of the mixing length, ℓ_*, across the turbulent two-dimensional boundary layer which is adopted for the three-dimensional case per the above discussion:

$$\ell_* = k_* y, \text{ for } 0 < y \leq \lambda y_\ell / k_*$$
$$\ell_* = \lambda y_\ell, \text{ for } \lambda y_\ell / k_* < y \tag{30}$$

where the values for the various numerical constants are taken to be $k_* = 0.435$ and $\lambda = 0.09$. The value of y at the point where the velocity in the boundary layer is equal to 0.99 of the velocity at the boundary-layer outer edge is used to define the distance y_ℓ. The above choices follow Patankar and Spalding and result in good agreement with the mixing-length model proposed by Maise and McDonald (Ref. 29) for compressible two-dimensional turbulent boundary layers.

By analogy with Stokes' solution for an infinite flat plate undergoing simple harmonic motion parallel to itself in an infinite fluid, van Driest (Ref. 30) concluded that in the vicinity of a wall the total shear stress in a turbulent two-dimensional fluid should be of the form

$$\tau = \mu \frac{\partial \bar{u}}{\partial y} + \bar{\rho}\, k_*^2 y^2 \left[1 - \exp\left(\frac{-y\sqrt{\tau_w \bar{\rho}}}{\mu A_*}\right)\right]^2 \left(\frac{\partial \bar{u}}{\partial y}\right)^2 \tag{31}$$

which results in an exponential damping of the turbulent part of the shear stress as the wall is approached and yields exactly the laminar shear stress form, $\tau = \mu(\partial \bar{u}/\partial y)$, at the wall. Although Eq. (31) was originally developed for incompressible flow, it can be applied to compressible flow by application of the suggestion by Patankar and Spalding (Ref. 2) that the local value of shear stress be used instead of the wall value as originally recommended by van Driest (Ref. 30). Hence, by analogy of Eq. (31) with Eqs. (25) and (26), the relationship for the three-dimensional near-wall shear stress as used in the present analysis is

$$\tau = \mu \frac{\partial \bar{G}}{\partial y} + \bar{\rho} k_*^2 y^2 \left[1 - \exp\left(\frac{-y\sqrt{\tau \bar{\rho}}}{\mu A_*}\right)\right]^2 \left(\frac{\partial \bar{G}}{\partial y}\right)^2 \tag{32}$$

where the constant A_* is taken to be 26.0 following the original van Driest proposal (Ref. 30). Note that the damping term in Eq. (32) reflects the application of the local total shear stress as opposed to the wall shear stress of Eq. (31) as discussed previously.

Based on Eqs. (26), (27), (30), and (32), the eddy-viscosity expression for the inner region is

$$\epsilon_i = \bar{\rho} k_*^2 y^2 \left[1 - \exp\left(\frac{-y\sqrt{\tau \bar{\rho}}}{\mu A_*}\right)\right]^2 \frac{\partial \bar{G}}{\partial y} \tag{33}$$

and for the outer region

$$\epsilon_o = \bar{\rho}\lambda^2 y_\ell^2 \frac{\partial \bar{G}}{\partial y} \tag{34}$$

with the constants k_*, A_*, λ, and y_ℓ defined previously. The constraint used to define the end of the inner region and the beginning of the outer region is the continuity of the eddy viscosity. From the wall outward, the expression for the inner eddy viscosity applies until $\epsilon_i = \epsilon_o$ from which point the outer eddy viscosity is used. A schematic of this variation in terms of the mixing lengths is shown below.

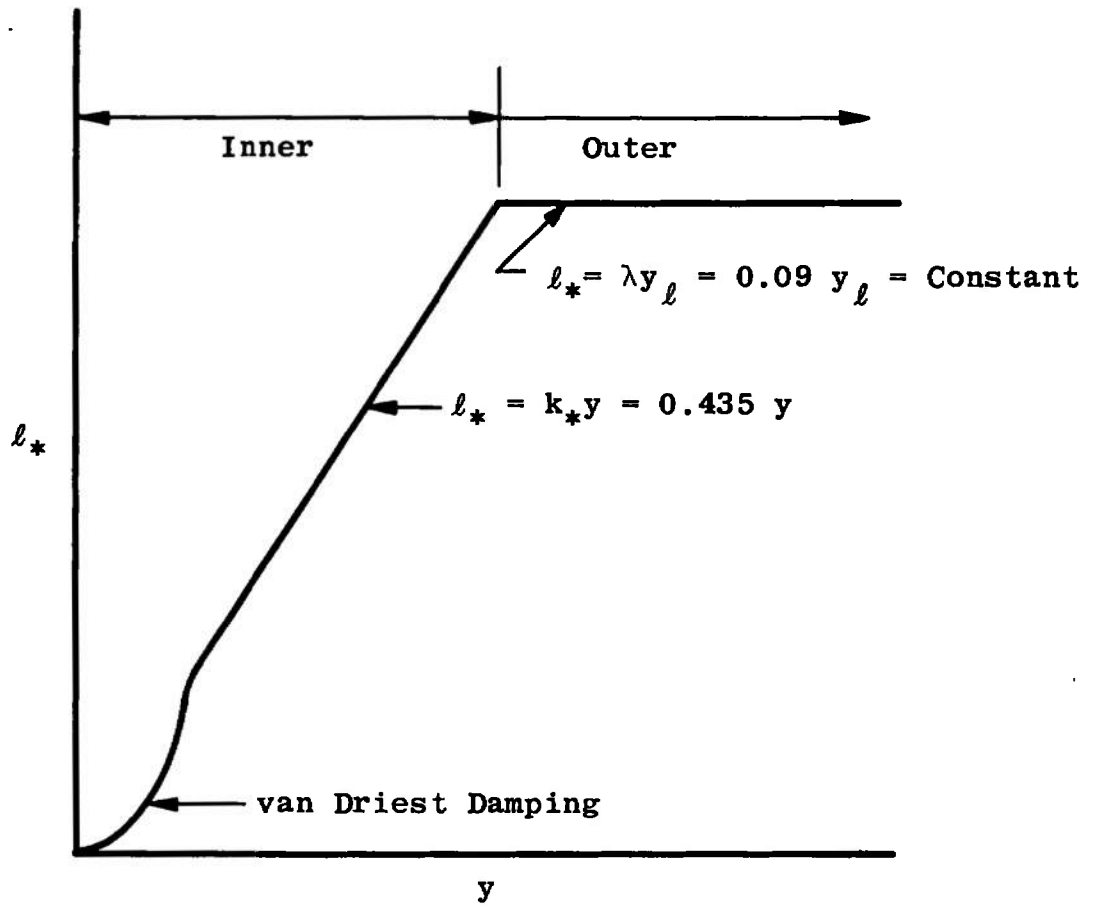

The turbulent Prandtl number defined as

$$Pr_t = \frac{C_p \epsilon}{\kappa} \tag{35}$$

is physically a measure of the ratio of eddy viscosity to eddy conductivity, that is, the ratio of the turbulent transport of momentum to the turbulent transport of heat. Since the flow in the outer region of a turbulent boundary layer shows some similarity to a turbulent wake flow,

one may advance arguments that a realistic formulation of turbulent Prandtl number requires a separate expression for the inner and outer region just as in the eddy-viscosity formalism. Recent reviews by Rotta (Refs. 31 and 32) and Meier and Rotta (Ref. 33) indicate that the turbulent Prandtl number varies in magnitude from approximately 0.8 near the boundary-layer outer edge to approximately 1.5 near the wall. Much experimental work remains to be done in defining the turbulent Prandtl number distribution as the reviews by Rotta point out. In the present work the turbulent Prandtl number defined by Eq. (35) is taken to remain constant at the value 0.90 across the entire boundary layer as recommended by Patankar and Spalding (Ref. 2) for two-dimensional turbulent boundary layers. This choice of turbulent Prandtl number is consistent with the analyses of Patankar and Spalding (Ref. 2), Martellucci, Rie, and Sontowski (Ref. 6), Mayne and Dyer (Ref. 7), and Adams (Ref. 8); the analysis by Smith and Cebeci (Ref. 1) assumed a value of unity. Bushnell and Beckwith (Ref. 5), as well as Hunt, Bushnell, and Beckwith (Ref. 17), employ a variable turbulent Prandtl number model.

2.5 SUMMARY OF GOVERNING THREE-DIMENSIONAL TURBULENT BOUNDARY-LAYER EQUATIONS AND GAS MODEL

Under the assumption of the invariant turbulence scalar eddy-viscosity model of three-dimensional turbulence presented above, the governing three-dimensional turbulent boundary-layer equations for a sharp cone at incidence flows under supersonic or hypersonic conditions, as given by Eqs. (1), (2), (3), (4), and (9), reduce to the following:

CONTINUITY

$$\frac{\partial}{\partial x}(\bar{\rho}\bar{u}r) + \frac{\partial}{\partial \phi}(\bar{\rho}\bar{w}) + \frac{\partial}{\partial y}(\bar{\rho}Vr) = 0 \tag{36}$$

x-MOMENTUM

$$\bar{\rho}\bar{u}\frac{\partial \bar{u}}{\partial x} + \frac{\bar{\rho}\bar{w}}{r}\frac{\partial \bar{u}}{\partial \phi} + \bar{\rho}V\frac{\partial \bar{u}}{\partial y} - \frac{\bar{\rho}(\bar{w})^2}{r}\frac{\partial r}{\partial x} = -\cancelto{0}{\frac{\partial \bar{p}}{\partial x}} + \frac{\partial}{\partial y}\left[\left(\mu + \epsilon\right)\frac{\partial \bar{u}}{\partial y}\right] \tag{37}$$

ϕ-MOMENTUM

$$\bar{\rho}\bar{u}\frac{\partial \bar{w}}{\partial x} + \frac{\rho\bar{w}}{r}\frac{\partial \bar{w}}{\partial \phi} + \bar{\rho}V\frac{\partial \bar{w}}{\partial y} + \frac{\bar{\rho}\bar{u}\bar{w}}{r}\frac{\partial r}{\partial x} = \frac{-1}{r}\frac{\partial \bar{p}}{\partial \phi} + \frac{\partial}{\partial y}\left[\left(\mu + \epsilon\right)\frac{\partial \bar{w}}{\partial y}\right] \tag{38}$$

y-MOMENTUM

$$\frac{\partial \bar{p}}{\partial y} = 0 \tag{39}$$

ENERGY

$$\bar{\rho}\,\bar{u}c_p\frac{\partial \overline{T}}{\partial x} + \frac{\bar{\rho}\bar{w}}{r}\,C_p\frac{\partial \overline{T}}{\partial \phi} + \bar{\rho}V\,C_p\frac{\partial \overline{T}}{\partial y} = \bar{u}\cancel{\frac{\partial \bar{p}}{\partial x}}^{\,0} + \frac{\bar{w}}{r}\frac{\partial \bar{p}}{\partial \phi} + (\mu+\epsilon)\left[\left(\frac{\partial \bar{u}}{\partial y}\right)^2 + \left(\frac{\partial \bar{w}}{\partial y}\right)^2\right]$$

$$+ \frac{\partial}{\partial y}\left[C_p\left(\frac{\mu}{Pr} + \frac{\epsilon}{Pr_t}\right)\frac{\partial \overline{T}}{\partial y}\right] \tag{40}$$

with the scalar eddy viscosity ϵ defined by Eq. (27) as

$$\epsilon = \bar{\rho}\ell_*^2\left[\left(\frac{\partial \bar{u}}{\partial y}\right)^2 + \left(\frac{\partial \bar{w}}{\partial y}\right)^2\right]^{1/2}$$

in conjunction with the following mixing-length model from Eqs. (33) and (34)

$$\begin{aligned}
&\text{Inner Region} \rightarrow \ell_* = Dk_*y \\
&\text{Outer Region} \rightarrow \ell_* = \lambda y_\ell \\
&\text{Switchover When } \epsilon_i = \epsilon_0
\end{aligned} \tag{41}$$

employing the following empirical constants

$k_* = 0.435$

$\lambda = 0.090$

D = van Driest wall damping term evaluated locally using $A_* = 26.0$

$$= 1 - \exp\left[\frac{-y\sqrt{\tau\bar{\rho}}}{\mu A_*}\right]$$

y_ℓ = y-value where $\dfrac{[(\bar{u})^2 + (\bar{w})^2]^{1/2}}{[U_e^2 + W_e^2]^{1/2}} = 0.99$

$Pr_t = 0.90$

and from Eq. (6),

$$V = \bar{v} + \frac{\overline{\rho' v'}}{\bar{\rho}}$$

The gas model used is thermally and calorically perfect air obeying the equation of state given by Eq. (12):

$$\bar{p} = \bar{\rho} R \overline{T}$$

where

$$R = 1716 \text{ ft}^2/\text{sec}^2\text{-}^\circ\text{R}$$
$$C_p = 6006 \text{ ft}^2/\text{sec}^2\text{-}^\circ\text{R}$$
$$\gamma = 1.40$$
$$Pr = 0.71$$

The laminar viscosity is given by Sutherland's law, Eq. (14), with $\overline{T}$ in units of °R:

$$\frac{\mu}{\mu_{ref}} = \frac{T_{ref} + 198.6}{\overline{T} + 198.6} \left(\frac{\overline{T}}{T_{ref}} \right)^{3/2}$$

From the sharp cone geometry as shown in Fig. 1,

$$r = x \sin \delta_v \tag{42}$$

so that

$$\frac{\partial r}{\partial x} = \sin \delta_v \tag{43}$$

which provides the necessary geometry information for use in the governing equations of motion (36-40).

2.6 PROCEDURE FOR NUMERICAL SOLUTION OF THE THREE-DIMENSIONAL BOUNDARY-LAYER EQUATIONS

For application in the present sharp cone at incidence investigation, the three-dimensional conical flow laminar boundary-layer analysis as presented in Appendix B of the report by McGowan and Davis (Ref. 34) has been modified to include the effects of three-dimensional turbulence through the use of the scalar eddy-viscosity model discussed previously. The basic McGowan and Davis laminar boundary-layer treatment is very similar to that of Dwyer (Ref. 35) and Boericke (Ref. 36) in that the limiting forms of the full three-dimensional compressible laminar boundary-layer equations for conical flow as originally derived by Moore (Ref. 25) are solved using a marching implicit finite-difference technique for numerical integration of the nonlinear parabolic partial differential equations written in similarity variable form. The similarity variable transformation reduces the number of independent variables from three to two in the transformed governing equations so that the

problem becomes two-dimensional in form. Since there are only two independent variables in this coordinate system, the implicit finite-difference techniques developed by Blottner (Refs. 37 and 38) can be used almost directly to solve the governing equations. The complete formalism of this numerical approach is discussed in Chapter III of the report by McGowan and Davis, to which the reader is referred for further information.

The necessary outer-edge conditions for input to the above-described boundary-layer analysis are determined based on results from an inviscid analysis of a sharp cone at incidence, which is discussed in the following subsection. The procedure for specifying the inviscid data necessary for input to the McGowan and Davis boundary-layer analysis is quite simple in that only the pressure distribution around the cone, along with the velocity and density on the windward streamline, must be specified. All other inviscid quantities are then internally calculated using the inviscid compressible Bernoulli and crossflow momentum equations applied at the cone surface, along with the restriction that the entropy remain constant on the surface; i. e., the cone surface is an isentropic surface. Complete details of this procedure are given in Section B of Chapter IV in the report by McGowan and Davis (Ref. 34).

Following Appendix B of McGowan and Davis (Ref 34), the governing three-dimensional turbulent boundary-layer equations (36-40) are transformed using similarity variables ξ, η, and ζ similar to those used by Dwyer (Ref. 35) and Boericke (Ref. 36) for three-dimensional laminar boundary layers. The definitions of ξ, η, and ζ are as follows:

$$\xi = \int_0^x r^2 dx = \int_0^x (x \sin \delta_v)^2 dx = \frac{1}{3} x^3 \sin^2 \delta_v \tag{44}$$

$$\eta = \sqrt{\frac{\rho_\infty U_\infty}{2 \xi \mu_\infty}} \int_0^y \frac{\bar{\rho}}{\rho_\infty} \sqrt{\frac{p_\infty}{\bar{p}}}\, r\, dy \tag{45}$$

$$\zeta = \phi \tag{46}$$

where $r = x \sin \delta_v$ for the sharp cone geometry of present interest, as shown in Fig. 1. Introducing the above similarity variables into the governing equations (36-40) and performing the standard transformation of variables manipulations yields the set of equations (B. 13-B. 16) in Appendix B of McGowan and Davis with the following two modifications:

1. The laminar viscosity, μ, must be replaced by the sum of the laminar and turbulent (eddy) viscosity $(\mu + \epsilon)$ in the transformed ξ- and ζ- momentum equations, as well as in the transformed energy equation.

Furthermore, in the energy equation the laminar heat conductivity term (μ/Pr) must be replaced by the sum of the laminar and turbulent (eddy) heat conductivity $[(\mu/Pr) + (\epsilon/Pr_t)]$.

2. The three-dimensional turbulent boundary-layer flow must be locally similar in the sense of a mathematical analysis under the constraint $(\partial/\partial\xi) = 0$ with the eddy viscosity ϵ evaluated at the local ξ condition. The applicability of this technique relies essentially on the condition that the external and body flow properties vary sufficiently slowly with the x-dependent variable ξ defined by Eq. (42). Experimental justification for the use of this assumption in the case of three-dimensional turbulent boundary-layer flow over a sharp cone at incidence in a supersonic stream is presented in Section IV of the present report.

Under the above local similarity restriction the transformed governing boundary-layer equations become mathematically parabolic in the η, ζ coordinates with ξ as a parameter. The "history" of the flow is contained only in the ϵ and η dependence on ξ and, hence, local similarity represents a "patching together" of local solutions.

The method for numerical solution of the governing three-dimensional boundary-layer equations in similarity ξ, η, ζ variables follows the iterative implicit finite-difference integration technique (integration in η-direction marching in ζ-direction windward to leeward ray) presented in Chapter III of the report by McGowan and Davis (Ref. 34). A variable η grid mesh is used following Adams (Ref. 8) to concentrate grid points in the near-wall region where the dependent variables change most rapidly in a turbulent flow. Digital computer run times are acceptable for practical usage (approximately 20 minutes, including printout, to integrate 180.0 degrees around a sharp cone at incidence using a 2.50-deg step size ζ-integration increment with 120 η grid points across the boundary layer on a CDC 1604-B digital computer).

Experience with the McGowan and Davis digital computer code reported in Ref. 34 has revealed few defects, and the present author highly recommends its use. It should be noted that the main emphasis of Ref. 34 is placed upon development and documentation of a very general three-dimensional laminar boundary-layer analysis for general body geometry, providing the inviscid flow field for the body in question is available from some source.

2.7 THREE-DIMENSIONAL INVISCID CONICAL FLOW

A recent investigation by Jones (Ref. 39) resulted in an accurate and efficient numerical integration procedure for solution of the governing partial differential equations describing the supersonic or hypersonic inviscid flow field around a sharp cone at incidence. Basically, Jones' method uses the condition of conicity to reduce the problem to a set of elliptic nonlinear partial differential equations in two independent variables. A transformation of coordinates is used to fix the boundaries, one of which is the unknown shock wave, between which the elliptic equations are to be satisfied. This transformation also has the effect of including the body shape in the coefficients of the partial differential equations and in the boundary conditions, so that the same method can be used for general conical body shapes simply by changing a few program statements to redefine the equation of the body. In fact, the method is, in many cases, only limited by the crossflow velocity expanding from subsonic to supersonic conditions which changes the mathematical character of the governing equations from elliptic to hyperbolic, by the entropy singularity moving too far away from the surface, or by the shock approaching very close to the Mach wave. In practice these restrictions limit the allowable angle-of-attack range to $\alpha/\delta_V \lessapprox 1.4$ (see Fig. 1 for clarification of nomenclature).

The method is efficient in computer time compared with other fully numerical techniques. One solution takes from about one-half minute to three minutes on an IBM 360/50 computer for the circular cone at incidence, the time increasing as the incidence increases. This is to be compared with a time requirement of approximately one-half hour on an IBM 360/50 computer for the technique developed by Moretti (Ref. 40) in which the flow field solution is obtained by marching step by step downstream (approximately 400 downstream steps are required) until a conicity condition is sufficiently well satisfied. Comparison of results between the Jones and Moretti approaches show excellent agreement, with the Jones digital computer code being a factor of approximately ten faster than the Moretti approach in solution time. An analysis very similar to that of Jones has recently been reported by South and Klunker (Ref. 41), whereas Holt and Ndefo (Ref. 42) have developed a method of integral relations approach to the problem. The important point to note is that all of the above-referenced analyses report excellent agreement with experiment for sharp circular cones at incidence under supersonic and hypersonic flow conditions, so that the choice of which analysis is indeed the best remains an open question. The present author's experience with use of the Jones digital computer code (Ref. 43) has been most favorable from a user's standpoint.

It should be pointed out in conclusion that Jones (Ref. 44) has recently published a very complete and thorough set of tables for inviscid supersonic and hypersonic flow about circular cones at incidence in a perfect gas, $\gamma = 1.40$, stream. These tables can be used to provide all of the needed inviscid information for input to the present boundary-layer analysis.

SECTION III
PRIOR EXPERIMENTAL INVESTIGATIONS OF THE SHARP CONE AT INCIDENCE UNDER SUPERSONIC AND HYPERSONIC FLOW CONDITIONS

The primary set of experimental data used for comparison with the present theory is taken from the work of Rainbird (Ref. 45) concerning turbulent boundary-layer growth and separation on a yawed 12.5-deg semivertex angle sharp cone. The investigation was conducted in the Canadian National Aeronautical Establishment 5-ft intermittent blowdown (air) supersonic wind tunnel at moderate relative incidence ($\alpha/\delta_V = 1$ to 2) under high Reynolds number conditions with essentially zero heat transfer either to or from the cone. Reference 45 presents experimentally determined surface pressure distributions, surface flow angles, and detailed turbulent boundary-layer profile traverses at various circumferential locations around the cone. Full details of the experimental techniques are given in Ref. 45, as well as in an earlier paper by Rainbird (Ref. 46) on essentially the same subject.

For the present investigation, attention is restricted solely to the free-stream Mach Number 1.80 and angle-of-incidence 15.78-deg condition of Rainbird (Ref. 45). The nominal free-stream conditions for this case are as follows (see Fig. 1 for the sharp cone geometry and nomenclature):

$$M_\infty = 1.80$$

$$p_\infty = 626.40 \text{ lbf/ft}^2$$

$$T_\infty = 321.60°\text{R}$$

$$Re_{\infty,L} = 2.56 \times 10^7$$

$$L = 41.58 \text{ in.}$$

The cone surface temperature is taken as equal to the free-stream stagnation temperature (530°R). Because of the conical nature of the flow field for a sharp cone at incidence (discussed in detail in Section 4.1 of this report), all boundary-layer surveys at various circumferential

locations around the cone were conducted at one axial location along the cone, namely, $x/L = 0.85$. As stated by Rainbird (Ref. 45), boundary-layer transition takes place quite close to the sharp cone apex ($x/L < 0.1$) because of the high stream turbulence level resulting from noise generated by the blowdown wind tunnel control valve.

The other set of experimental data used for comparison with the present theory is taken from the study by Martellucci and Neff (Ref. 47) concerning the effects of asymmetric boundary-layer transition on reentry vehicle characteristics under hypersonic flow conditions. The experimental phase of this investigation was conducted in the Hypersonic Wind Tunnel (B) of the von Kármán Gas Dynamics Facility (VKF), Arnold Engineering Development Center (AEDC), on a 7.20-deg semivertex angle sharp cone at 1.0-, 2.0-, and 4.0-deg angle of attack. The model, which was fabricated of stainless steel, had a nominal wall thickness of 0.050 in. and was instrumented with approximately 100 thermocouples located on five conical rays (ϕ = 0, 45, 90, 135, and 180 deg) to record the aerodynamic heat-transfer rate via the thin-skin technique. Tunnel free-stream conditions are as follows (see Fig. 1 for the sharp cone geometry and nomenclature):

$$M_\infty = 8.0$$

$$p_\infty = 12.69 \text{ lbf/ft}^2$$

$$T_\infty = 96.84°\text{R}$$

$$Re_{\infty,L} = 1.38 \times 10^7$$

$$L = 43.89 \text{ in.}$$

which are based upon nominal tunnel stagnation conditions of

$$p_0 \approx 860 \text{ lbf/in.}^2$$

$$T_0 \approx 1340°\text{R}$$

The cone surface temperature is taken to be a constant 535.0°R, which results in a constant wall to stagnation temperature ratio, T_W/T_O, of approximately 0.4. Figure 2 presents the spatial distribution of the end of boundary-layer transition with respect to angle of attack as reported in Fig. 3 of Ref. 47 for the above tunnel free-stream conditions. Here the end of transition is defined to be the point where the aerodynamic heat-transfer rate in the transition front region is a maximum. The important point to note from Fig. 2 is that the three-dimensional boundary layer will be in a fully turbulent state for $x/L > 0.5$ for all three angles of attack under the present high Reynolds number free-stream condition.

SECTION IV
RESULTS AND DISCUSSION

4.1 JUSTIFICATION OF LOCALLY SIMILAR TURBULENT BOUNDARY-LAYER ANALYSIS

The assumption made in Section II of a locally similar boundary-layer analysis with the eddy viscosity ϵ evaluated at the local ξ condition appears very questionable for application to general three-dimensional turbulent flows because of the failure to include details of the "upstream history." However, for the special case of a sharp cone at incidence in a supersonic or hypersonic stream where the boundary layer is in a state of fully developed turbulent flow, i. e., far downstream of transition with a constant wall temperature, experimental measurements reported by Rainbird (Refs. 45 and 46) establish that the flow field, even with separation present, is essentially conical and symmetrical, thus permitting all detailed measurements to be made at one lengthwise station. The evidence in support of this finding is as follows (taken from Ref. 45):

a. Overall force and moment measurements show zero side force and yawing moment and give a fixed center-of-pressure position at 0.682L that is in excellent agreement with the theoretical conical flow value of $(2/3)L/\cos \delta_V$.

b. Integration of circumferential pressure distributions to give local normal-force coefficients shows good agreement with overall balance measurements.

c. Measurements of surface pressure distributions along generators of the cone show pressures constant except for some extreme angle-of-attack conditions where a forward-propagating base effect is present.

d. Flow visualization using the oil-dot technique gives values of surface flow angle ω_S, i. e., the direction of surface shear stress, as well as primary separation position which are independent of distance from the cone apex, x/L, within a measuring accuracy of about 1.5 deg.

Because of the importance of the invariance of the surface flow angle with lengthwise location at a given circumferential location in the present theoretical analysis, a comparison is given in Fig. 3 (taken from Ref. 45) of surface flow angle measurements at various x/L stations up to separation for the rather severe condition of $\alpha/\delta_V = 2$. See

Fig. 1 for the definition of the surface flow angle relative to the conical geometry of present interest. The results show that surface flow angle is essentially independent of distance from the cone apex, which means that under such a flow condition (conical inviscid and fully turbulent boundary layer) a locally similar turbulent boundary-layer analysis which neglects "upstream history" may be a plausible assumption. One purpose of the present report is to assess if indeed such is a reasonable approach based on comparison of theory relative to experimental measurements taken under flow conditions which satisfy the restrictions imposed above (conical inviscid flow field with a fully turbulent boundary layer under constant wall temperature conditions).

4.2 PRESENTATION OF PRESENT RESULTS

4.2.1 Supersonic Flow

Turning now to representative results from the present investigation, one sees in Fig. 4 a comparison of the calculated surface pressure distribution around the sharp cone based on the Jones analysis (Refs. 39 and 43) relative to the experimental measurements of Rainbird (Ref. 45). As is clearly shown in Fig. 4, the agreement is excellent over the entire cone. Figure 5 presents the corresponding calculated inviscid flow parameters (streamwise and crossflow velocities, as well as static temperature) on the cone surface. It should be noted that these surface values are the so-called isentropic surface values (see Ref. 39 for clarification of this terminology).

With respect to the above, it should be noted that Rainbird (Ref. 45) experimentally observed turbulent boundary-layer separation to occur at approximately 159 deg around the cone for the present flow condition and angle of incidence (M_∞ = 1.80, $Re_{\infty, L}$ = 2.56 x 10^7, α = 15.78 deg). As discussed by Rainbird in Ref. 45, the development of flow separation about sharp cones as the incidence angle is increased is a gradual, progressive, steady, and essentially conical process involving the formation of symmetrical lobes of vortical fluid which develop into vortices and which remain comparatively close to the cone surface on either side of, and near, the leeward generator. For the angle of incidence of present interest (α = 15.78 deg) Rainbird observed the formation of two symmetrically disposed lobes of vortical fluid on either side of the leeward generator. At a higher angle of incidence (α = 22.75 deg) these lobes of vortical fluid roll up to form a pair of symmetrically disposed vortices close to the cone surface which, in turn, result in the formation of internal shock waves with their attendant local increases in pressure. Since there are no vortices present in the separated flow

field of current interest, the influence of separation on the external inviscid flow is small, which is reflected in the excellent agreement shown in Fig. 4 between inviscid theory and experiment.

Figures 6 and 7 present the calculated mean velocity and static temperature profiles across the turbulent boundary layer at the location $x/L = 0.85$ on the most windward ray ($\phi = 0$ deg) of the sharp cone. The calculated profiles are generally in good agreement with the measured profiles by Rainbird, which reveals the validity of the presently proposed three-dimensional eddy-viscosity model for windward ray applications. Shown in Fig. 7 are comparisons of the present windward ray profiles relative to calculated results from Fig. 16b of the recent windward plane of symmetry turbulent boundary-layer analysis by Adams (Ref. 48). The basic approach of Ref. 48 involved formulation and application of a laminar, transitional, and turbulent boundary-layer analysis for the windward streamline of a sharp cone at incidence in a supersonic or hypersonic flow. The governing nonsimilar boundary-layer equations in the windward plane of symmetry were numerically integrated on a digital computer using an implicit finite-difference technique which marched along the windward ray starting at the apex of the cone with a laminar similar solution. The same two-layer (inner-outer) eddy viscosity-mixing length model of turbulence was used for calculation of the windward ray turbulent boundary layer as in the present work. The transition zone was treated through an eddy viscosity-intermittency factor approach. Inviscid edge conditions along the windward ray were obtained from the same Jones digital computer code (Refs. 39 and 43) used in the present work. The excellent agreement shown in Figs. 7a and b between the nonsimilar analysis of Ref. 48 and the present locally similar analysis offers further analytical justification for the applicability of the locally similar type analysis for sharp cone at incidence flows with a turbulent boundary layer. It should be mentioned in this connection that Schmidt, Boldman, and Todd (Ref. 49) have recently reported a locally similar turbulent boundary-layer analysis for axisymmetric nozzle flow applications. They point out that through this approach the nozzle exit boundary layer can be calculated directly without the requirement of the usual step-by-step marching calculation method of the nonsimilar boundary layer. The same statement applies to the present sharp cone at incidence boundary layer where, as in the current work, the analysis can be performed for the body station location of interest without having to perform the step-by-step marching calculation of the complete three-dimensional nonsimilar boundary layer.

Also shown in Figs. 7a and b are rough indications of the physical boundaries for the inner and outer regions of the turbulent boundary

layer, as discussed by Bradshaw (Ref. 50) in his recent review. The location of the inner-outer boundary at $y/\delta_t \approx 0.2$ can easily be derived from Eq. (30) by equating the inner and outer mixing lengths to yield

$$\frac{y}{y_\ell} = \frac{\lambda}{k_*} = \frac{0.090}{0.435} = 0.206 \tag{47}$$

where y_ℓ is the value of y at the point where the velocity in the boundary layer is equal to 0.99 of the velocity at the boundary-layer outer edge, and, hence, $y_\ell \approx \delta_t$ where δ_t is the boundary-layer thickness defined as the normal distance from the surface where the boundary-layer velocity equals 0.995 of the outer-edge velocity. Further, observe from Figs. 7a and b that the experimentally determined turbulent boundary-layer thickness is slightly larger than predicted by the present theory.

Using the implicit finite-difference integration technique to obtain the solution around the cone at the body location $x/L = 0.85$ yields the calculated profiles shown in Figs. 8a, b, and c for the angular locations $\phi = 45.0$, 90.0, and 135.0 deg, respectively. As can be seen from these figures, agreement between the calculated profiles and the experimental profiles are in good agreement for the $\phi = 45.0$-deg case, differ somewhat in the near-wall region for the $\phi = 90.0$-deg case, and differ somewhat in character across the entire profile at $\phi = 135.0$ deg. Figure 9 presents the streamline direction within the boundary layer which shows good agreement between calculated and measured values for the $\phi = 45.0$-deg case and progressive disagreement as the ϕ-angle is increased. This behavior can be partially traced to the use of the isentropic surface values of the inviscid flow quantities as the boundary-layer outer-edge conditions. As discussed by Rainbird (Ref. 45) in the concluding paragraph of his paper, it is perhaps more appropriate to use "near" surface conditions (rather than isentropic surface conditions) as the external flow for boundary-layer calculations. More work remains to be done in this connection.

Distributions of the surface flow angle, ω_s, and the external flow angle, ω_e, relative to experimental measurements are presented in Fig. 10. The condition that $\omega_s = 0$ on a conical surface is used as a criterion for boundary-layer separation following Rainbird (Refs. 45 and 46). As can be seen from Fig. 10, the present three-dimensional turbulent boundary-layer analysis predicts separation to occur somewhere between $\phi = 162.5$ and 165.0 deg, whereas Rainbird (Ref. 45) experimentally observed separation at $\phi \approx 159$ deg. Further note that the magnitude of the crossflow influence on the turbulent boundary-layer turning is very small, e.g., $\omega_s - \omega_e \approx 7$ deg at $\phi = 90.0$ deg. Also shown in Fig. 10 is the calculated surface flow angle distribution for a laminar boundary layer under the same flow conditions. Much larger

crossflow influence on the laminar boundary-layer turning is observed, i.e., $\omega_s - \omega_e \approx 26$ deg at $\phi = 90.0$ deg. Laminar boundary-layer separation is predicted to occur much earlier than for the turbulent case, somewhere between $\phi = 130.0$ and 132.5 deg. No attempt has been made in the present study to attempt more accurate location of the calculated separation location by use of a very small ϕ integration increment near separation; all of the present calculations employed a constant ϕ integration increment of 2.50 deg. The above results confirm quite clearly the statement by Vaglio-Laurin (Ref. 11) that "due to the larger shearing stress, smaller three-dimensional effects can be expected for turbulent layers as compared with laminar layers subject to the same boundary conditions."

The calculated eddy-viscosity, ϵ, distributions across the three-dimensional turbulent boundary layer at various angular locations around the cone are presented in Fig. 11. As is apparent the eddy viscosity reaches its maximum value ($\epsilon_{max} \approx 200$ to 300 μ) in the outer region of the boundary layer with $\epsilon >> \mu$ even in regions near the wall; i.e., $\epsilon \approx 10\mu$ at $y \approx 0.0025$ in. It should be noted that the laminar viscosity, μ, in the above is evaluated at the same local conditions as the corresponding eddy viscosity.

To illustrate the differences in three-dimensional laminar and turbulent boundary-layer structure at a common body location, Figs. 12a, b, and c present calculated boundary-layer profiles at the circumferential location $\phi = 90.0$ deg for the present sharp cone at incidence flow. The differences in the laminar and the turbulent profiles are apparent. It is interesting to note that the turbulent boundary-layer thickness, δ_t, is approximately a factor of ten greater than the laminar value, δ_ℓ, for this particular flow condition.

4.2.2 Hypersonic Flow

Turning now to the hypersonic flow past a 7.20-deg semivertex angle sharp cone at 1.0-, 2.0-, and 4.0-deg angles of attack under AEDC-VKF Tunnel B (Mach 8) conditions, one sees in Fig. 13 the calculated inviscid flow parameters around the (isentropic) cone surface based on the Jones analysis (Refs. 39 and 43). As is obvious from Fig. 13, the inviscid parameters most sensitive to increasing angle of attack are the surface pressure, temperature, and crossflow velocity; the streamwise velocity component remains almost constant at a value slightly less than the free-stream velocity over the entire cone. The small magnitude of the inviscid crossflow velocity at even 4-deg angle of attack indicates that the inviscid crossflow turning, i.e., the inviscid

streamline direction, ω_e, at the outer edge of the boundary layer, will be small. More will follow on this point later.

One of the primary objectives of the experimental investigation reported by Martellucci and Neff (Ref. 47) was the detection of boundary-layer transition on cones at angle of attack via surface heat-transfer measurements, as discussed in Section III. To establish the basic validity of the McGowan and Davis (Ref. 34) analysis of the three-dimensional laminar boundary layer on a sharp cone at incidence under hypersonic conditions, Fig. 14 presents a comparison of calculated laminar boundary-layer heat-transfer rate (as reflected through the Stanton number, St_∞, based on free-stream conditions) relative to experimental measurements for a 4.0-deg angle-of-attack laminar flow condition reported in Ref. 47. Note that the heat transfer is presented in laminar boundary-layer similarity format; i.e., the Stanton number is multiplied by the square root of the normalized surface distance from the apex. Free-stream conditions for this laminar case are presented in the figure. In general, the agreement between the McGowan and Davis analytical analysis and the experimental measurements of Ref. 47 is excellent for this laminar flow condition, which illustrates the basic validity of the McGowan and Davis analysis for laminar boundary layers on sharp cones at incidence under hypersonic conditions. It should be noted here that Boericke (Ref. 36) has also reported good agreement with the experimental measurements of Ref. 47 for a sharp cone at incidence under laminar boundary-layer hypersonic conditions.

The end of transition locations presented previously in Fig. 2 show that the boundary layer will be in a fully turbulent state for $x/L > 0.5$ at all three angle-of-attack conditions under the high Reynolds number free-stream conditions discussed in Section III. The calculated turbulent heat-transfer-rate distributions from the present three-dimensional turbulent boundary-layer analysis (as again reflected through the Stanton number based on free-stream conditions) for $x/L > 0.5$ and all three angles of attack (α = 1.0, 2.0, and 4.0 deg) at various circumferential locations around the cone are presented in Fig. 15 relative to the experimental heat-transfer-rate measurements of Ref. 47. The present calculations were performed at the x/L locations indicated by the x-marks on the figure, and the solid line was faired between the marked calculated values. In general, good agreement between the present analytical analysis and experiment is observed at all three angle-of-attack conditions with the circumferential distribution also well defined.

It is well-known that in the free-stream Reynolds number range $5 \times 10^5 < Re_{\infty,L} < 10^7$ the turbulent heat-transfer rate to a flat plate in incompressible flow can be expressed in the form (see, e.g., Ref. 51, pp. 492-499, 536-539)

$$St_\infty \propto (Re_{\infty,x})^{-0.2} \tag{48}$$

which means physically that for two x-locations along the plate, say locations x_1 and x_2, the corresponding turbulent heat-transfer rates at these two locations are related according to

$$\frac{(St_\infty)_{x_1}}{(St_\infty)_{x_2}} = \left(\frac{x_2}{x_1}\right)^{0.2} \tag{49}$$

As discussed in Ref. 51, Eq. (49) may be carried over reasonably well to turbulent compressible flows, providing the wall temperature remains constant and the external flow at the outer edge of the boundary layer does not vary along the body. Since these criteria are met in the present sharp cone at incidence flow for the case of the streamwise directed velocity component, it is of interest to note that the scaling criterion suggested by Eq. (49) works very well when applied to the results of Fig. 15 in the interval $0.5 \leq x/L \leq 1.0$ for all three angle-of-attack conditions. This means that for practical applications the present analytical calculation of the three-dimensional turbulent boundary layer need only be performed at one x/L location, say the x/L = 0.80 location, as depicted in Fig. 16 for the present flow condition, and then these results for the one station scaled through the use of Eq. (49) to other x/L locations at a given circumferential location. An illustration of the applicability of this approximate technique is given in Table I for the α = 4.0-deg flow condition of present interest with the x/L = 0.8 station of Fig. 16 used as the reference station for the scaling application. Examination of Table I reveals that for the present body, angle of attack, and flow condition the maximum error in the use of Eq. (49) relative to the present three-dimensional turbulent boundary-layer analysis (denoted as "exact" in Table I) is only approximately 2 percent, which is for the x/L = 0.50 station on the leeward ray (ϕ = 180.0 deg). Through the use of this approximate scaling technique, rapid calculations of three-dimensional turbulent heat-transfer rates on sharp cones at incidence can be performed for use in design tradeoff studies, ablation heat shield design, or evaluation of experimental data with a minimum requirement of digital computer time (one numerical calculation of the three-dimensional turbulent boundary layer using the present analytical analysis). Needless to say the applicability of the technique should be first established for the flow conditions and geometry of interest in a new problem, since Eq. (49) is not universally applicable for all values

of the free-stream Reynolds number (see Chapters XIX and XXI of Ref. 51 for further discussion of this point).

Since the favorable agreement between results from the present theory and experiment indicates that the present analytical analysis is indeed applicable to calculation of turbulent heat transfer on a sharp cone at incidence in hypersonic flow under cold wall conditions, it is now in order to examine certain details of the flow field. Figure 17 presents the calculated windward ray (ϕ = 0.0 deg) turbulent boundary-layer profiles at the body station x/L = 0.80 for the 4.0-deg angle-of-attack condition. Also included in Fig. 17 are the calculated profiles based on the nonsimilar, windward plane of symmetry, turbulent boundary-layer analysis by Adams (Ref. 48). The same comments made previously with respect to discussion of Figs. 7a and b apply equally as well to Fig. 17. Further note from Fig. 17 that the present locally similar analysis and the nonsimilar analysis of Ref. 48 are in excellent agreement in the inner region of the turbulent boundary layer. This is because of the "local equilibrium" and "independence" in the inner layer of a turbulent boundary layer, as discussed by Bradshaw (Ref. 50). A slight discrepancy between the two analyses is observed in the outer region of the turbulent boundary layer, especially for the static temperature. This is because it is the outer layer of the turbulent boundary layer where the "memory" of the turbulence becomes important (see Ref. 50 for further discussion of this point).

The calculated turbulent boundary-layer parameters (heat-transfer rate, skin friction, and displacement thickness) along the windward ray of the present sharp cone at 4.0-deg angle of attack are shown in Fig. 18. The excellent agreement in heat-transfer rate to the wall (through the Stanton number St_∞) and wall shear stress (through the skin-friction coefficient C_{f_∞}) between the present locally similar type of analysis and the nonsimilar analysis of Ref. 48 is directly due to the excellent agreement in mean velocity and static temperature profiles in the inner region of the turbulent boundary layer, as shown in the previous figure. The small difference in magnitude of the displacement thickness $\delta^*_{2\text{-D}}$ between the two analyses is due to the difference in static temperature profiles across the outer region of the turbulent boundary layer, as shown previously in Fig. 17. It should be noted that the displacement thickness definition used in the present work (see the NOMENCLATURE) is for a two-dimensional boundary layer; see Adams (Ref. 48, p. 22) for a discussion of the differences between two- and three-dimensional displacement thickness definitions for the windward ray of a sharp cone at incidence.

The calculated turbulent boundary-layer profiles for the leeward ray (ϕ = 180.0 deg) at the body station x/L = 0.80 and the 4.0-deg angle-of-attack condition are given in Fig. 19. As originally shown by Moore (Ref. 52) and recently discussed in great detail by Murdock (Ref. 53), the laminar boundary-layer equations for the leeward plane of symmetry do not have a mathematically unique solution because of a defect in the basic boundary-layer model on the lee ray of a sharp cone at incidence. Furthermore, Boericke (Ref. 36) shows by integration of the three-dimensional laminar boundary-layer equations around a sharp cone at incidence from the windward to the leeward ray that smooth solutions do not exist in the leeward plane of symmetry; the same type results and conclusions have also been obtained by McGowan and Davis (Ref. 34, pp. 32-33). As can be seen by a careful study of the analysis by Murdock (Ref. 53), the problem with the leeward ray plane of symmetry boundary-layer equations can be traced to the convective terms in the crossflow momentum equation and, hence, the above discussion of the laminar equations also applies to the turbulent case of present interest, since the only modifications for turbulence involve inclusion of the turbulent shear stress and conductivity terms. Indeed, it has been found in the present work that numerical solutions could not be obtained by integrating the three-dimensional turbulent boundary-layer equations around a sharp cone at incidence from the windward to the leeward ray—a converged solution in the leeward plane of symmetry could not be generated. In view of these difficulties, the profiles presented in Fig. 19 are the results of extrapolating the numerical solutions at the two previous ϕ-stations off the leeward ray into the leeward ray using a second-order extrapolation process. While this procedure is certainly not rigorously justifiable, the favorable results presented previously in Fig. 15 with respect to lee ray, turbulent heat-transfer calculations suggest that the present extrapolation technique yields reasonable turbulent boundary-layer profiles. What is needed here for completeness are detailed, lee ray, turbulent boundary-layer profile measurements for comparison with the present analytical approach.

Calculated, three-dimensional, turbulent boundary-layer profiles at three ϕ-locations (ϕ = 45.0, 90.0, and 135.0 deg) are presented in Fig. 20 for the 4.0-deg angle-of-attack condition at the body location x/L = 0.8. Note the increasing crossflow influence on the profiles as the ϕ-angle is increased, especially with respect to the overshoot in the crossflow velocity profiles of Fig. 20b. Most of the hypersonic three-dimensional turbulent boundary-layer turning relative to the inviscid flow occurs in the outer region ($y > 0.2\delta_t$) of the layer, as can be seen from Fig. 20d. For the ϕ = 90.0-deg case in Fig. 20d with $\delta_t/L \approx 8 \times 10^{-3}$, $\omega_e \approx 4$ deg, and $\omega_s \approx 10$ deg at $y/L = 10^{-5}$; $\omega \approx 8$ deg at $y/L = 1.6 \times 10^{3}$, which is the location where $y/L \approx 0.2\delta_t/L$. The

three-dimensional eddy-viscosity profiles shown in Fig. 20e are very similar in appearance to the zero-angle-of-attack eddy-viscosity profiles presented in Fig. 13 of the hypersonic sharp cone work by Adams (Ref. 8). Further note the somewhat dissimilar character between the eddy-viscosity profiles in Fig. 11 for the supersonic hot wall flow condition and the Fig. 20e cold wall hypersonic flow profiles. This difference in character is directly related to the differences in static temperature profiles between the two flows, as can be seen by comparison of Figs. 8a, b, and c with Fig. 20c, which, in turn, are related to the basic differences between a hot wall supersonic flow and a cold wall hypersonic flow over a sharp cone at incidence.

Returning to the subject of three-dimensional boundary-layer turning relative to the inviscid flow direction on a sharp cone at incidence under hypersonic conditions, Fig. 21 shows calculated surface and external (inviscid) flow angles for both laminar and turbulent boundary layers at the body location $x/L = 0.8$ for the 4.0-deg angle-of-attack condition of present interest. At the $\phi = 110.0$-deg circumferential location where maximum turning occurs, Fig. 21 shows that $\omega_s \approx 25$ deg for the three-dimensional laminar boundary layer, whereas $\omega_s \approx 11$ deg for the three-dimensional turbulent boundary layer; $\omega_e \approx 4$ deg for the inviscid external flow at this location. Hence, the maximum laminar boundary-layer turning angle is approximately a factor of six greater than the inviscid flow turning angle, whereas the maximum turbulent boundary-layer turning angle is slightly less than a factor of three greater than the corresponding inviscid value. These findings again confirm the statement by Vaglio-Laurin (Ref. 11) quoted earlier that "due to the larger shearing stress, smaller three-dimensional effects can be expected for turbulent layers as compared with laminar layers subject to the same boundary conditions" for the case of sharp cones at incidence in a hypersonic flow under cold wall conditions.

A knowledge of wall temperature effects on the three-dimensional hypersonic turbulent boundary layer is of interest for the extrapolation of results from ground test (wind tunnel) measurements to the flight condition. Adams (Ref. 54) has recently examined the three-dimensional laminar boundary layer on sharp cones at incidence under hypersonic conditions and found that the surface upwash angle, ω_s, may be substantially increased between cold wall ($T_w/T_o \rightarrow 0$) conditions representative of hypersonic atmospheric flight and hot wall ($T_w/T_o \approx 0.9$) conditions representative of force testing in hypersonic wind tunnels. Figure 22 presents the same type of information for the present three-dimensional hypersonic turbulent boundary layer on the 7.2-deg half-angle sharp cone at 4.0-deg angle of attack. Note from Fig. 22 that maximum turning in the present three-dimensional turbulent boundary layer occurs at

$\phi \approx 110$ deg irrespective of wall temperature ratio in the range considered. A value of $T_w/T_o = 0.8$ is representative of force tests in the AEDC-VKF Tunnel B, whereas $T_w/T_o = 0.4$ is representative of heat-transfer tests via the thin-skin technique; a value of $T_w/T_o = 0.025$ is representative of hypersonic atmospheric flight under the same Mach number–Reynolds number combination as the wind tunnel. Figure 22 shows that the maximum calculated surface upwash angle, ω_s, is approximately 8 deg for the cold wall flight condition. This is a factor of two greater than the maximum calculated inviscid turning angle of $\omega_e \approx 4$ deg as determined from the Jones analysis (Refs. 39 and 43). For the hot wall, force test condition the maximum calculated surface upwash angle is approximately 13 to 14 deg, a factor of three greater than the maximum calculated inviscid turning angle of $\omega_e \approx 4$ deg as determined from the Jones analysis (Refs. 39 and 43) and a factor of almost two greater than the maximum cold wall flight value. This means that for the present sharp cone, angle of attack, and flow conditions the maximum surface upwash angle, ω_s, of the three-dimensional turbulent boundary layer may be increased approximately 70 to 80 percent between cold wall flight conditions and hot wall hypersonic wind tunnel force test conditions. Although this difference in surface turning angle between hot and cold wall conditions for the three-dimensional turbulent boundary layer is not as large as the differences found by Adams (Ref. 54) for the three-dimensional laminar boundary layer, these findings indicate to the vehicle designer that proper interpretation of hot wall ground test measurements on slender bodies at incidence under hypersonic conditions with either a laminar or turbulent boundary layer is necessary relative to cold wall flight conditions for aerodynamic parameters where the boundary-layer flow direction is important.

Details of the various three-dimensional turbulent boundary-layer profiles at the $\phi = 90.0$-deg circumferential location and $x/L = 0.8$ body station for the present sharp cone at 4.0-deg angle of attack are presented in Fig. 23 relative to wall temperature effects. Note from Figs. 23a and b that in the near-wall region ($y/L < 10^{-4}$) of the three-dimensional turbulent boundary layer, the colder the wall, the larger the numerical value for both the streamwise and crossflow velocity at a fixed y/L location. Furthermore, Fig. 23c shows that increasing the wall cooling will increase the gas density near the surface (recall that $\bar{\rho} \propto 1/\overline{T}$, since the static pressure is constant across the boundary layer). Hence, the effects of compressibility on the three-dimensional turbulent boundary layer are such as to result in increased momentum in the lower portions of the boundary layer as the wall cooling is increased.

Such is reflected in greater turning for the hot wall boundary layer relative to the cold wall case, as shown in Fig. 23d. Further observe, from Fig. 23b, that in the outer regions of the three-dimensional turbulent boundary layer, the hotter the wall, the larger the amount of crossflow velocity profile overshoot relative to the inviscid crossflow velocity value. This again is reflected in Fig. 23d where the hot wall boundary-layer turning is greater than the cold wall case. As shown in Fig. 23c, the hot wall ($T_w/T_o = 0.8$) condition representative of hypersonic wind tunnel force testing results in essentially an adiabatic wall condition, i.e., $(\partial T/\partial y)_{y \to 0} \approx 0$. Little effect is seen in Fig. 23e on the maximum value of the eddy-viscosity ratio with respect to wall temperature. However, keep in mind that the maximum eddy viscosity, ϵ, must increase with increasing wall temperature, since the laminar viscosity, μ, increases as the wall temperature is increased, with the maximum ϵ/μ ratio remaining constant. All of the above findings indicate that, in general, the hotter the wall, the greater the turning effect on the hypersonic three-dimensional turbulent boundary layer attributable to crossflow. The prior work by Adams (Ref. 54) found exactly the same trend for the hypersonic three-dimensional laminar boundary layer.

SECTION V
CONCLUDING SUMMARY

The results of the present investigation indicate that numerical calculation of the three-dimensional compressible turbulent boundary layer on a sharp cone at incidence in a supersonic or hypersonic stream is indeed feasible and reasonable, based on comparisons with experimental measurements. The assumption of a locally similar turbulent boundary-layer analysis neglecting "upstream history" on the sharp cone appears to result in acceptable calculations for the mean flow profiles, including crossflow, when used in conjunction with the three-dimensional invariant turbulence scalar eddy-viscosity model. The main advantage of the present approach over the previously used integral techniques is that no assumptions as to the form or character of the profiles are required; the present profiles are the result of numerical integration of the complete governing three-dimensional turbulent boundary-layer equations, with the only assumptions being the three-dimensional eddy-viscosity formalism, the choice of mixing-length model, and the locally similar method of solution. The degree of success experienced in the present investigation indicates that the invariant turbulence scalar eddy-viscosity approach should be applicable to numerical calculation of general three-dimensional turbulent boundary-layer flows. However, much more work, especially carefully controlled

experimental investigations of the three-dimensional compressible turbulent boundary-layer structure, remains to be done before the question of variance or invariance can be completely resolved.

REFERENCES

1. Smith, A. M. O. and Cebeci, T. "Numerical Solution of the Turbulent Boundary-Layer Equations." Douglas Aircraft Company Report DAC 33735, May 1967.
2. Patankar, S. V. and Spalding, D. B. Heat and Mass Transfer in Boundary Layers. CRC Press, Cleveland, Ohio, 1968.
3. Herring, H. J. and Mellor, G. L. "A Method of Calculating Compressible Turbulent Boundary Layers." NASA CR-1144, September 1968.
4. Anon. "Compressible Turbulent Boundary Layers." NASA SP-216, Symposium held at the Langley Research Center, Hampton, Virginia, December 1968.
5. Bushnell, D. M. and Beckwith, I. E. "Calculation of Nonequilibrium Hypersonic Turbulent Boundary Layers and Comparisons with Experimental Data." AIAA Paper 69-684 presented at the AIAA Fluid and Plasma Dynamics Conference, San Francisco, California, June 1969. See also AIAA J., Vol. 8, No. 8, August 1970, pp. 1462-1469.
6. Martellucci, A., Rie, H. and Sontowski, J. F. "Evaluation of Several Eddy Viscosity Models Through Comparison with Measurements in Hypersonic Flows." AIAA Paper 69-688 presented at the AIAA Fluid and Plasma Dynamics Conference, San Francisco, California, June 1969.
7. Mayne, A. W., Jr. and Dyer, D. F. "Comparisons of Theory and Experiment for Turbulent Boundary Layers on Simple Shapes at Hypersonic Conditions." Proceedings of the 1970 Heat Transfer and Fluid Mechanics Institute, Stanford University Press, 1970, pp. 168-188.
8. Adams, J. C., Jr. "Eddy Viscosity-Intermittency Factor Approach to Numerical Calculation of Transitional Heating on Sharp Cones in Hypersonic Flow." AEDC-TR-70-210 (AD714058), November 1970.

9. Harris, J.E. "Numerical Solution of the Equations for Compressible Laminar, Transitional, and Turbulent Boundary Layers and Comparisons with Experimental Data." NASA TR R-368, August 1971.

10. Braun, W. H. "Turbulent Boundary Layer on a Yawed Cone in a Supersonic Stream." NASA TR R-7, 1959.

11. Vaglio-Laurin, R. "Turbulent Heat Transfer on Blunt-Nosed Bodies in Two-Dimensional and General Three-Dimensional Hypersonic Flow." WADC Technical Note 58-301, September 1958. See Also J. Aero. Sci., Vol. 27, No. 1, January 1960, pp. 27-36.

12. Cooke, J. C. "Three-Dimensional Turbulent Boundary Layers." Aeronautical Research Council C. P. No. 635, June 1961.

13. Smith, P. D. "Calculation Methods for Three-Dimensional Turbulent Boundary Layers." Aeronautical Research Council R. & M. No. 3523, December 1966.

14. Bradley, R. G. "Approximate Solutions for Compressible Turbulent Boundary Layers in Three-Dimensional Flow." AIAA J., Vol. 6, No. 5, May 1968, pp. 859-864.

15. Shanebrook, J.R. and Hatch, D.E. "A Family of Hodograph Models for the Cross Flow Velocity Component of Three-Dimensional Turbulent Boundary Layers." ASME Paper 71-FE-1 presented at the Fluids Engineering Conference, Pittsburgh, Pennsylvania, May 1971.

16. Zakkay, V. and Calarese, W. "Theoretical Investigation of Cross-flow Effects on Compressible Turbulent Boundary Layer Over Bodies of Revolution." New York University School of Engineering and Science Report No. F-69-5, December 1969. See also Israel J. Techn., Vol. 8, No. 1-2, 1970, pp. 127-138.

17. Hunt, J. L., Bushnell, D. M., and Beckwith, I.E. "Finite-Difference Analysis of the Compressible Turbulent Boundary Layer on a Blunt Swept Slab with Leading-Edge Blowing." Paper 19 in "Analytic Methods in Aircraft Aerodynamics," NASA SP-228, Symposium held at NASA Ames Research Center, Moffett Field, California, October 1969, pp. 417-472. See also NASA TN D-6203, March 1971.

18. Bradshaw, P. "Calculation of Three-Dimensional Turbulent Boundary Layers." J. Fluid Mech., Vol. 46, Pt. 3, April 1971, pp. 417-445.

19. Nash, J. F. "The Calculation of Three-Dimensional Turbulent Boundary Layers in Incompressible Flow." J. Fluid Mech., Vol. 37, Pt. 4, July 1969, pp. 625-642.

20. Cooper, P. "Turbulent Boundary Layer on a Rotating Disk Calculated with an Effective Viscosity." AIAA J., Vol. 9, No. 2, February 1971, pp. 255-261.

21. Cebeci, T. and Smith, A. M. O. "A Finite-Difference Solution of the Incompressible Turbulent Boundary-Layer Equations by an Eddy Viscosity Concept." Douglas Aircraft Company Report DAC 67130, October 1968.

22. Nash, J. F. "An Explicit Scheme for the Calculation of Three-Dimensional Turbulent Boundary Layers." ASME Paper 71-FE-19 presented at the Fluid Engineering Conference, Pittsburgh, Pennsylvania, May 1971.

23. McCroskey, W. J., Nash, J. F., and Hicks, J. G. "Turbulent Boundary-Layer Flow Over a Rotating Flat-Plate Blade." AIAA J., Vol. 9, No. 1, January 1971, pp. 188-189.

24. Hicks, J. G. and Nash J. F. "The Calculation of Three-Dimensional Turbulent Boundary Layers on Helicopter Rotors." NASA CR-1845, May 1971.

25. Moore, F. K. "Three-Dimensional Compressible Laminar Boundary-Layer Flow." NACA TN 2279, March 1951.

26. Prandtl, L. "On a New Representation of Fully Developed Turbulence." Jet Propulsion Lab. Publ. No. 13, California Inst. Technology, August 1952.

27. Glushko, G. S. "Turbulent Boundary Layer on a Flat Plate in an Incompressible Fluid." NASA TT F-10,080, April 1966.

28. Escudier, M. P. "The Distribution of the Mixing Length in Turbulent Flows Near Walls." Mechanical Eng. Dept. Report TWF/TN/1, Imperial College, London, March 1965.

29. Maise, G. and McDonald, H. "Mixing Length and Kinematic Eddy Viscosity in a Compressible Boundary Layer." AIAA J., Vol. 6, No. 1, January 1968, pp. 73-80.

30. van Driest, E. R. "On Turbulent Flow Near a Wall." J. Aero Sci., Vol. 23, No. 11, November 1956, pp. 1007-1011, 1036.

31. Rotta, J. C. "Heat Transfer and Temperature Distribution in Turbulent Boundary Layers at Supersonic and Hypersonic Flow." AGARDograph 97, Pt. I, May 1965, pp. 35-63.

32. Rotta, J. C. "Recent Developments in Calculation Methods for Turbulent Boundary Layers with Pressure Gradients and Heat Transfer." J. Applied Mech., Vol. 33, No. 2, June 1966, pp. 429-437.

33. Meier, H. U. and Rotta, J. C. "Experimental and Theoretical Investigation of Temperature Distributions in Supersonic Boundary Layers." AIAA Paper 70-744 presented at the AIAA 3rd Fluid and Plasma Dynamics Conference, Los Angeles, California, June 1970.

34. McGowan, J. J., III, and Davis, R. T. "Development of a Numerical Method to Solve the Three-Dimensional Compressible Laminar Boundary-Layer Equations with Application to Elliptical Cones at Angle of Attack." ARL 70-0341, December 1970.

35. Dwyer, H. A. "Boundary Layer on a Hypersonic Sharp Cone at Small Angle of Attack." AIAA J., Vol. 9, No. 2, February 1971, pp. 277-284.

36. Boericke, R. R. "Laminar Boundary Layer on a Cone at Incidence in Supersonic Flow." AIAA J., Vol. 9, No. 3, March 1971, pp. 462-468.

37. Blottner, F. G. "Viscous Shock Layer at the Stagnation Point with Nonequilibrium Air Chemistry." AIAA J., Vol. 7, No. 12, December 1969, pp. 2281-2288.

38. Blottner, F. G. "Finite Difference Methods of Solution of the Boundary-Layer Equations." AIAA J., Vol. 8, No. 2, February 1970, pp. 193-205.

39. Jones, D. J. "Numerical Solutions of the Flow Field for Conical Bodies in a Supersonic Stream." National Research Council of Canada Aeronautical Report LR-507, July 1968. See also C. A. S. I. Transactions, Vol. 3, No. 1, March 1970, pp. 62-71.

40. Moretti, G. "Inviscid Flow Field Past a Pointed Cone at Angle of Attack. Part I-Analysis." GASL TR-577, December 1965. See also AIAA J., Vol. 5, No. 4, April 1967, pp. 789-791.

41. South, J. C., Jr. and Klunker, E. B. "Methods for Calculating Nonlinear Conical Flows." Paper 8 in "Analytic Methods in Aircraft Aerodynamics," NASA SP-228, Symposium held at NASA Ames Research Center, Moffett Field, California, October 1969, pp. 131-158. See also NASA TR R-374, October 1971.

42. Holt, M. and Ndefo, D.E. "A Numerical Method for Calculating Steady Unsymmetrical Supersonic Flow Past Cones." J. Computational Physics, Vol. 5, 1970, pp. 463-486.

43. Jones, D.J. ."Use of the Jones Computer Programme to Determine the Flow Field for Conical Flow Situations. Part I: The Circular Cone at Incidence." National Research Council of Canada NAE LTR-HA-1, June 1969.

44. Jones, D.J. "Tables of Inviscid Supersonic Flow About Circular Cones at Incidence $\gamma = 1.4$, Parts I and II." AGARDograph 137, November 1969.

45. Rainbird, W. J. "Turbulent Boundary-Layer Growth and Separation on a Yawed Cone." AIAA J., Vol. 6, No. 12, December 1968, pp. 2410-2416.

46. Rainbird, W.J. "The External Flow Field About Yawed Circular Cones." Paper 19 in "Hypersonic Boundary Layers and Flow Fields," AGARD C. P. No. 30, Specialists' Meeting of the Fluid Dynamics Panel of AGARD held at the Royal Aeronautical Society, London, England, May 1968, pp. 19-1 through 19-18.

47. Martellucci, A. and Neff, R.S. "The Influence of Asymmetric Transition on Re-Entry Vehicle Motion." AIAA Paper 70-987 presented at the AIAA Guidance, Control, and Flight Mechanics Conference, Santa Barbara, California, August 1970. See also J. Spacecraft and Rockets, Vol. 8, No. 5, May 1971, pp. 476-482.

48. Adams, J. C., Jr. "Implicit Finite-Difference Analysis of Compressible Laminar, Transitional, and Turbulent Boundary Layers along the Windward Streamline of a Sharp Cone at Incidence." AEDC-TR-71-235 (AD734535), December 1971.

49. Schmidt, J.F., Boldman, D.R., and Todd, C. "Similar Solutions for Turbulent Boundary Layers with Large Favorable Pressure Gradients (Nozzle Flow with Heat Transfer)." NASA TN D-6439, August 1971.

50. Bradshaw, P. "Turbulent Boundary Layers." The Aeronautical Journal of the Royal Aeronautical Society, Vol. 72, May 1968, pp. 451-459.

51. Schlichting, H. Boundary Layer Theory, Fourth Edition. McGraw-Hill, Inc., New York, 1960.

52. Moore, F.K. "Laminar Boundary Layer on Cone in Supersonic Flow at Large Angle of Attack." NACA TN 2844, November 1952.

53. Murdock, J.W. "The Solution of Sharp Cone Boundary Layer Equations in the Plane-of-Symmetry." Aerospace Report No. TR-0172 (S2816-60)-1, July 1971.

54. Adams, J.C., Jr. "Three-Dimensional Laminar Boundary-Layer Analysis of Upwash Patterns and Entrained Vortex Formation on Sharp Cones at Angle of Attack." AEDC-TR-71-215 (AD736880), December 1971.

APPENDIXES

I. ILLUSTRATIONS

II. TABLE

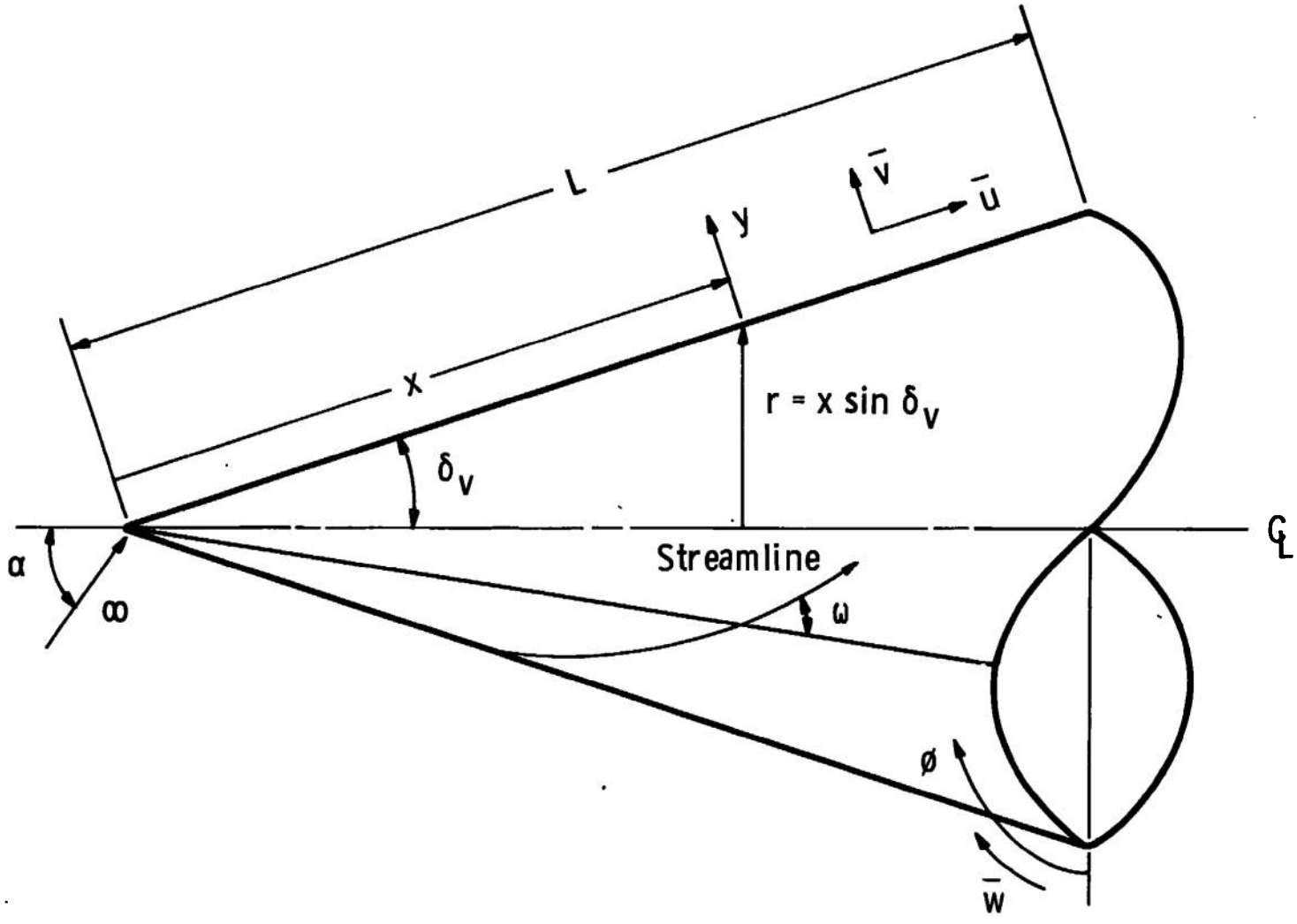

Fig. 1 Sharp Cone at Angle of Attack Geometry and Nomenclature

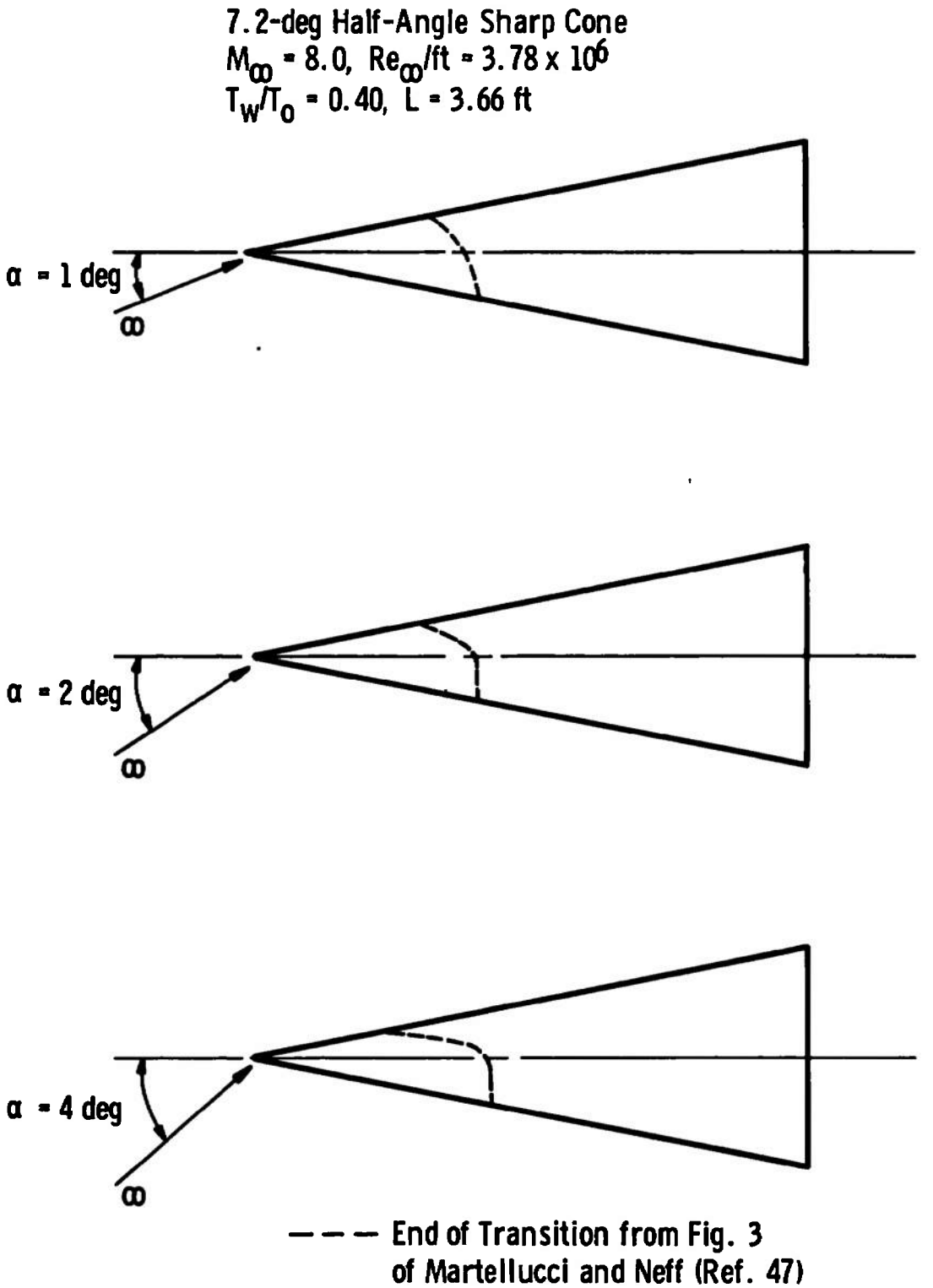

Fig. 2 Spatial Distribution of End of Transition with Respect to Angle of Attack under Hypersonic Conditions

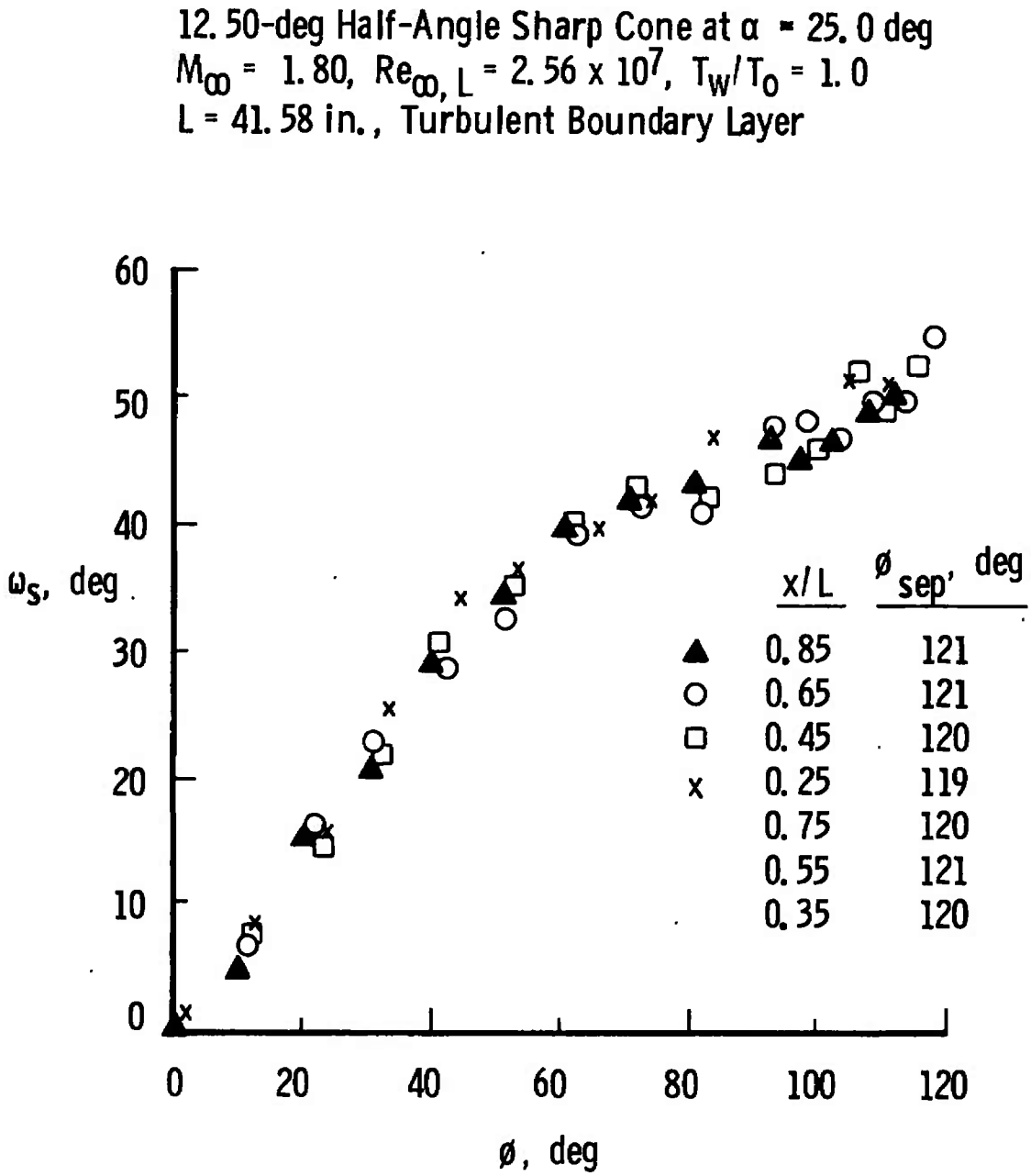

Fig. 3 Experimentally Determined Surface Flow Angles at Various Lengthwise Stations from Rainbird (Ref. 45)

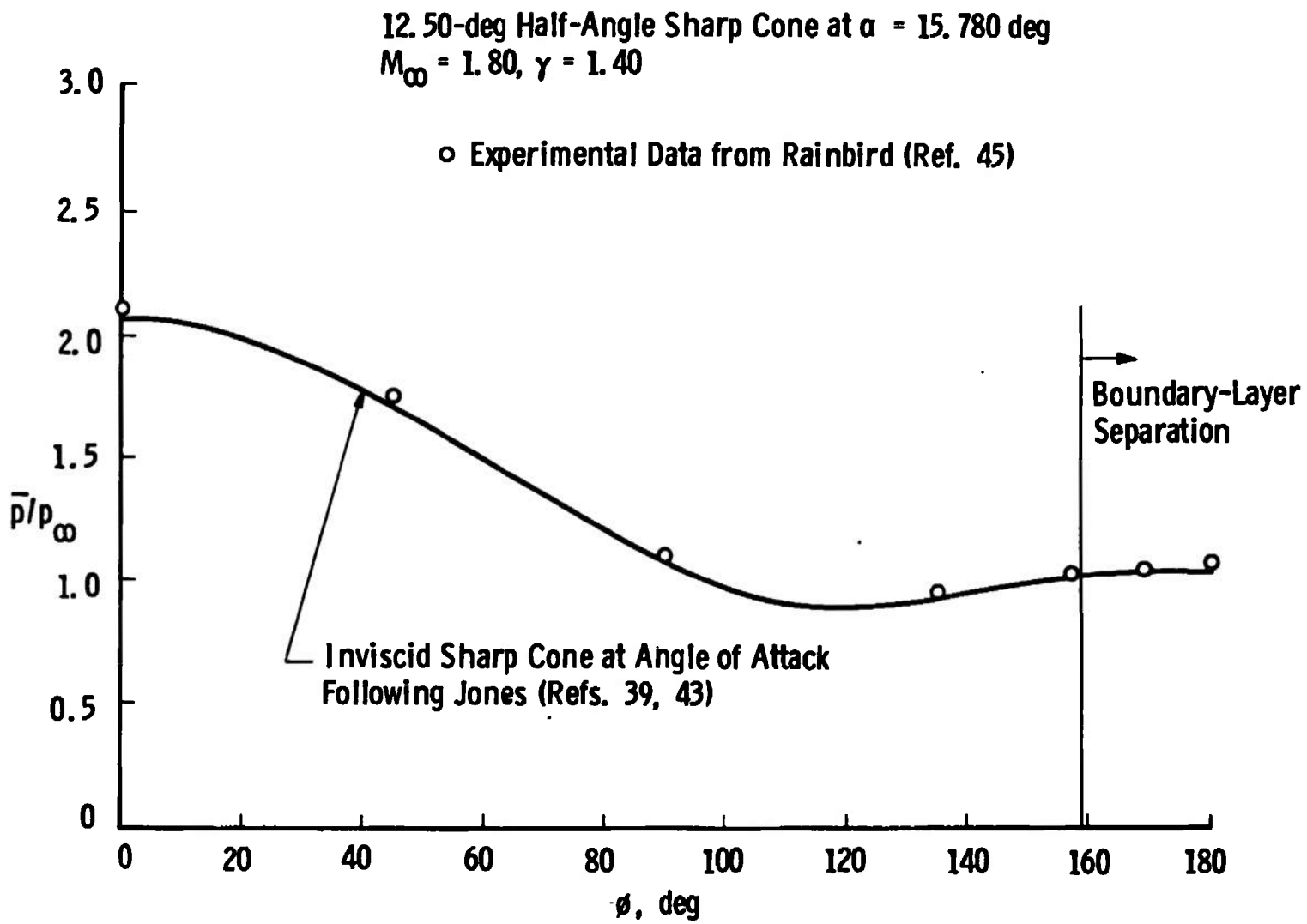

Fig. 4 Surface Pressure Distribution under Supersonic Conditions

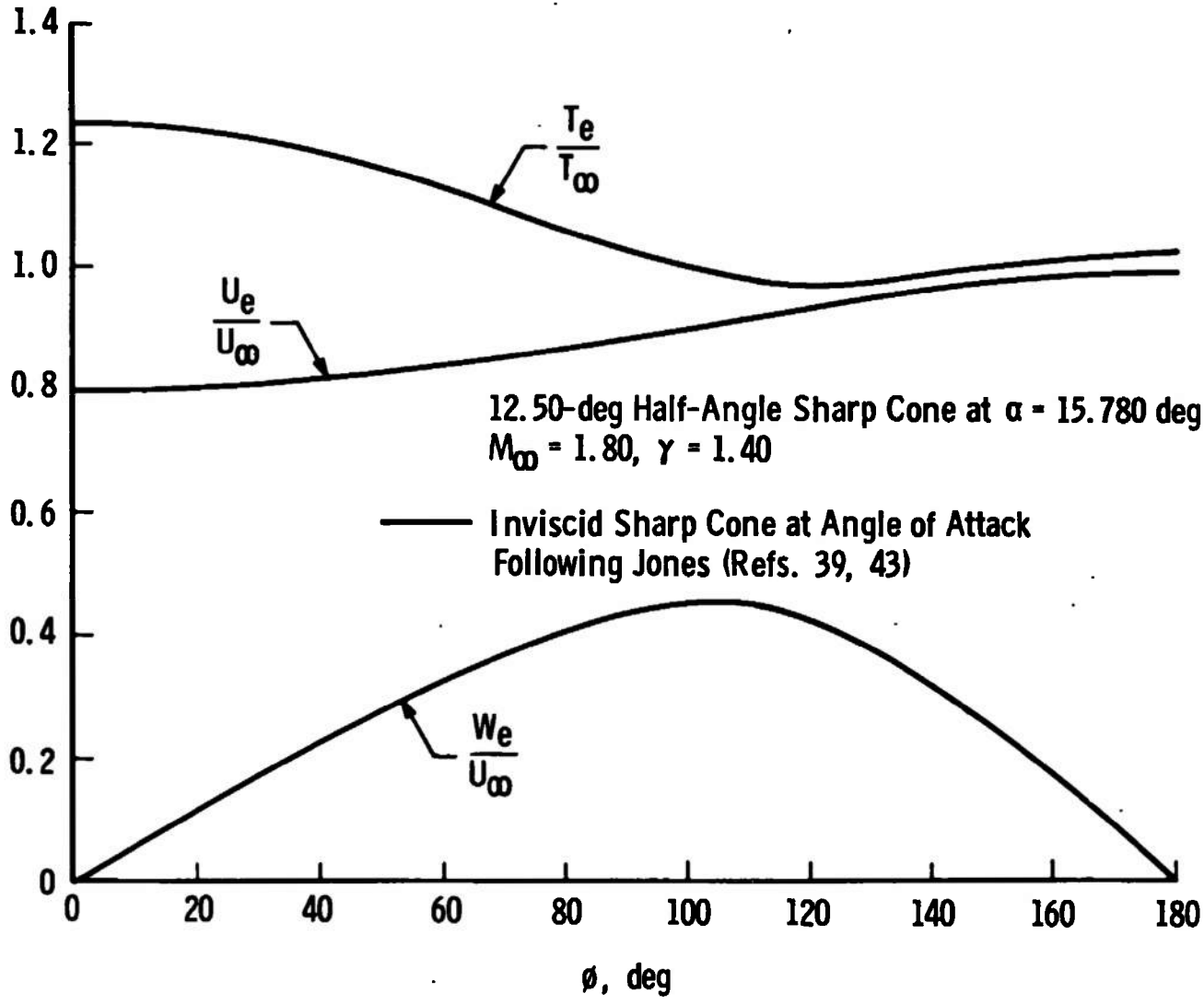

Fig. 5 Calculated Inviscid Flow Parameters on Cone Surface under Supersonic Conditions

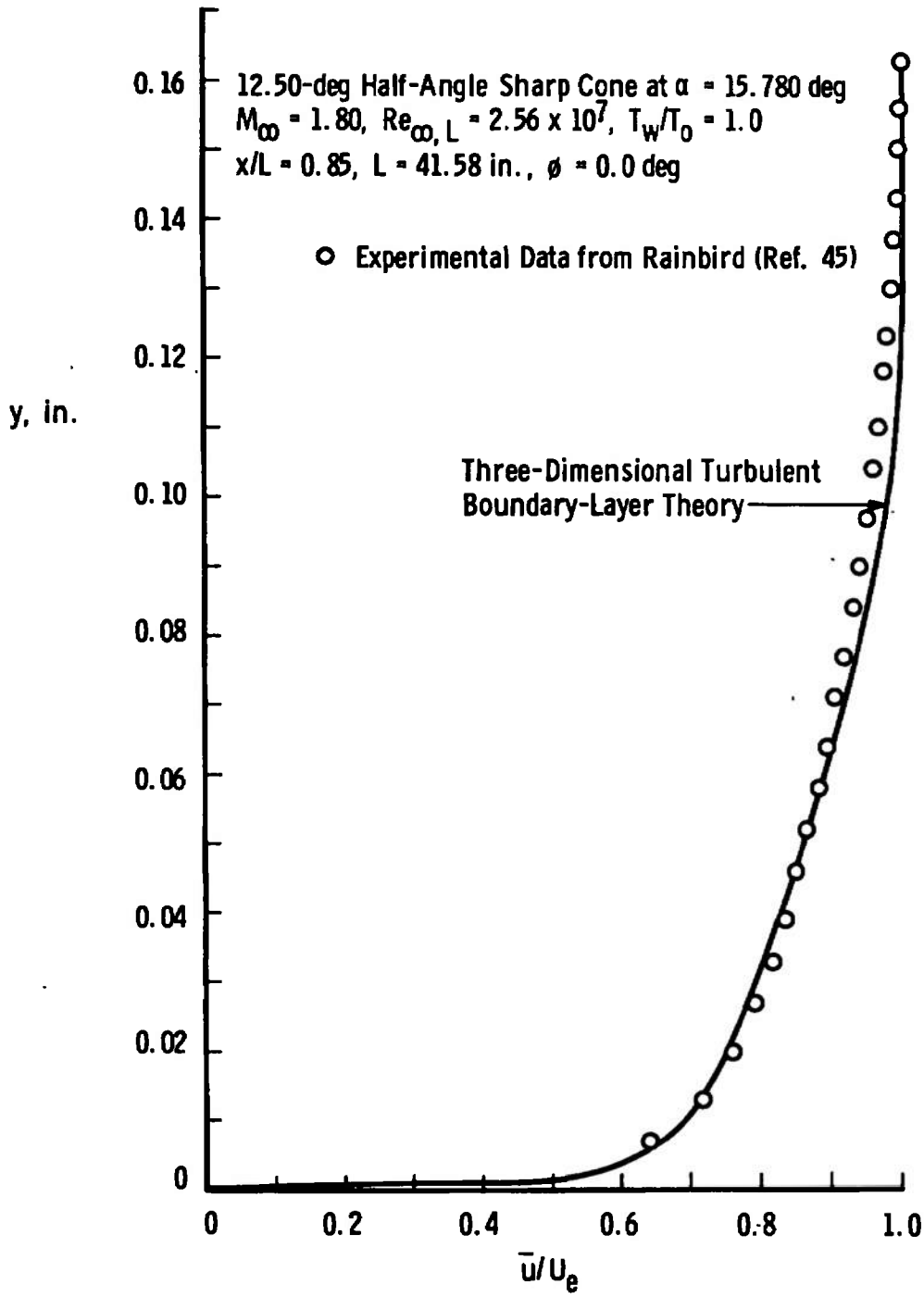

a. Streamwise Velocity Ratio

Fig. 6 Windward Ray Turbulent Boundary-Layer Profiles under Supersonic Conditions

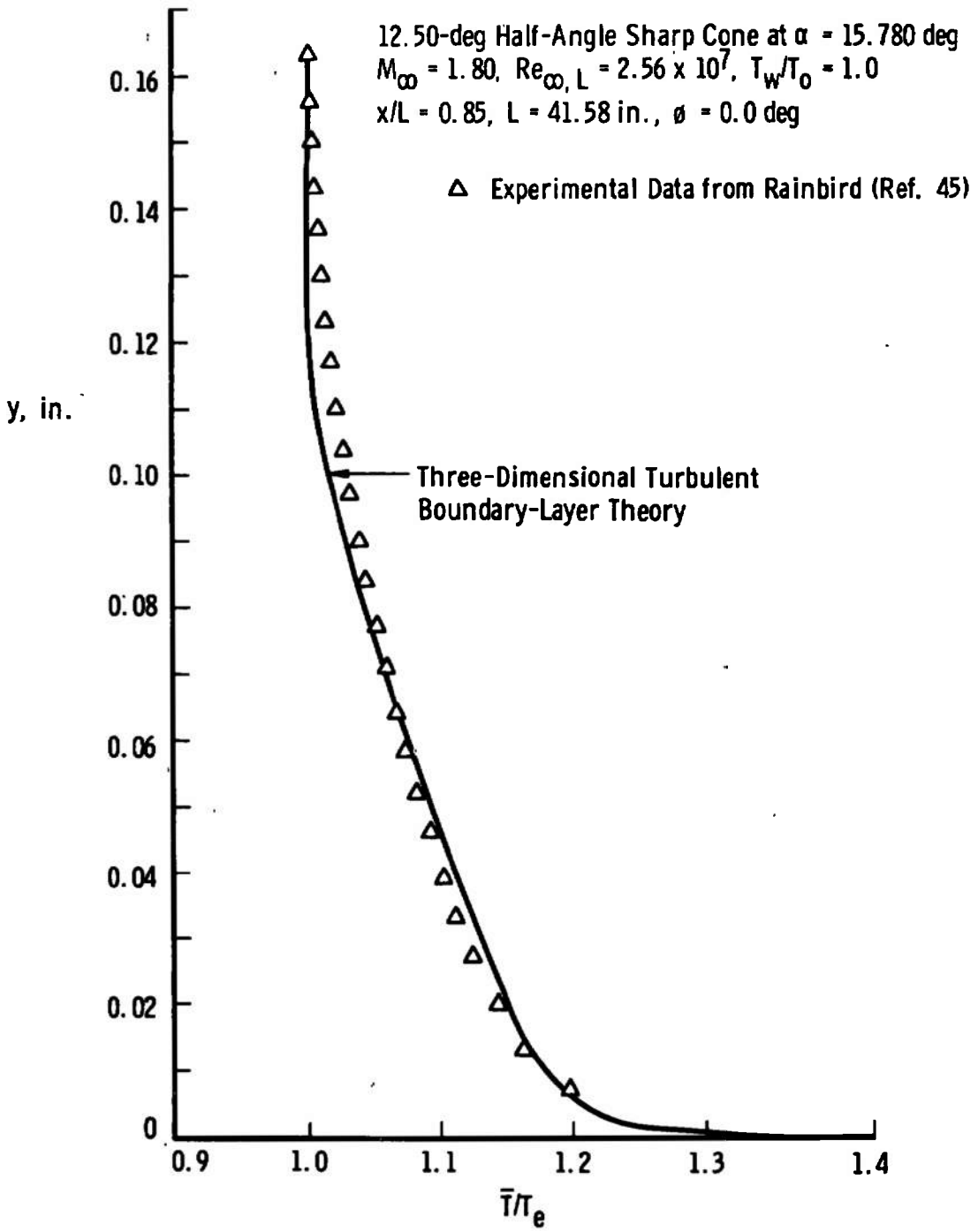

b. Static Temperature Ratio

Fig. 6 Concluded

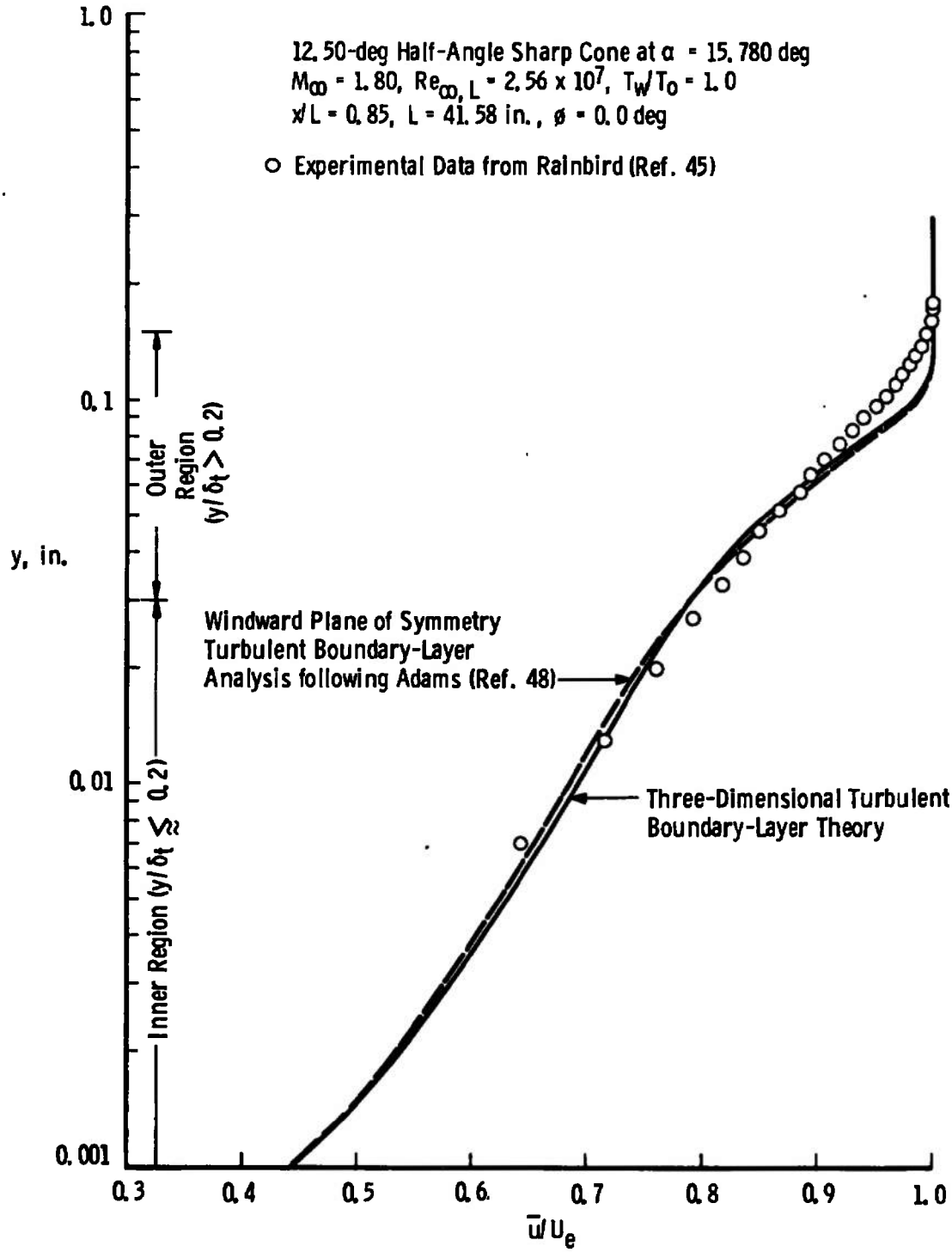

a. Streamwise Velocity Ratio

Fig. 7 Comparison of Windward Ray Turbulent Boundary-Layer Profiles with Previous Analysis by Adams (Ref. 48)

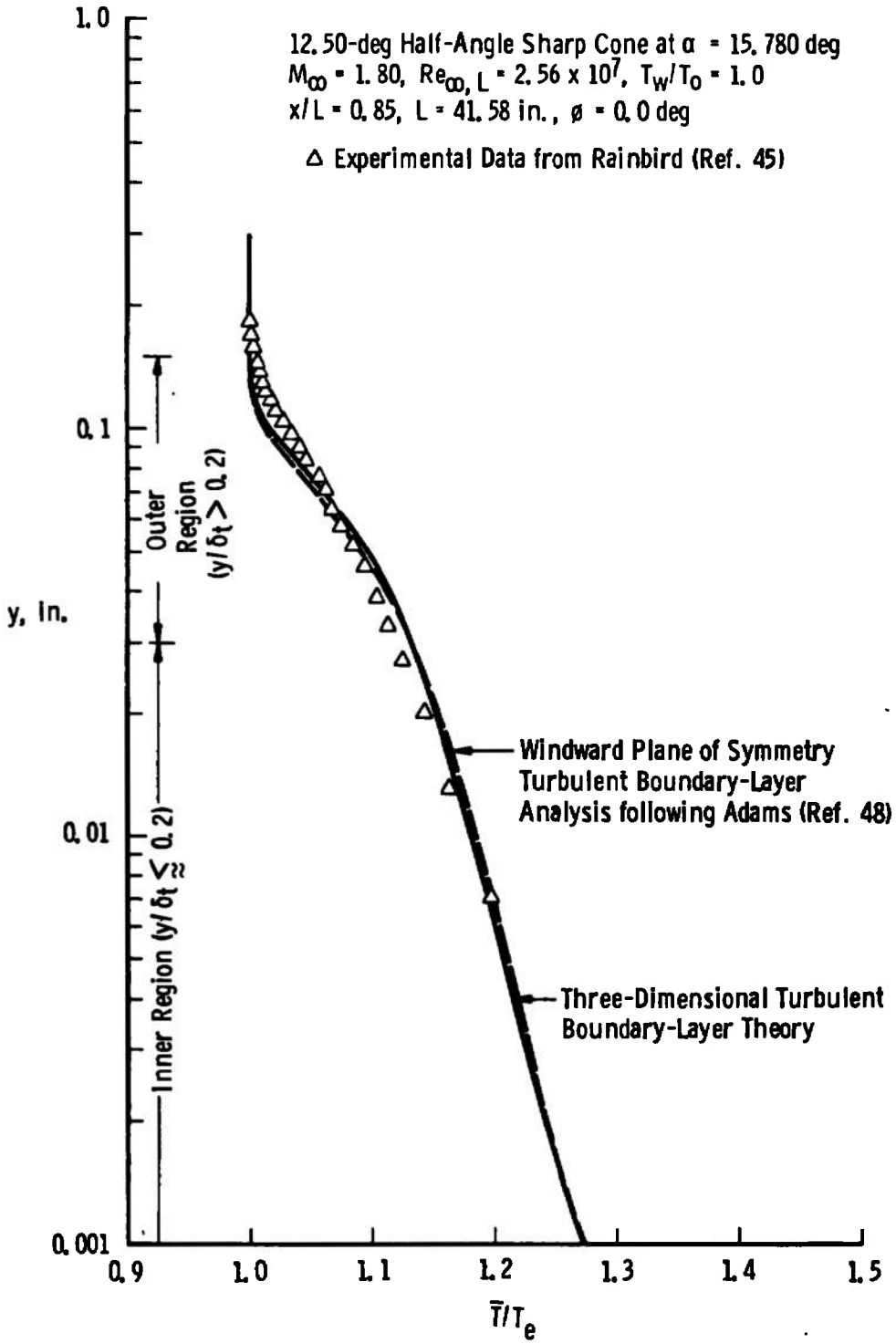

b. Static Temperature Ratio

Fig. 7 Concluded

12.50-deg Half-Angle Sharp Cone at α = 15.780 deg
M_∞ = 1.80, $Re_{\infty,L}$ = 2.56 x 10^7, T_W/T_0 = 1.0
x/L = 0.85, L = 41.58 in., ϕ = 45.0 deg

——— Three-Dimensional Turbulent Boundary-Layer Theory
□ . ○ △ Experimental Data from Rainbird (Ref. 45)

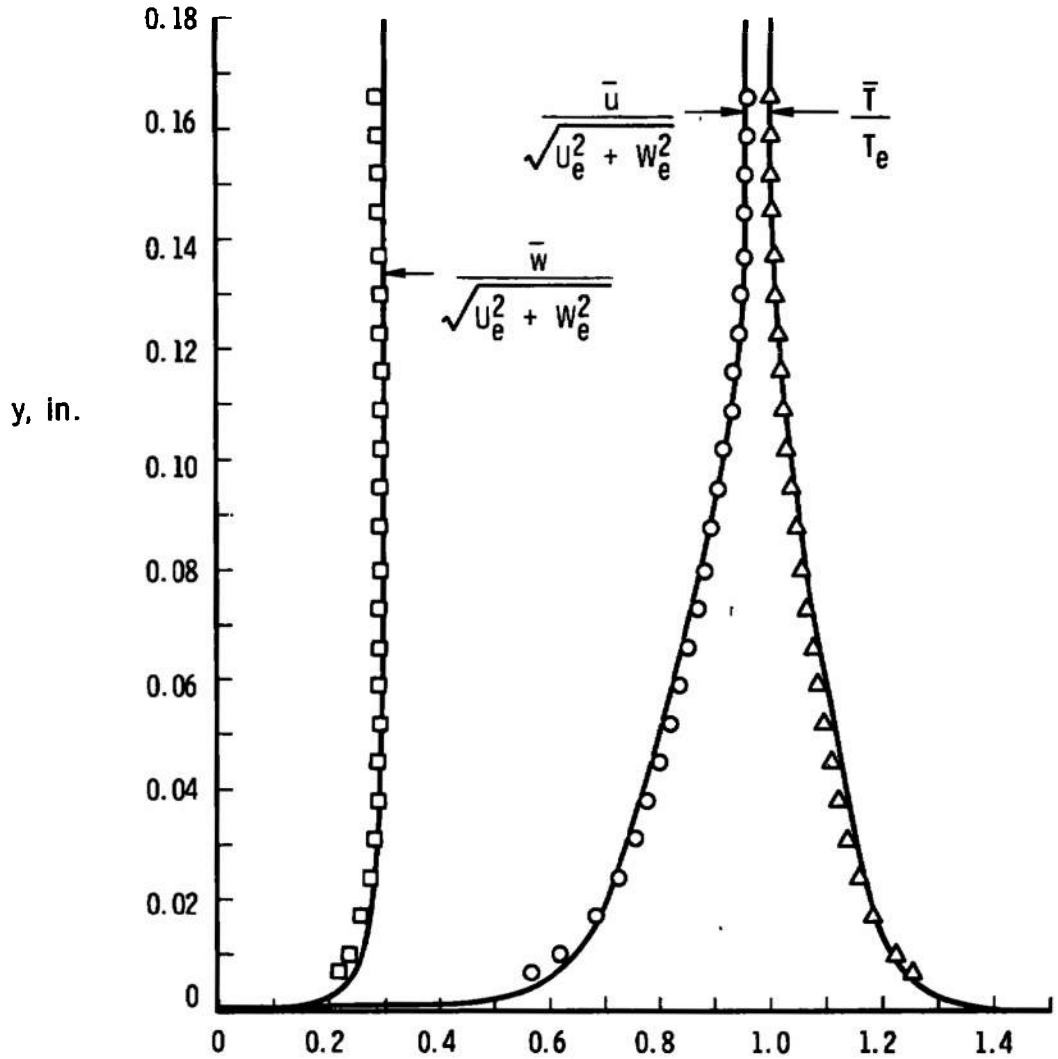

a. ϕ = 45.0 deg

Fig. 8 Three-Dimensional Turbulent Boundary-Layer Profiles under Supersonic Conditions

12.50-deg Half-Angle Sharp Cone at α = 15.780 deg
M_∞ = 1.80, $Re_{\infty, L}$ = 2.56 x 10^7, T_w/T_o = 1.0
x/L = 0.85, L = 41.58 in., ϕ = 90.0 deg

——— Three-Dimensional Turbulent Boundary-Layer Theory
□ ○ △ Experimental Data from Rainbird (Ref. 45)

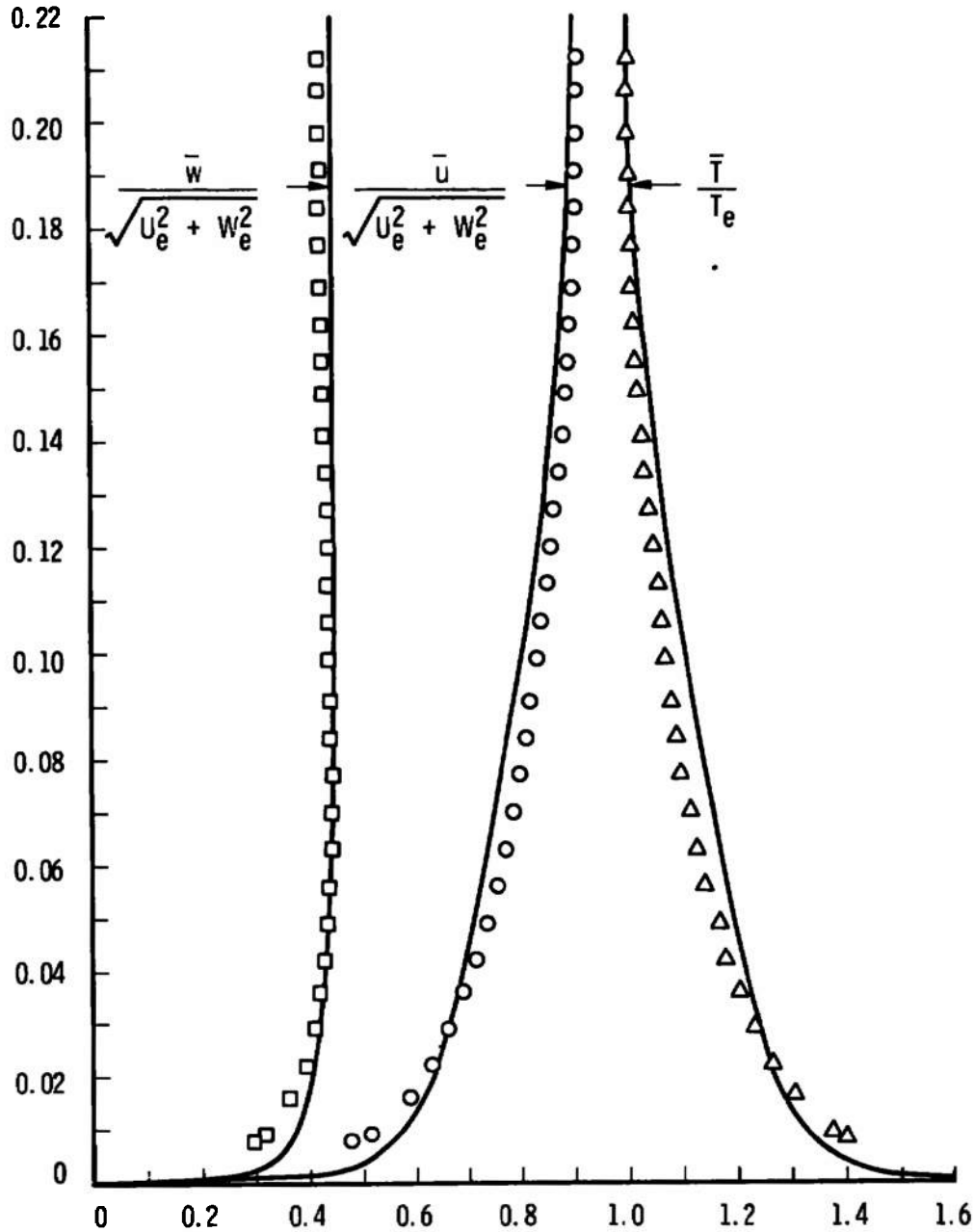

b. ϕ = 90.0 deg
Fig. 8 Continued

12.50-deg Half-Angle Sharp Cone at α = 15.780 deg
M_∞ = 1.80, $Re_{\infty, L}$ = 2.56 x 10^7, T_w/T_0 = 1.0
x/L = 0.85, L = 41.58 in., ϕ = 135.0 deg

——— Three-Dimensional Turbulent Boundary-Layer Theory
□ ○ △ Experimental Data from Rainbird (Ref. 45)

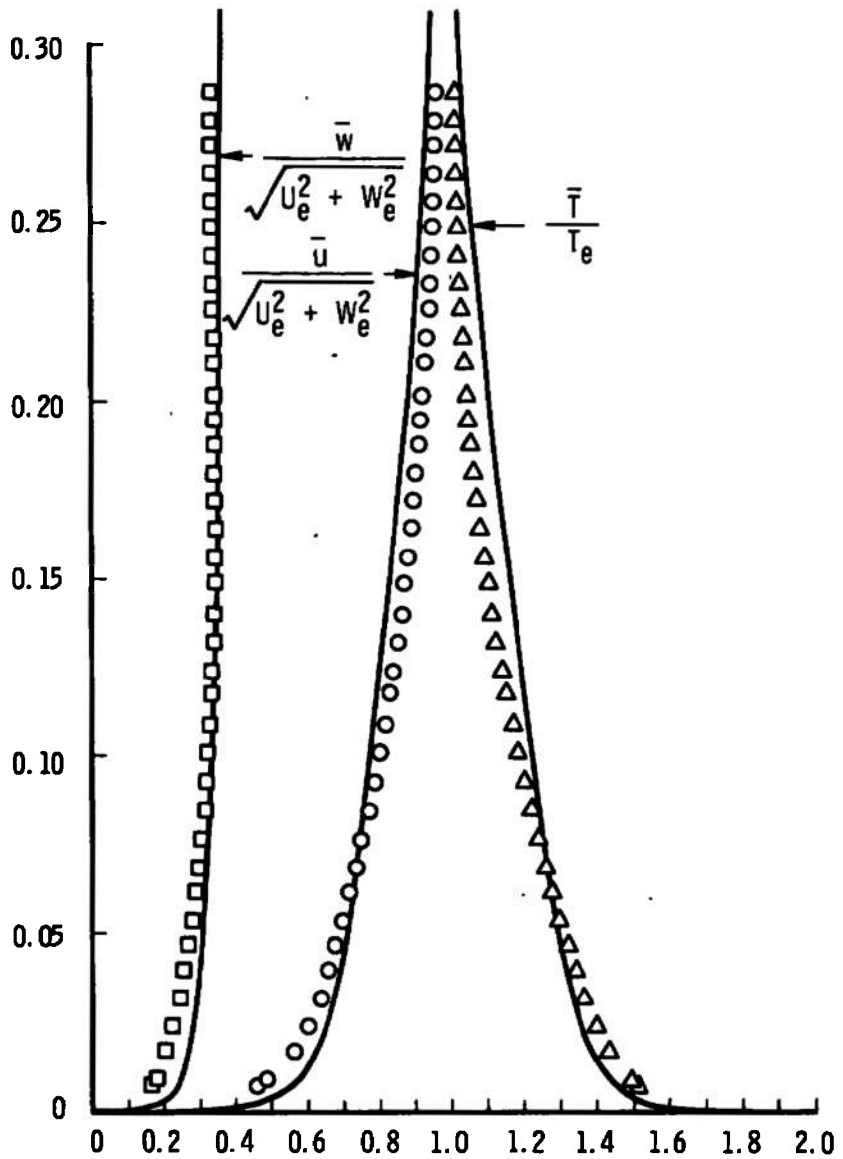

c. ϕ = 135.0 deg
Fig. 8 Concluded

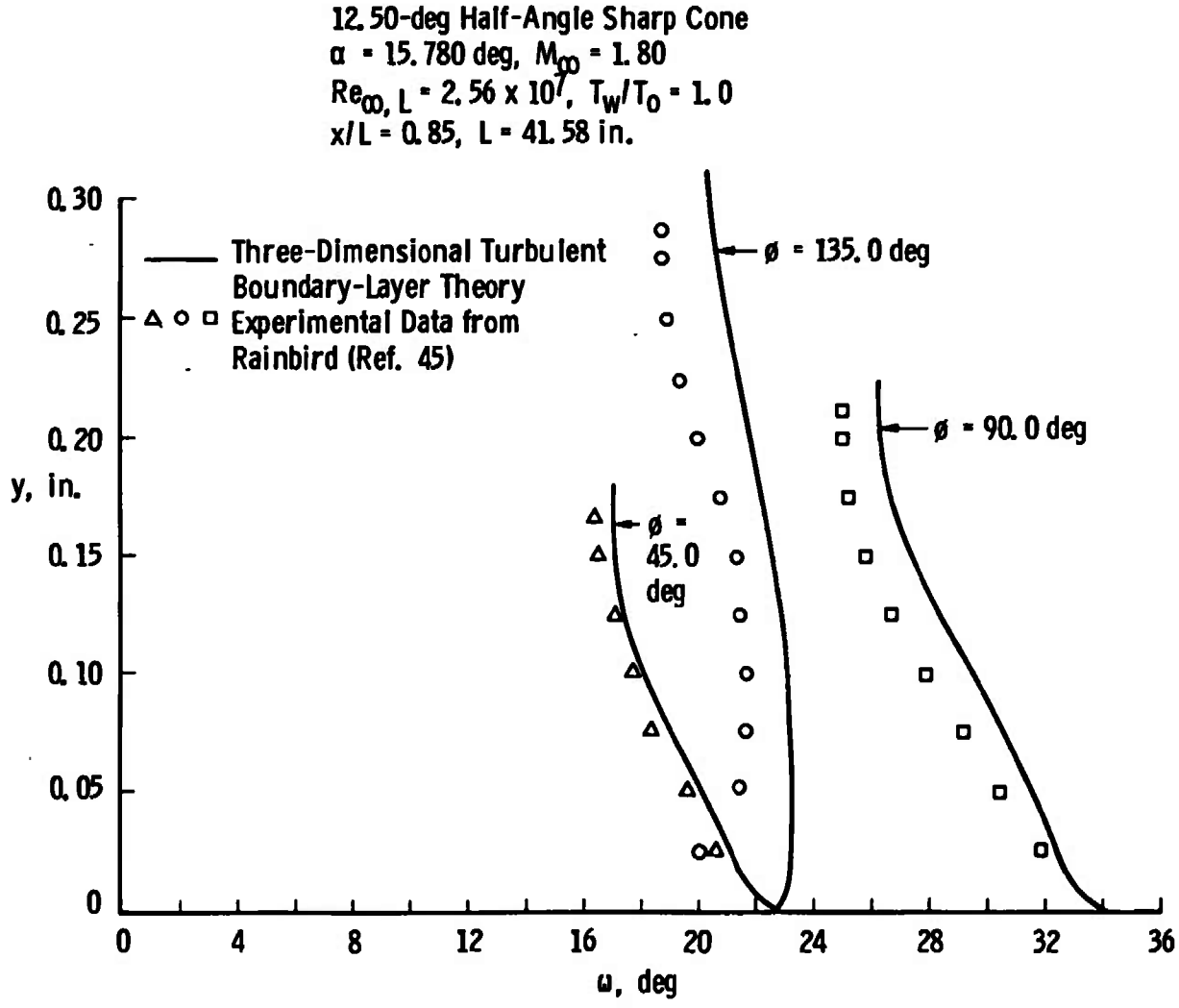

Fig. 9 Streamline Directions within the Three-Dimensional Turbulent Boundary Layer under Supersonic Conditions

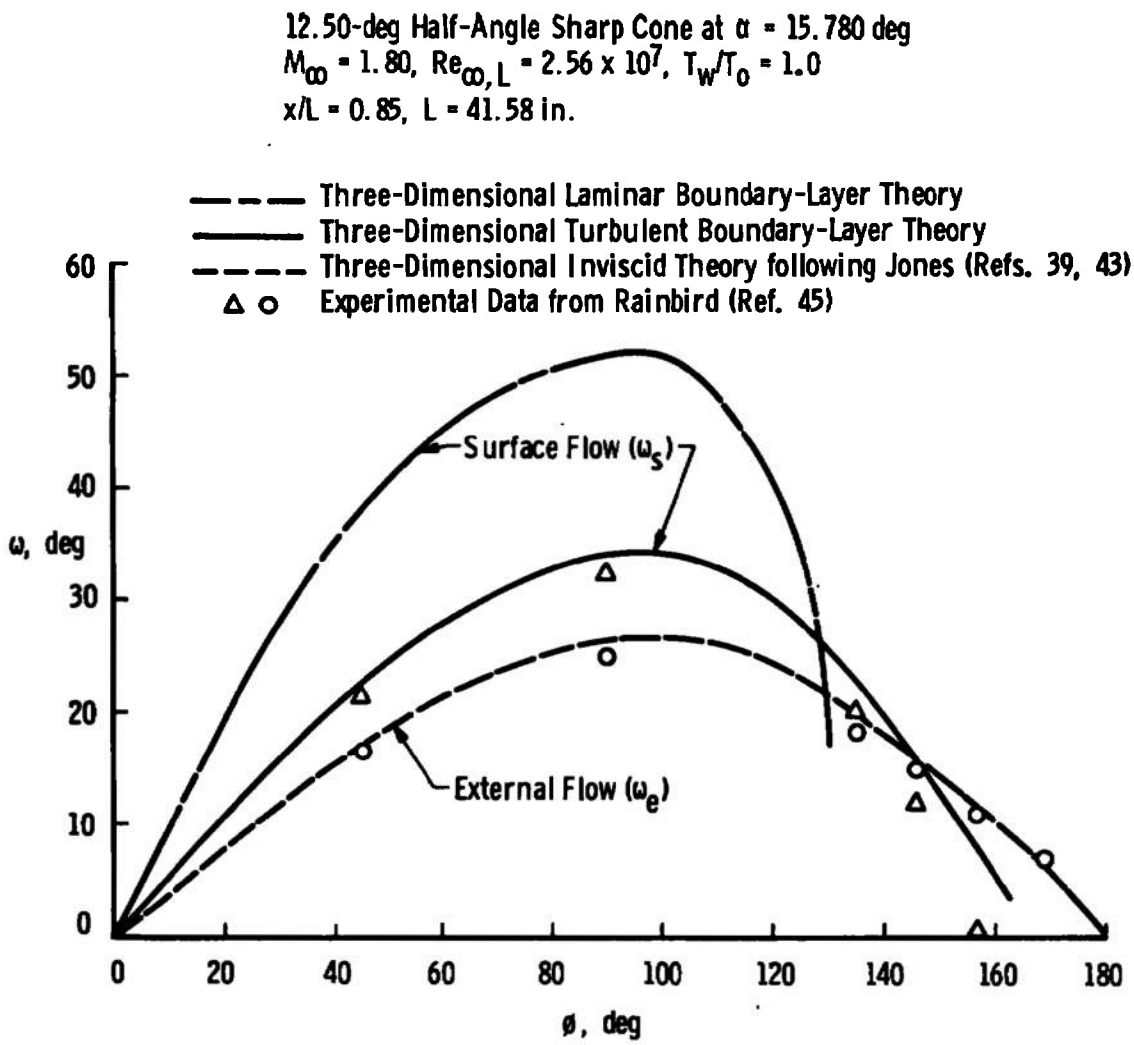

Fig. 10 Surface and External Flow Directions under Supersonic Conditions

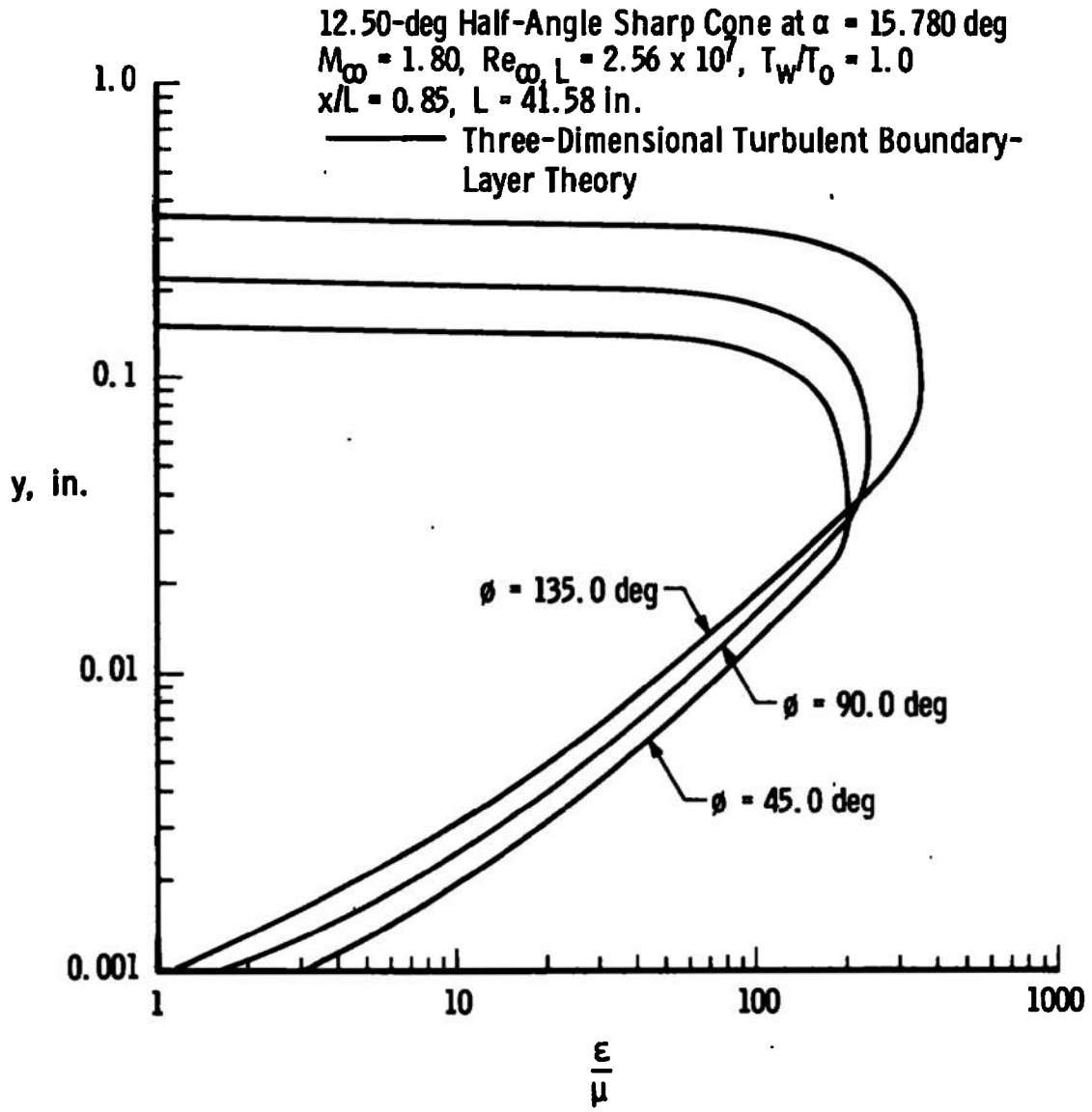

Fig. 11 Eddy-Viscosity Distributions at Various Angular Locations under Supersonic Conditions

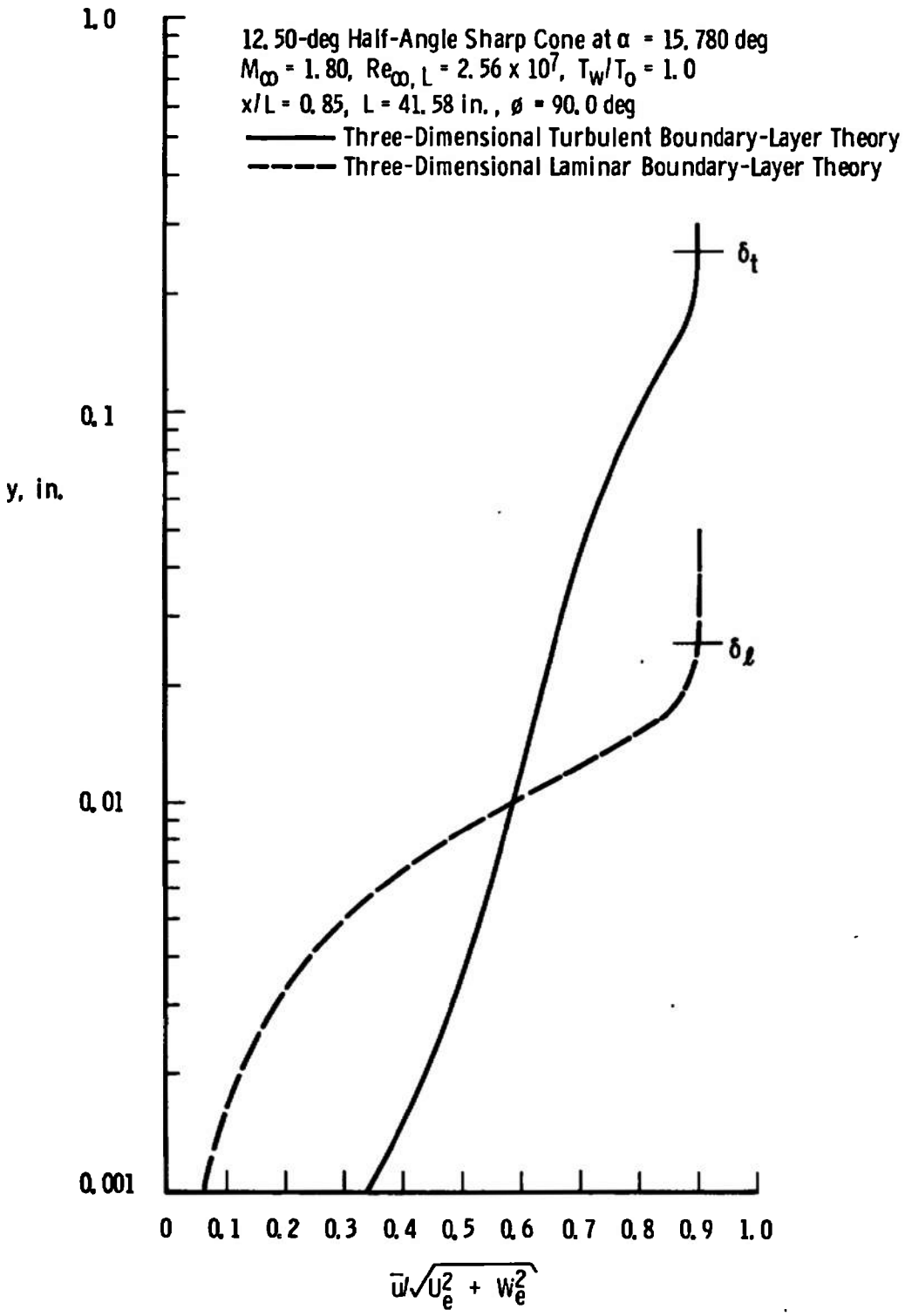

a. $\bar{u}$ - Velocity Ratio

Fig. 12 Comparison of Laminar and Turbulent Three-Dimensional Boundary-Layer Profiles at Angular Location ϕ = 90.0 deg under Supersonic Conditions

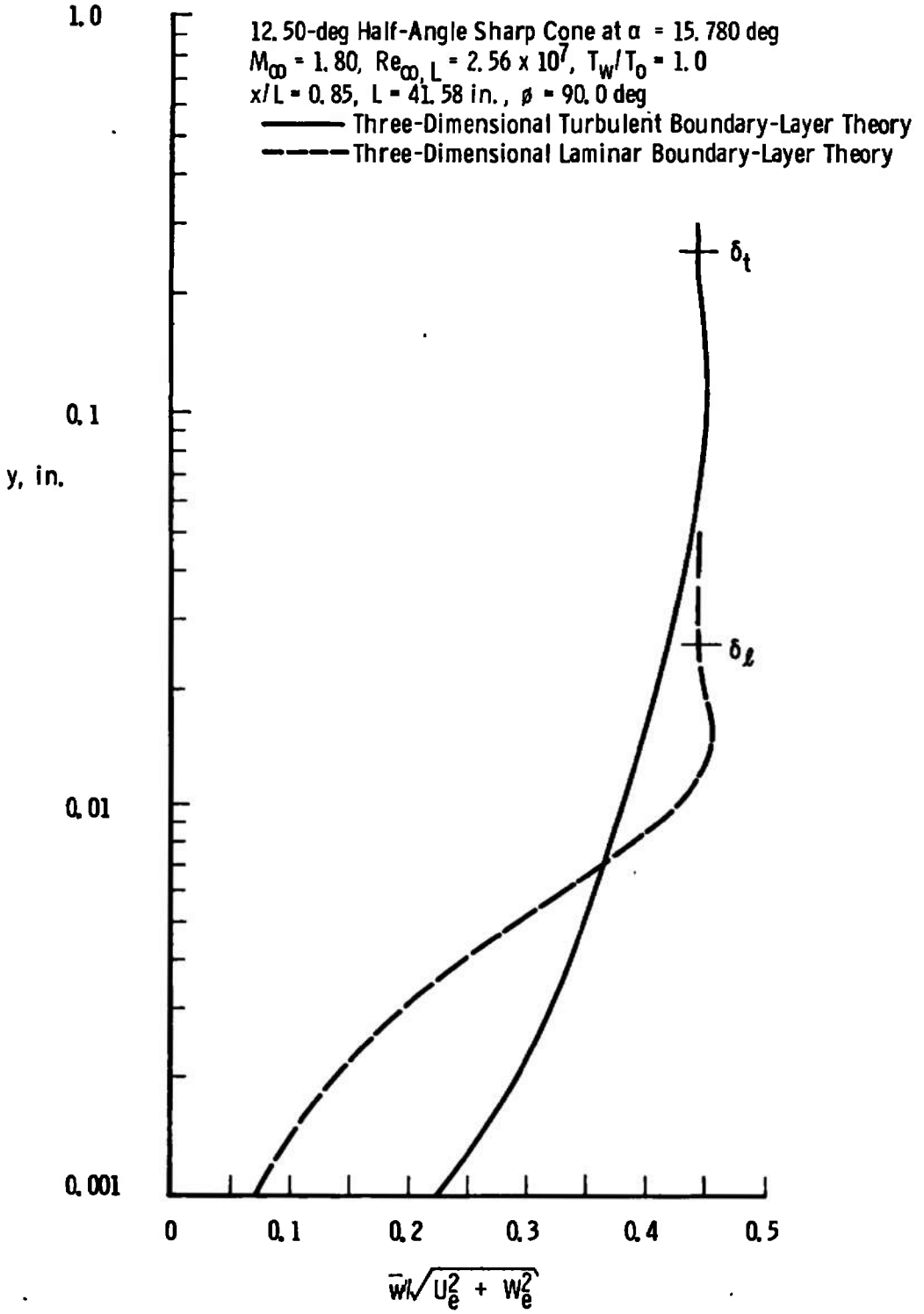

b. $\bar{w}$ - Velocity Ratio
Fig. 12 Continued

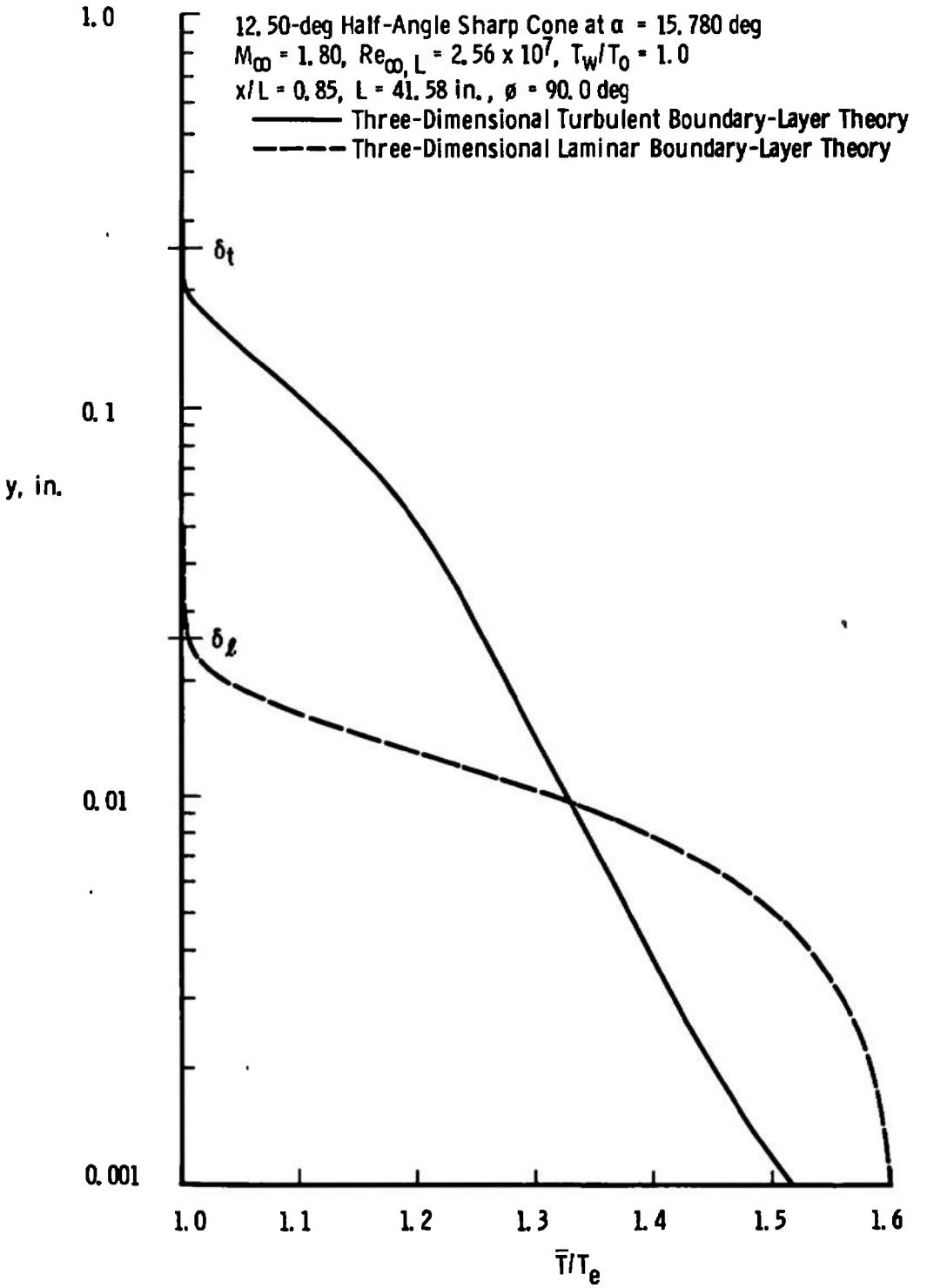

c. Static Temperature Ratio
Fig. 12 Concluded

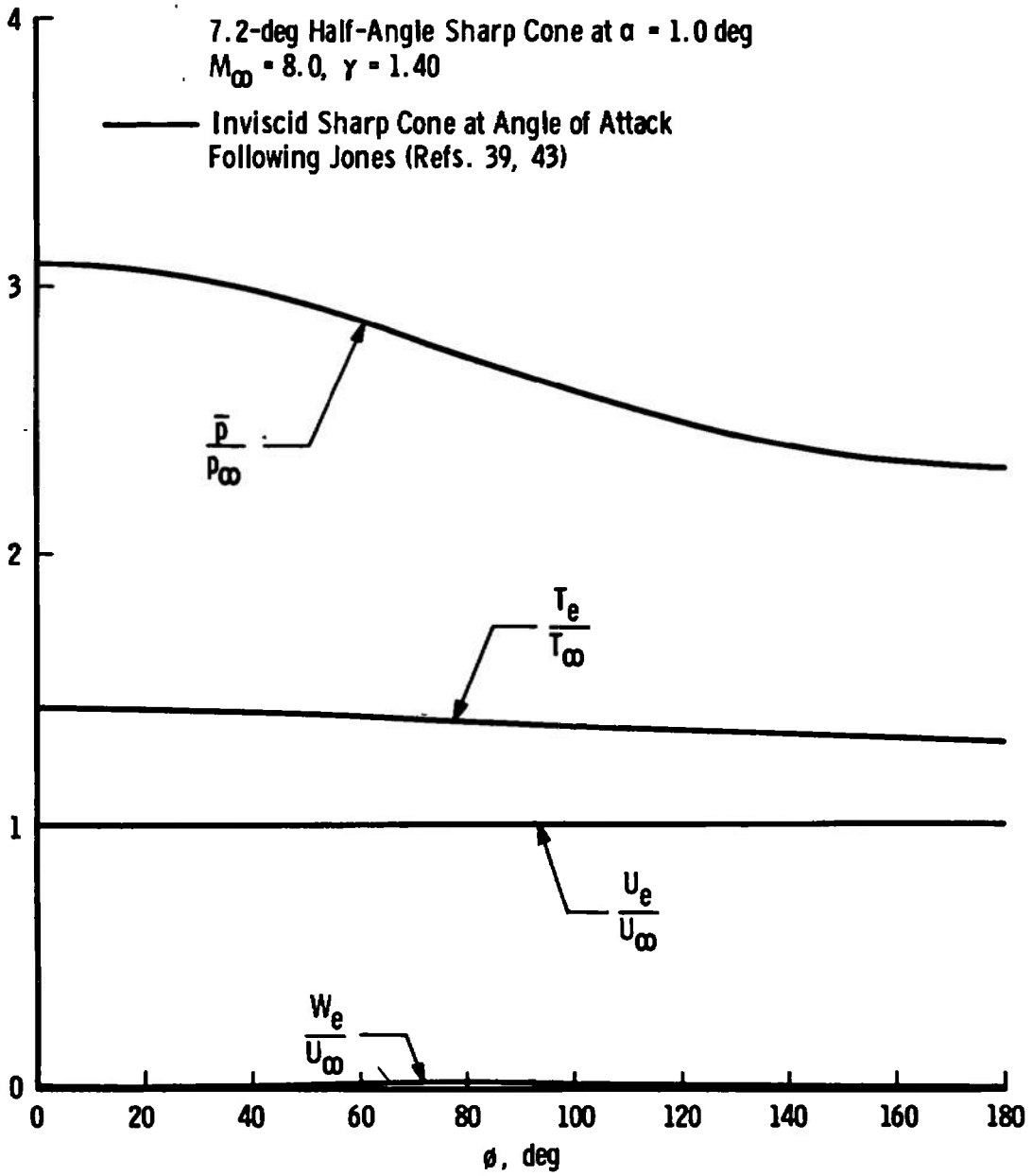

a. α = 1.0 deg

Fig. 13 Calculated Inviscid Flow Parameters on Cone Surface under Hypersonic Conditions

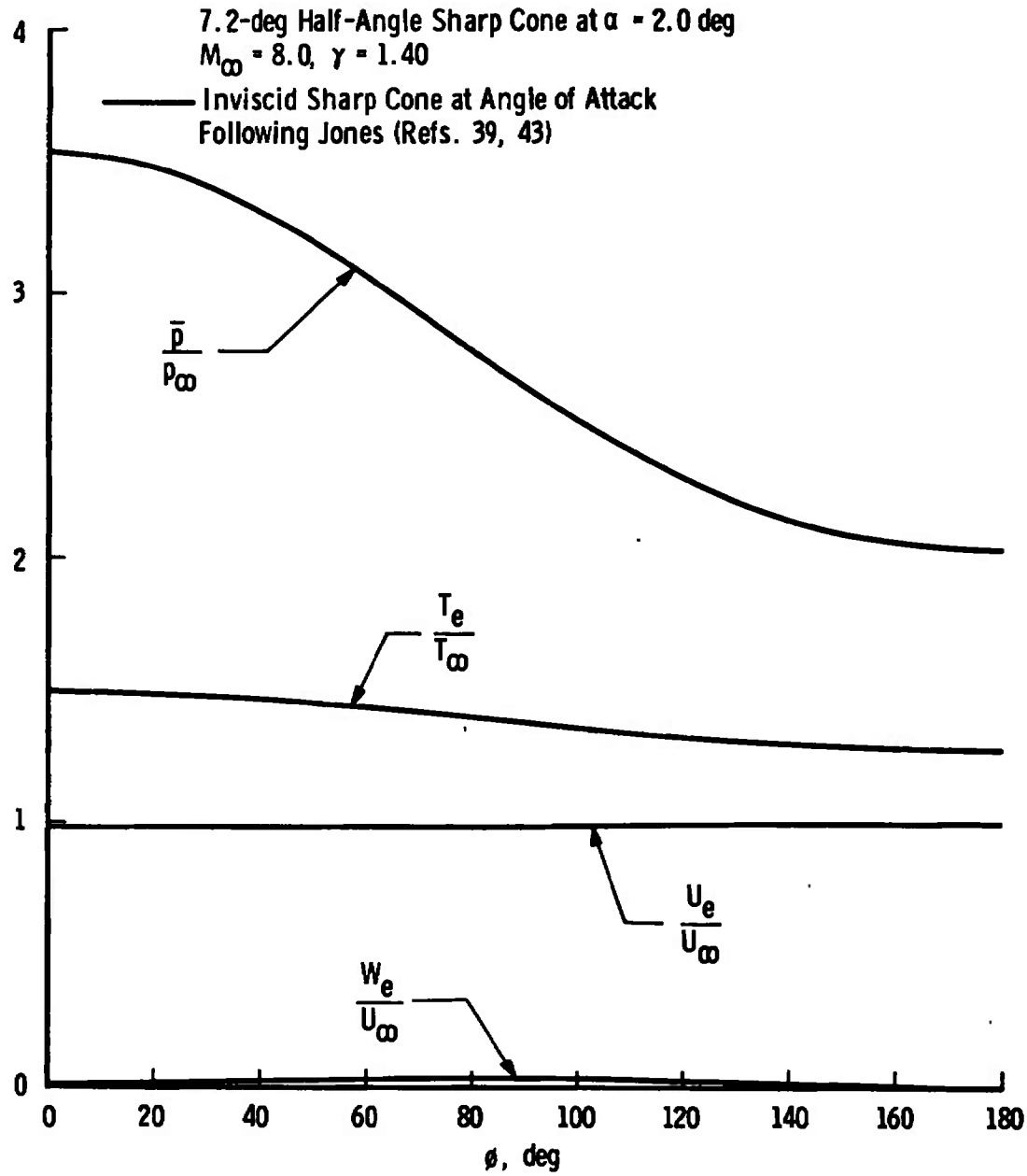

b. α = 2.0 deg
Fig. 13 Continued

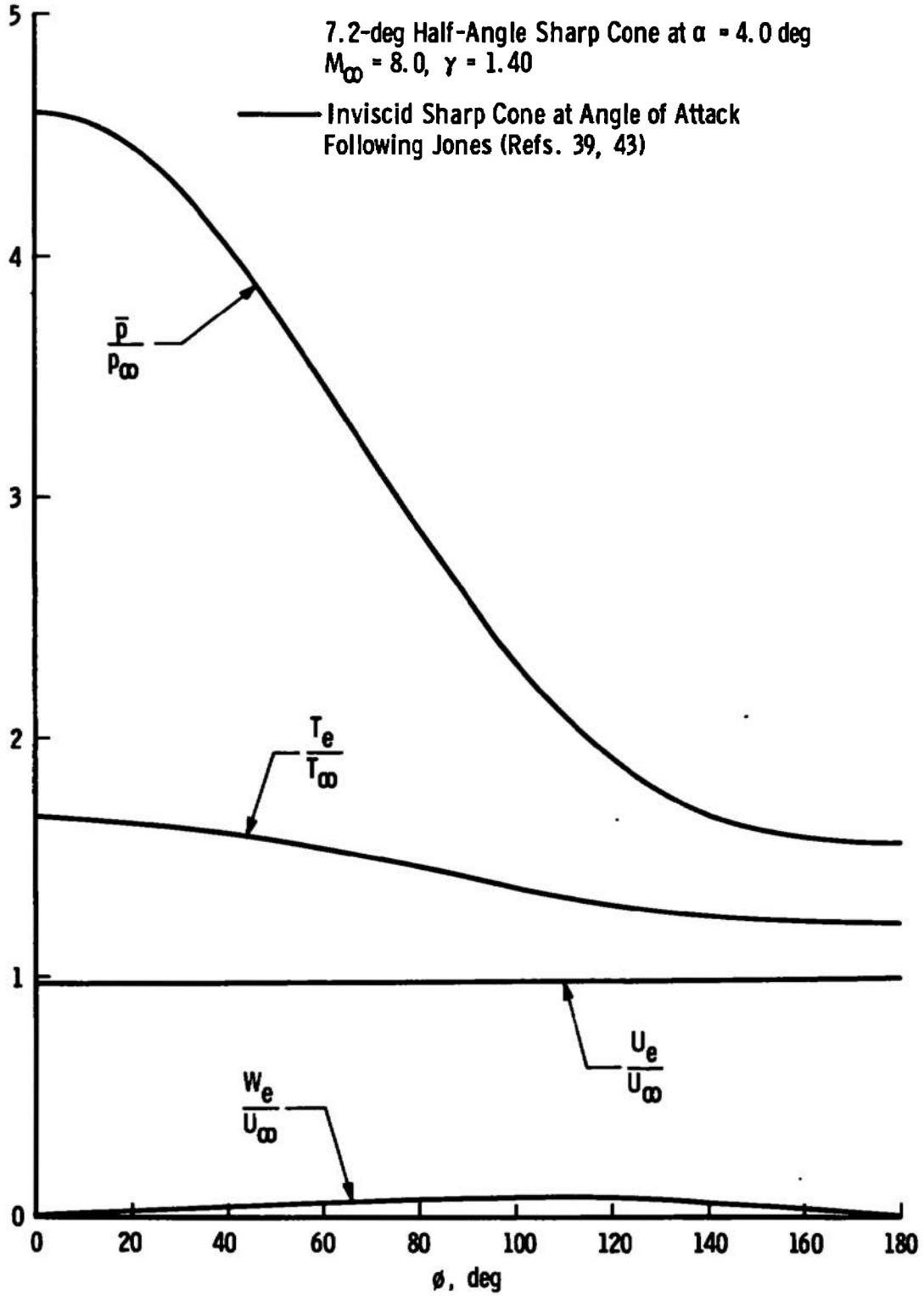

c. α = 4.0 deg

Fig. 13 Concluded

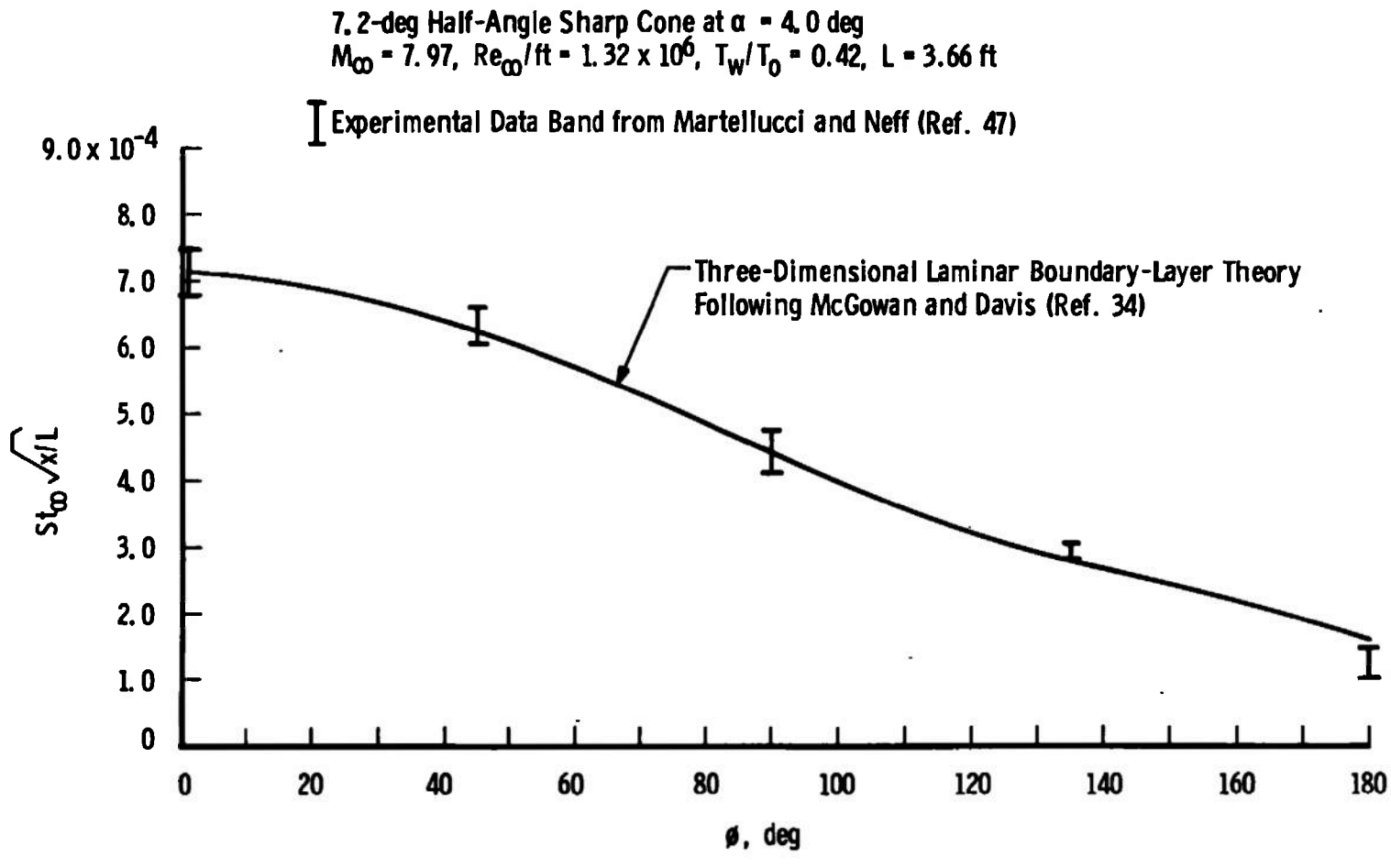

Fig. 14 Laminar Heat-Transfer Distribution on a Sharp Cone at Incidence under Hypersonic Conditions

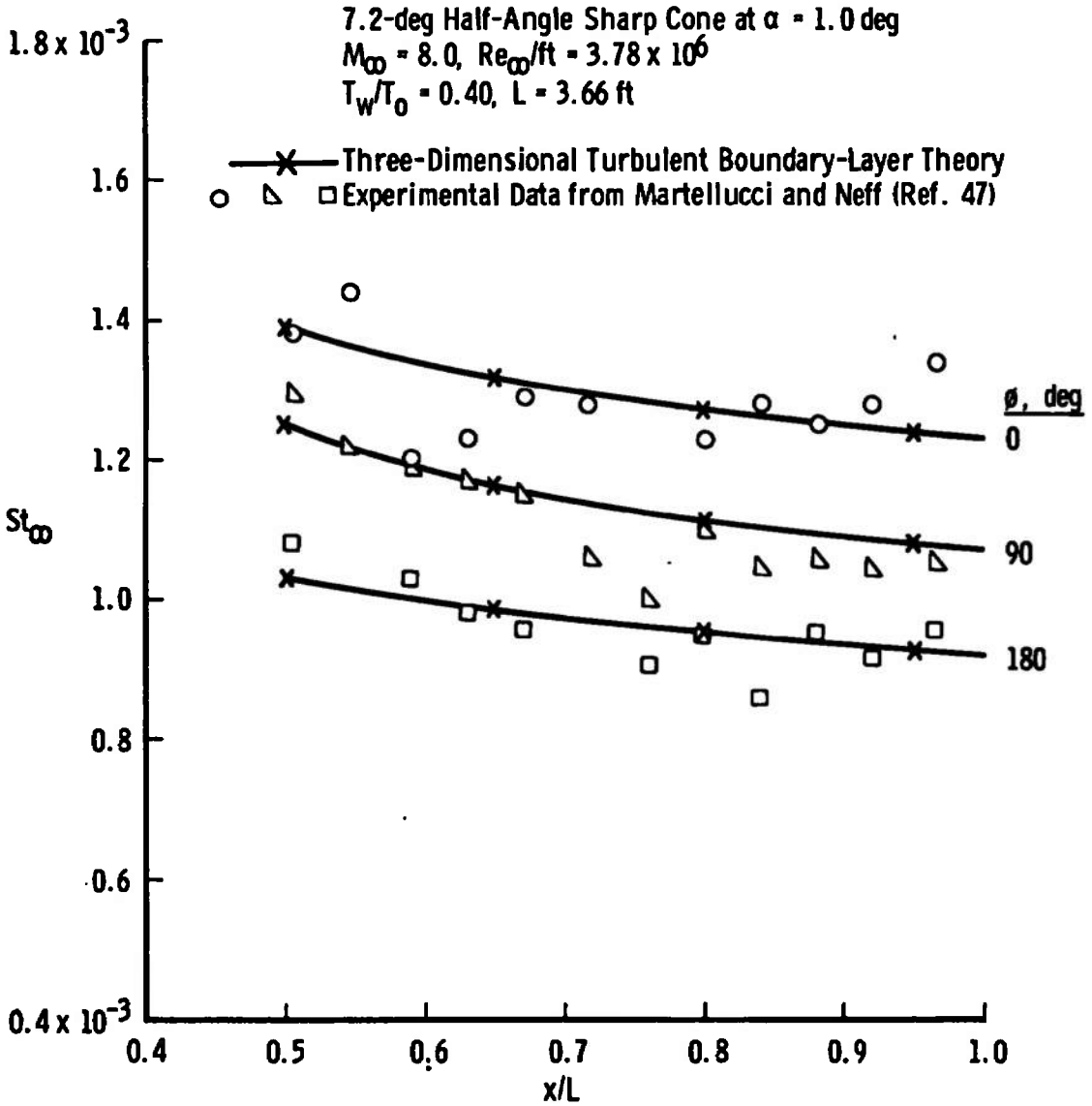

a. α = 1.0 deg

Fig. 15 Turbulent Heat-Transfer Distribution on a Sharp Cone at Incidence under Hypersonic Conditions

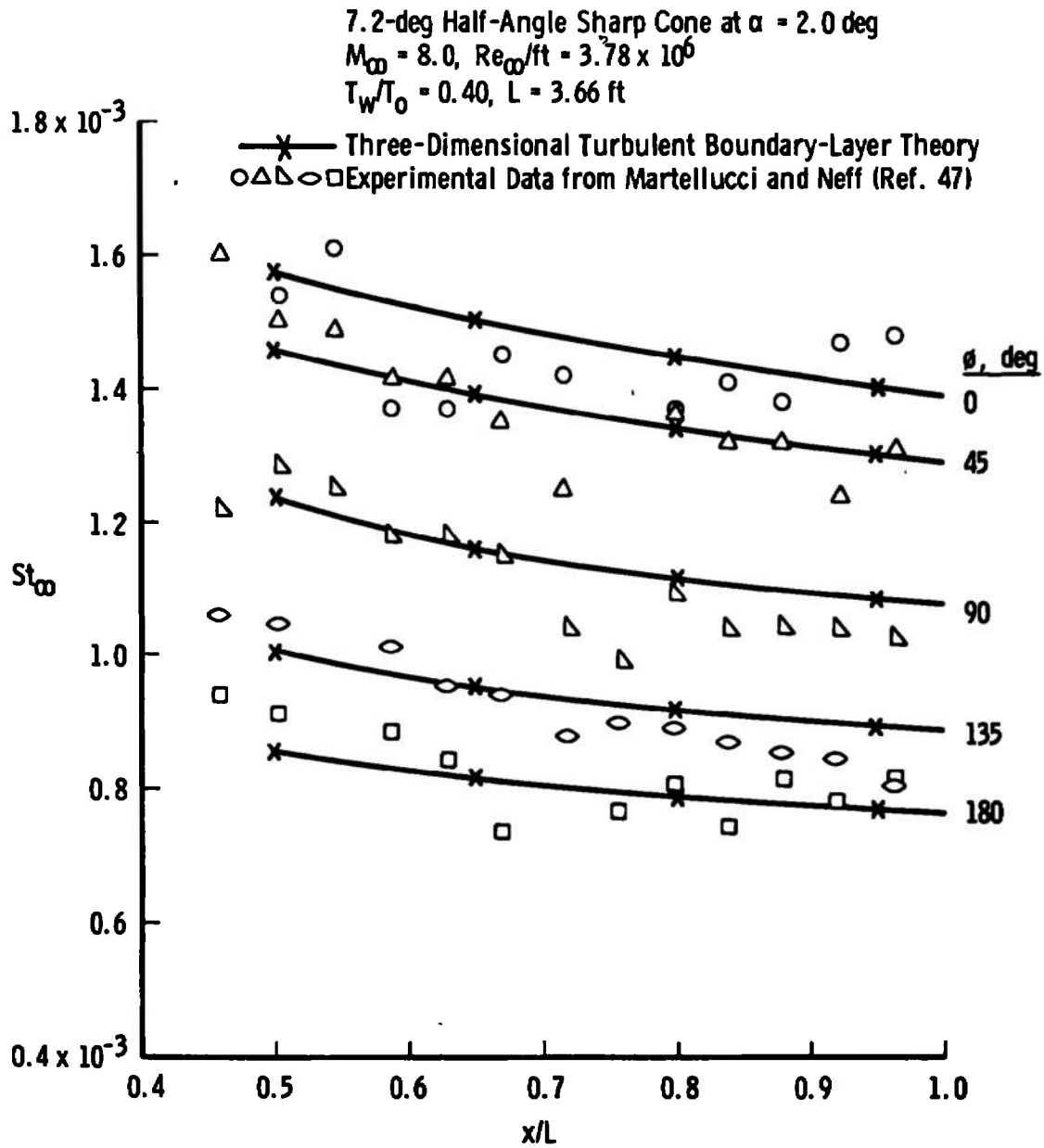

b. α = 2.0 deg
Fig. 15 Continued

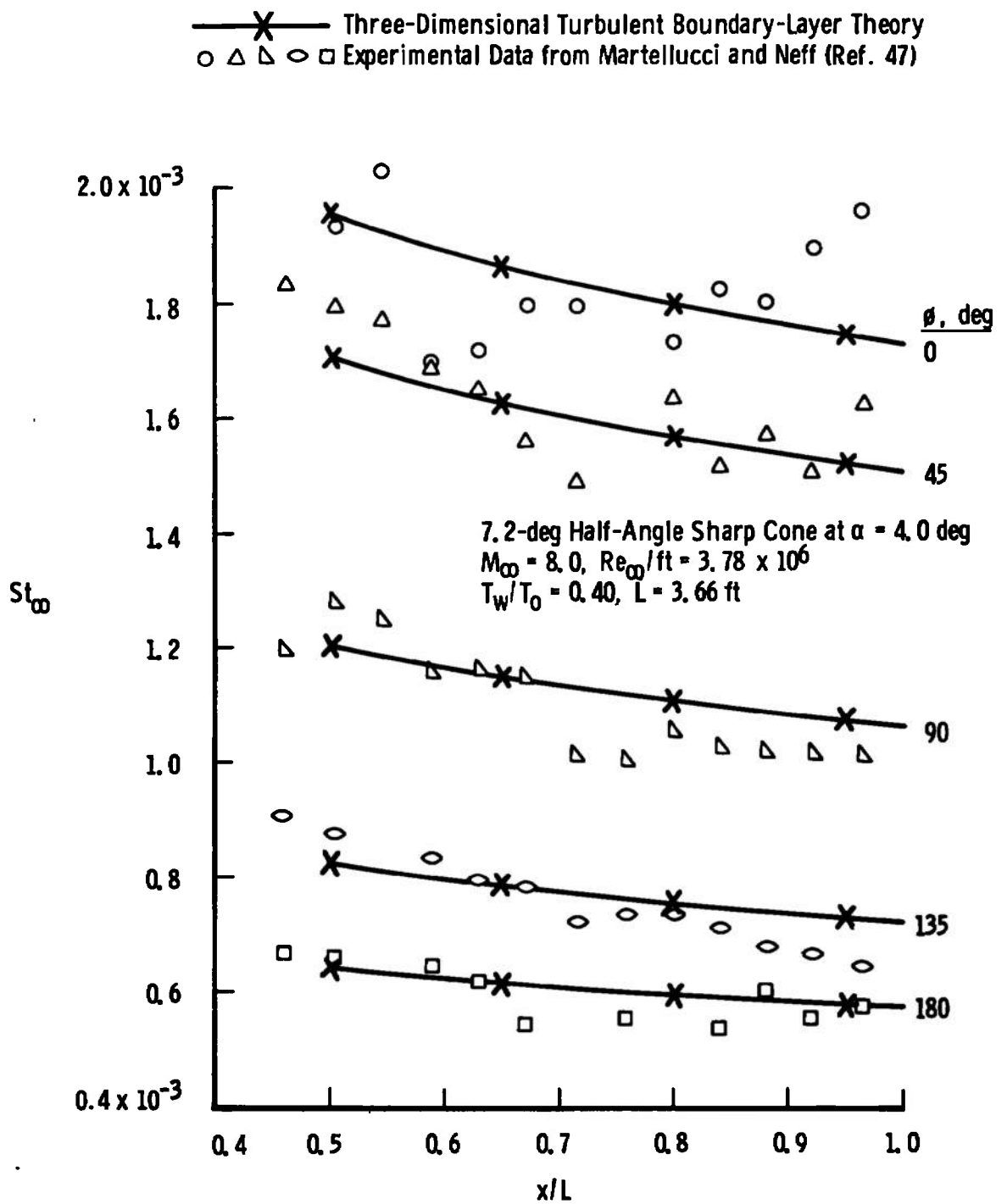

c. α = 4.0 deg

Fig. 15 Concluded

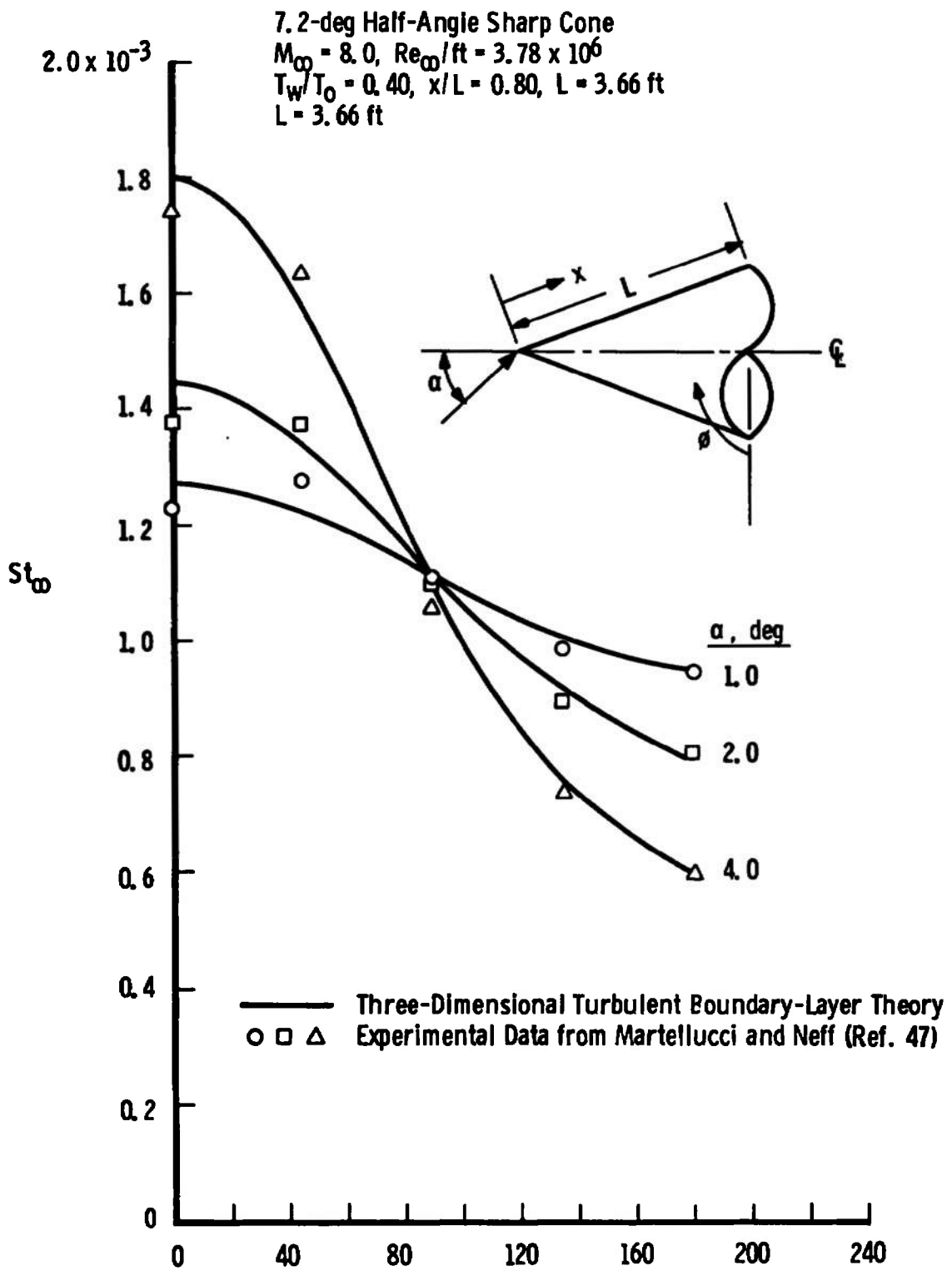

Fig. 16 Circumferential Turbulent Heat-Transfer Distribution on a Sharp Cone at Incidence under Hypersonic Conditions

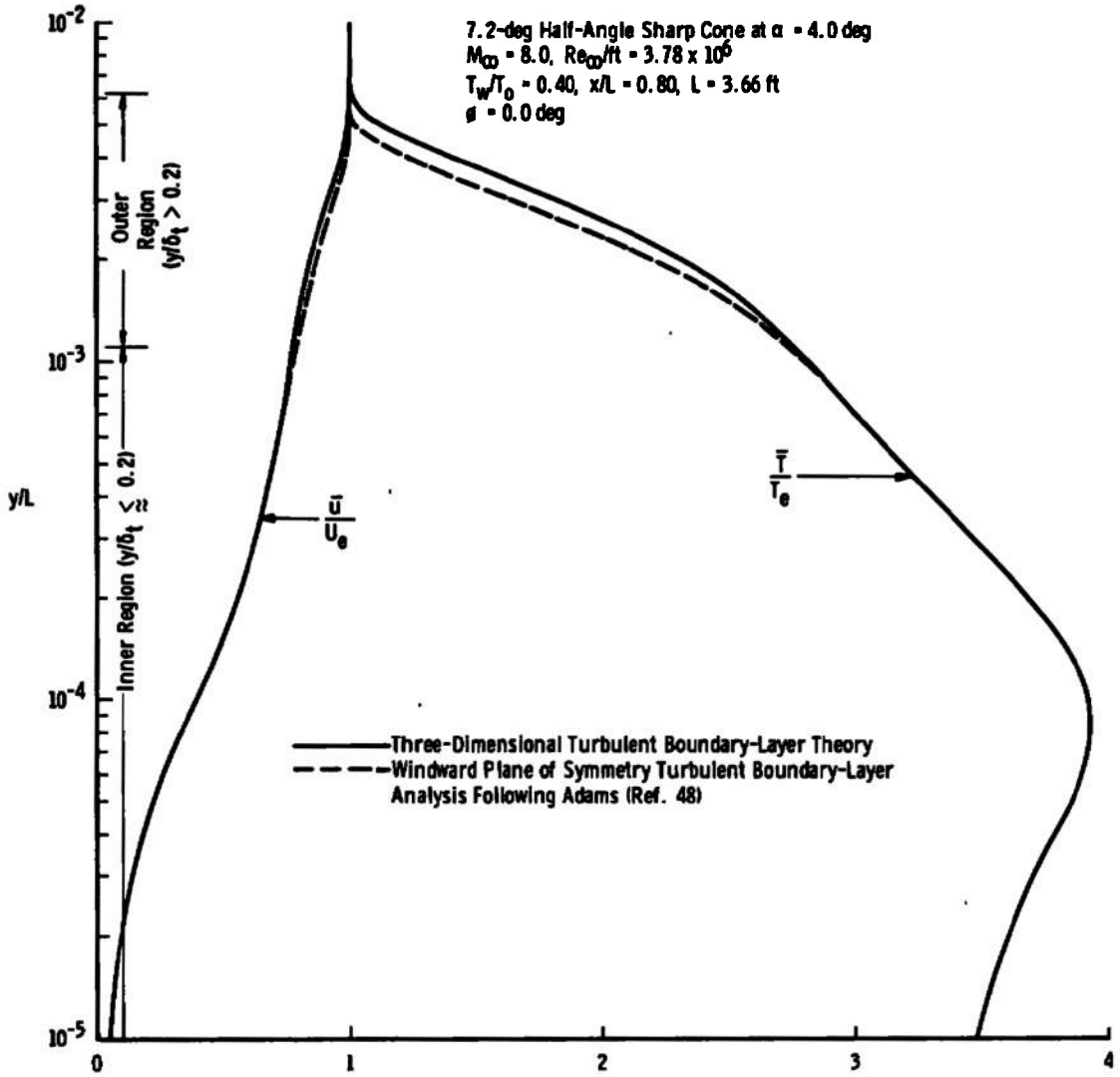

Fig. 17 Windward Ray Turbulent Boundary-Layer Profiles Under Cold Wall Hypersonic Conditions

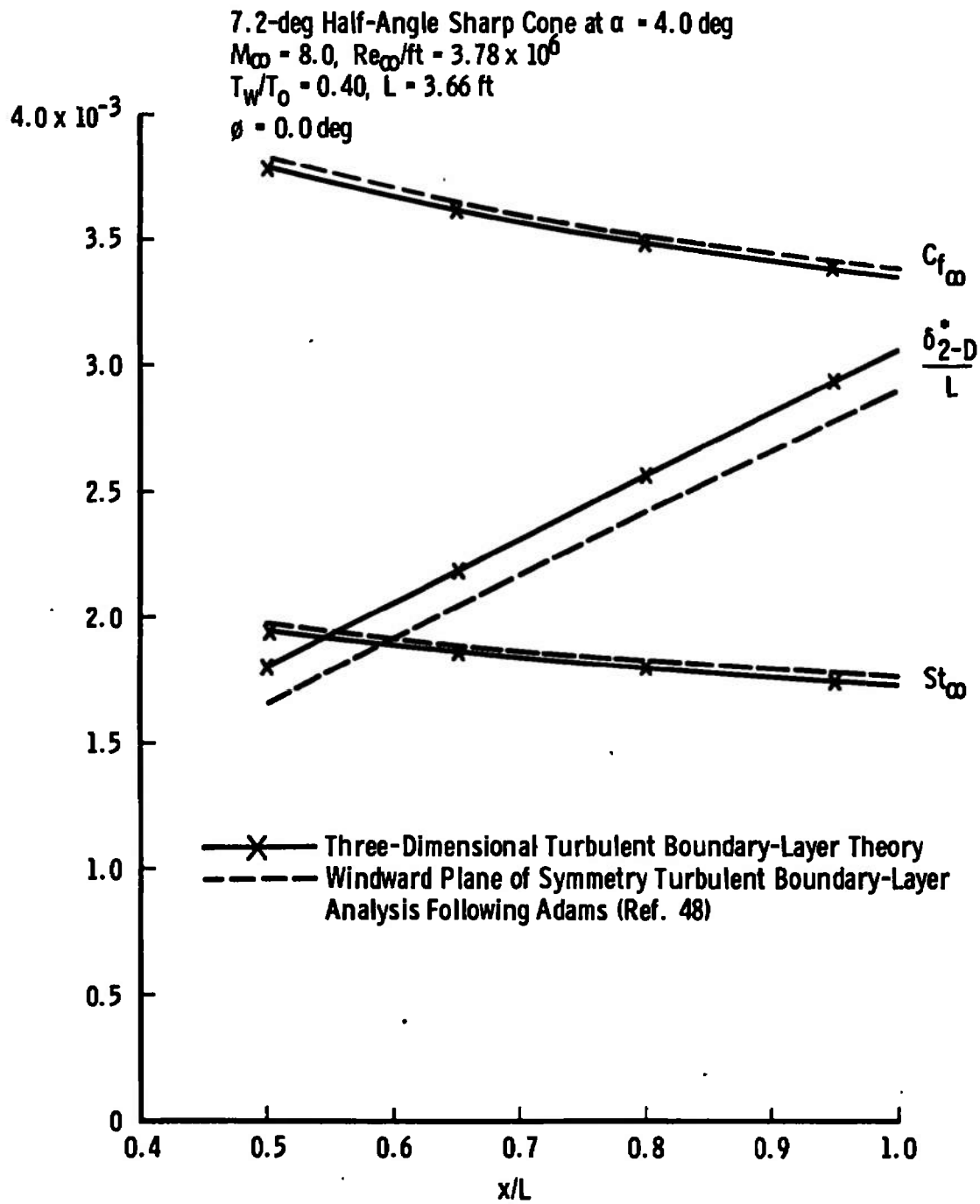

Fig. 18 Windward Ray Turbulent Boundary-Layer Parameters under Cold Wall Hypersonic Conditions

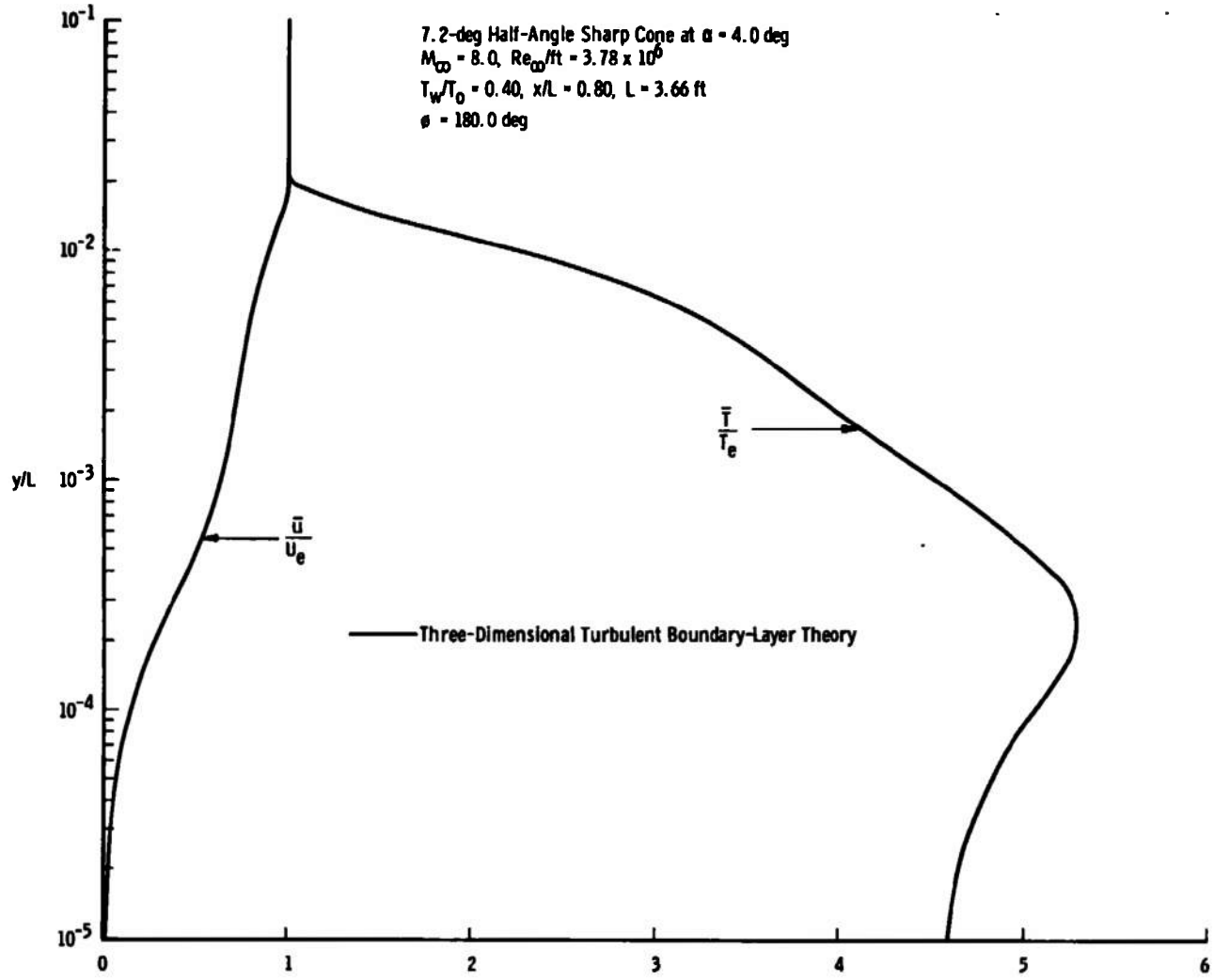

Fig. 19 Leeward Ray Turbulent Boundary-Layer Profiles under Cold Wall Hypersonic Conditions

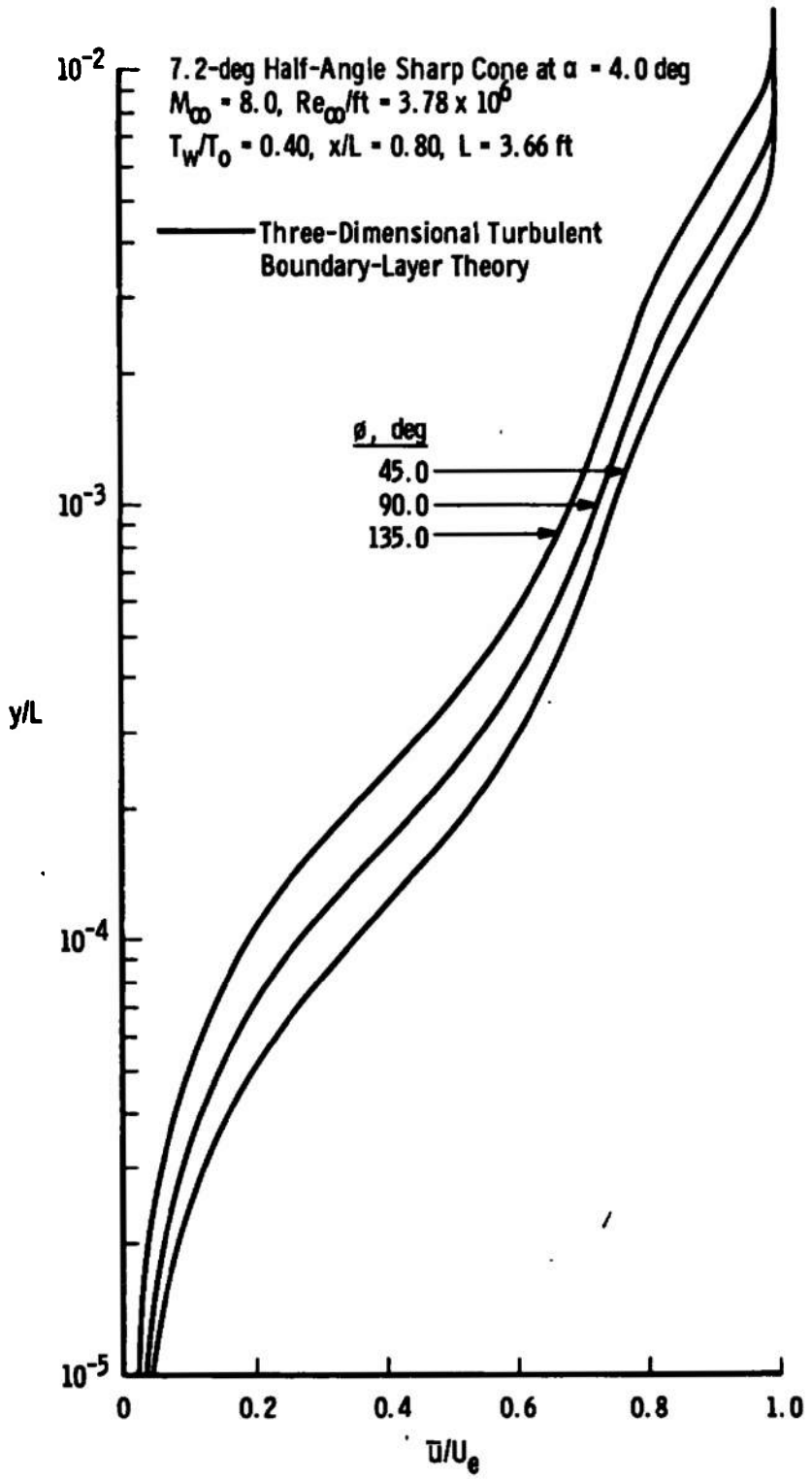

a. Streamwise Velocity Ratio

Fig. 20 Three-Dimensional Turbulent Boundary-Layer Profiles under Cold Wall Hypersonic Conditions

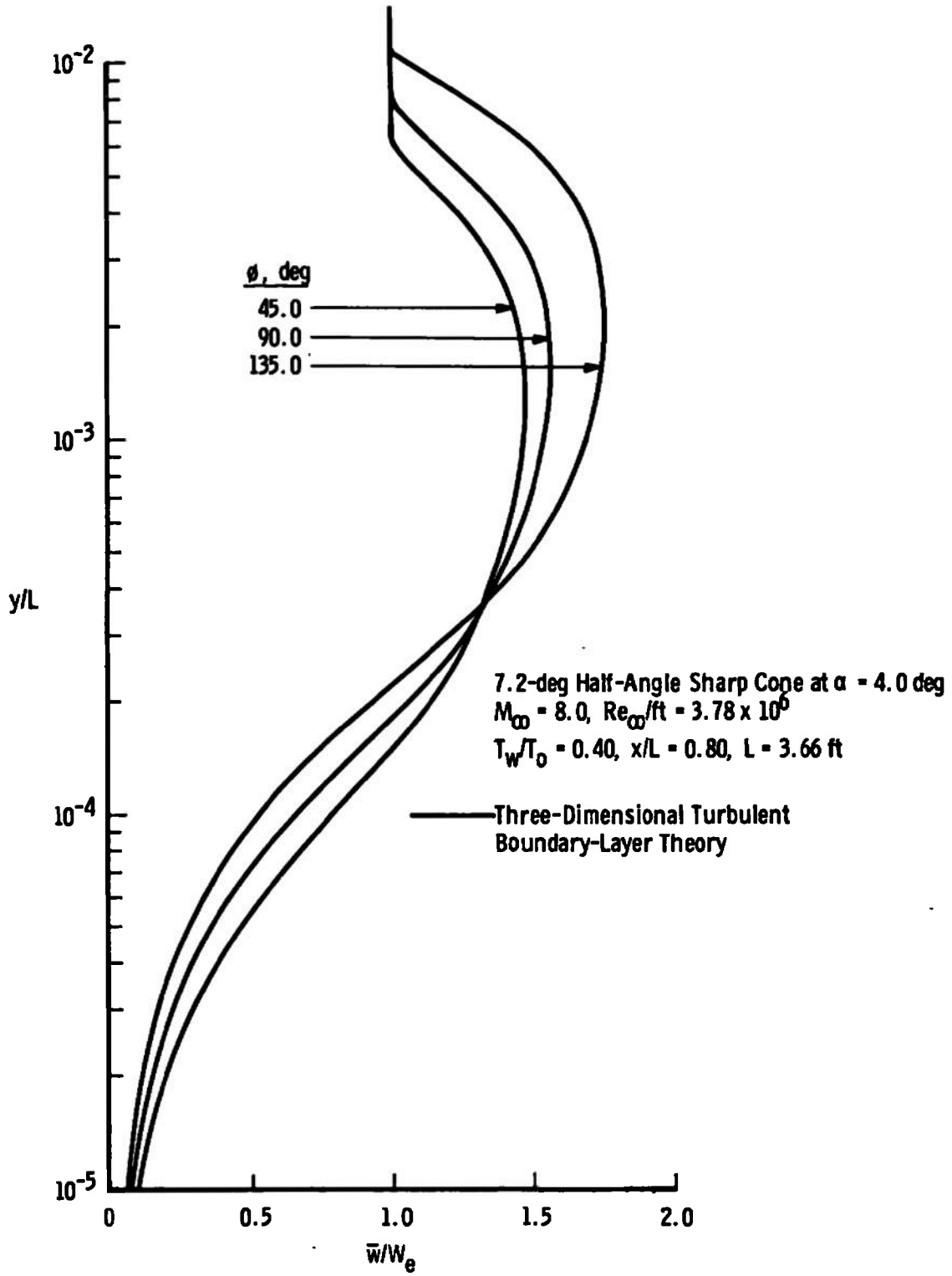

b. Crossflow Velocity Ratio
Fig. 20 Continued

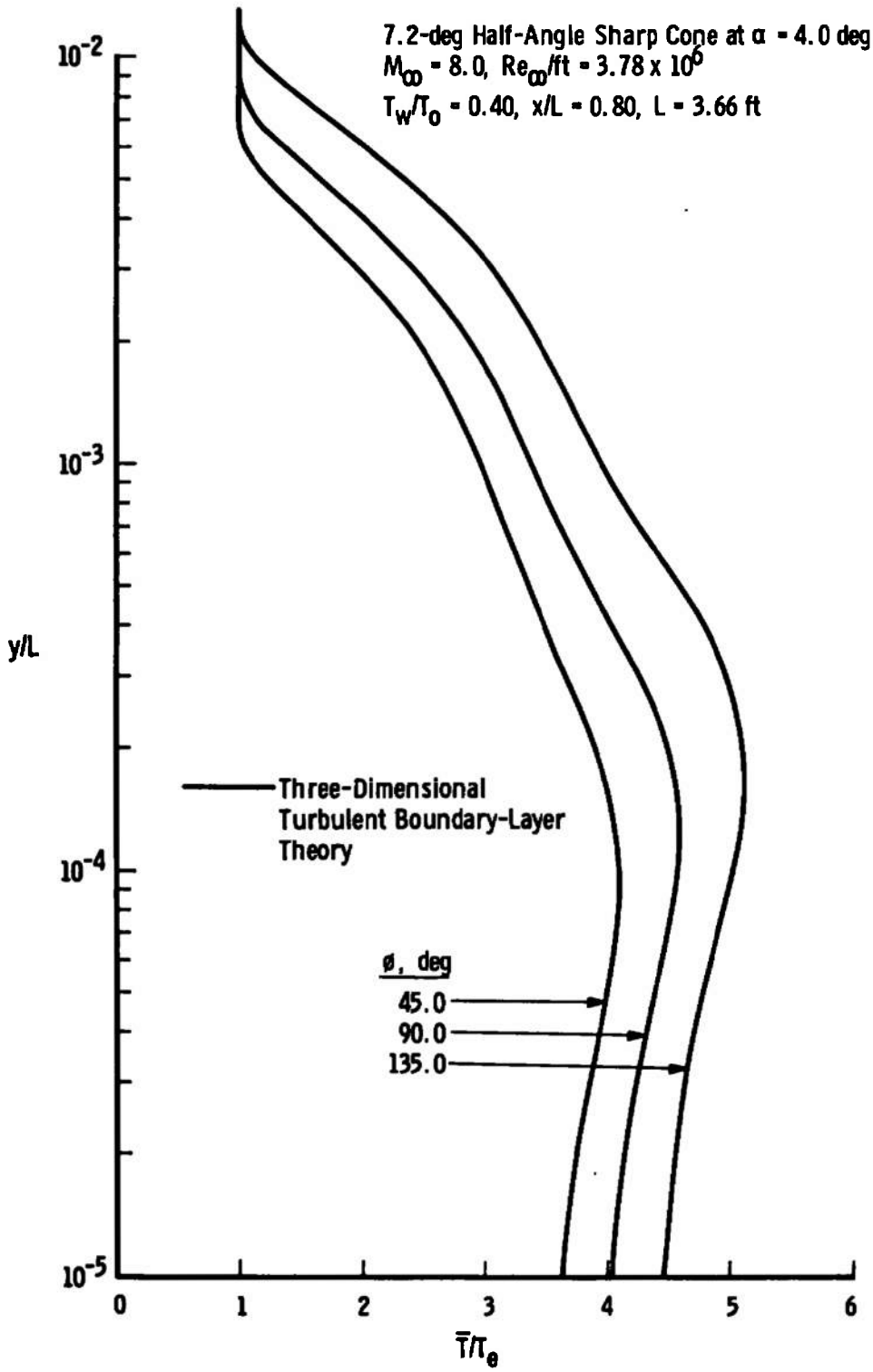

c. Static Temperature Ratio
Fig. 20 Continued

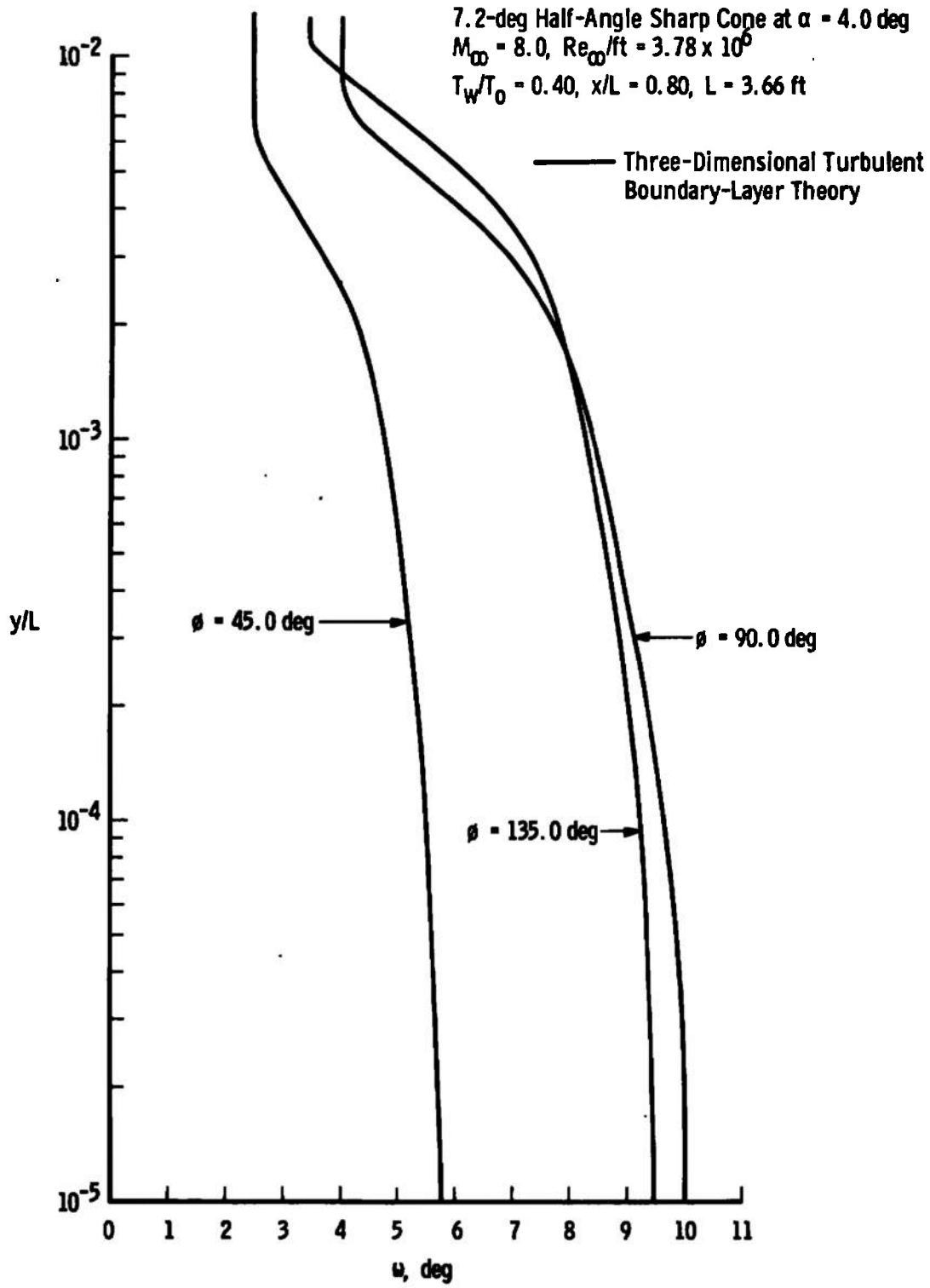

d. Streamline Directions in Boundary Layer
Fig. 20 Continued

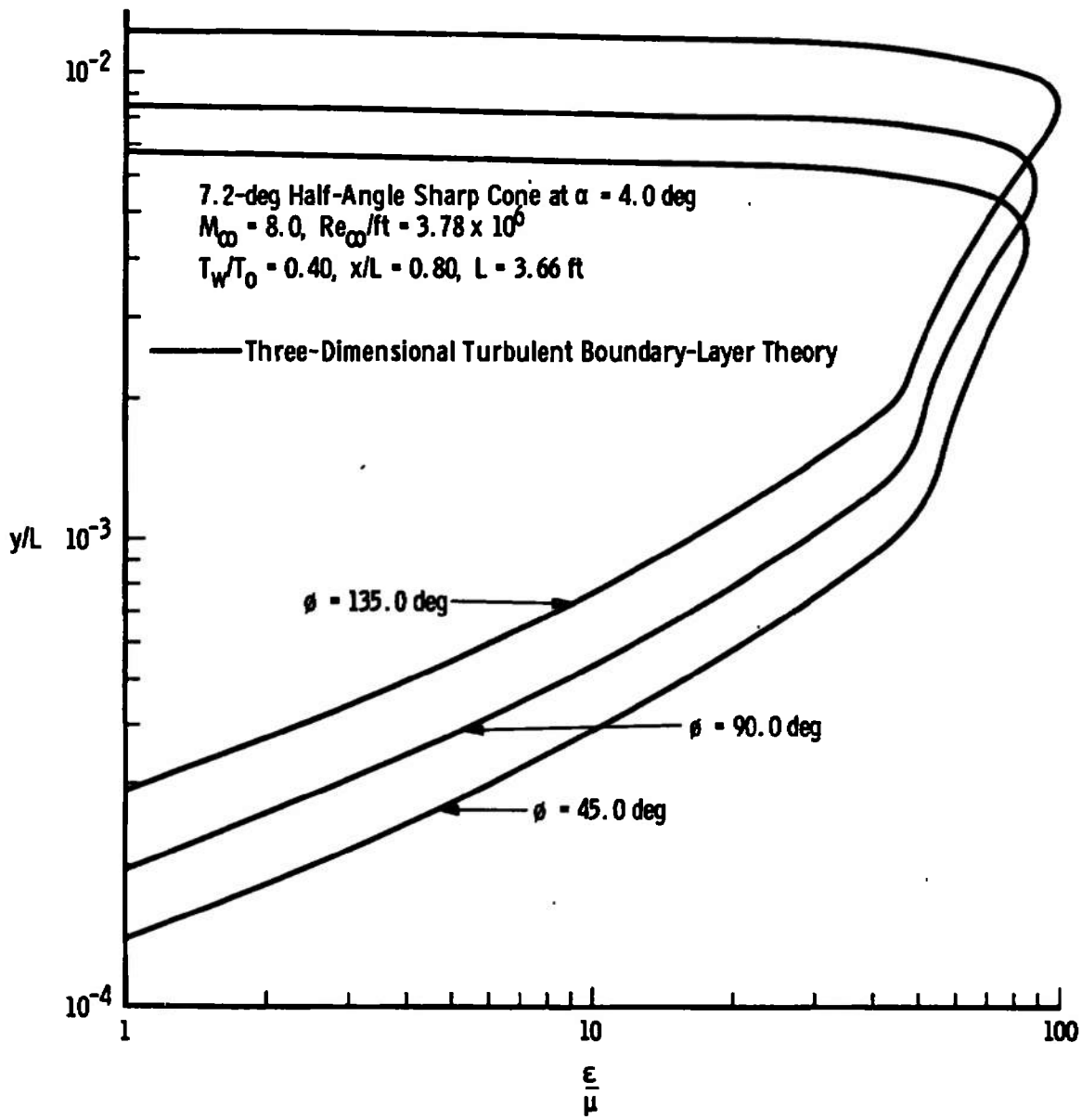

e. Eddy-Viscosity Ratio
Fig. 20 Concluded

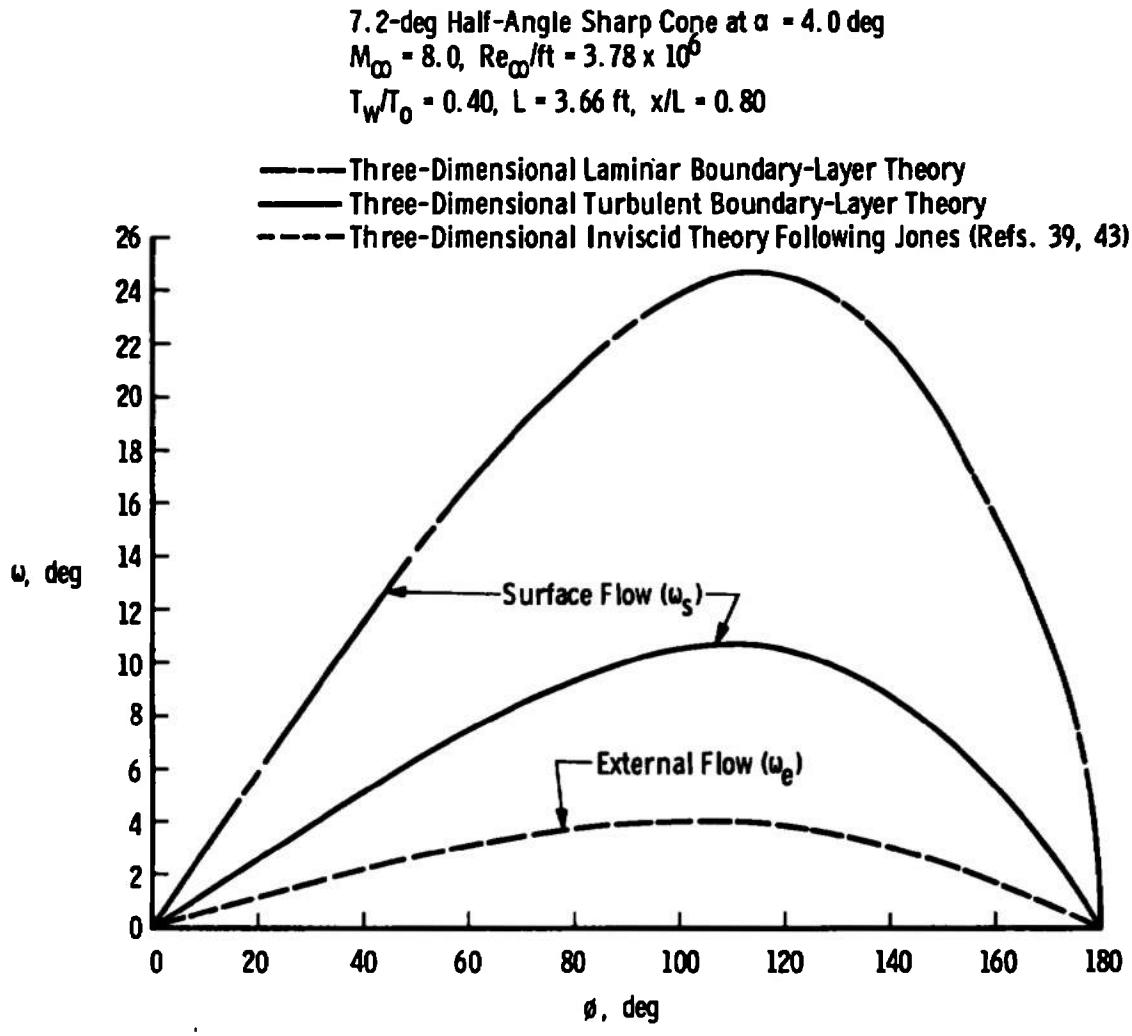

Fig. 21 Surface and External Flow Directions under Cold Wall Hypersonic Conditions

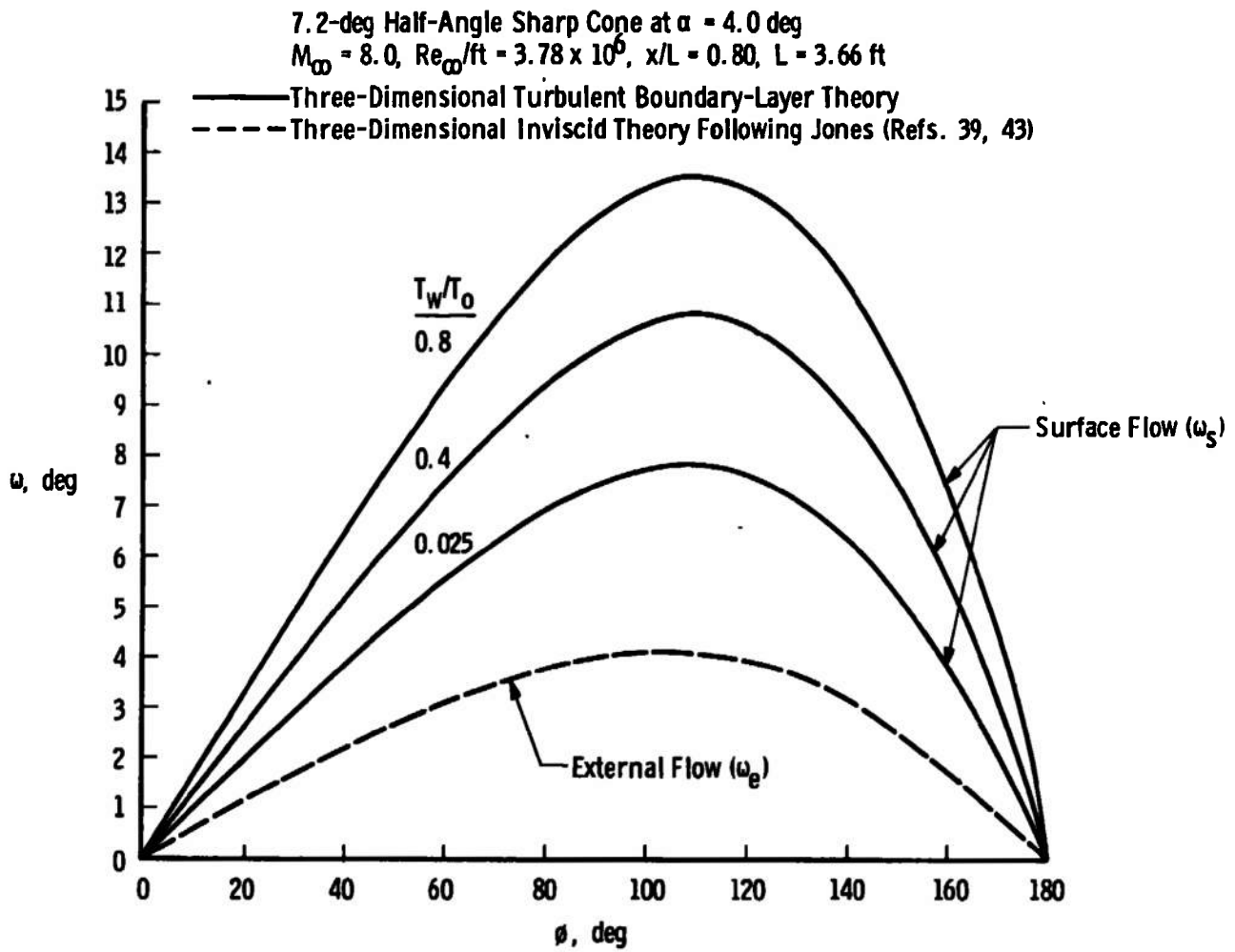

Fig. 22 Effects of Wall Temperature on Surface Flow Direction under Hypersonic Conditions

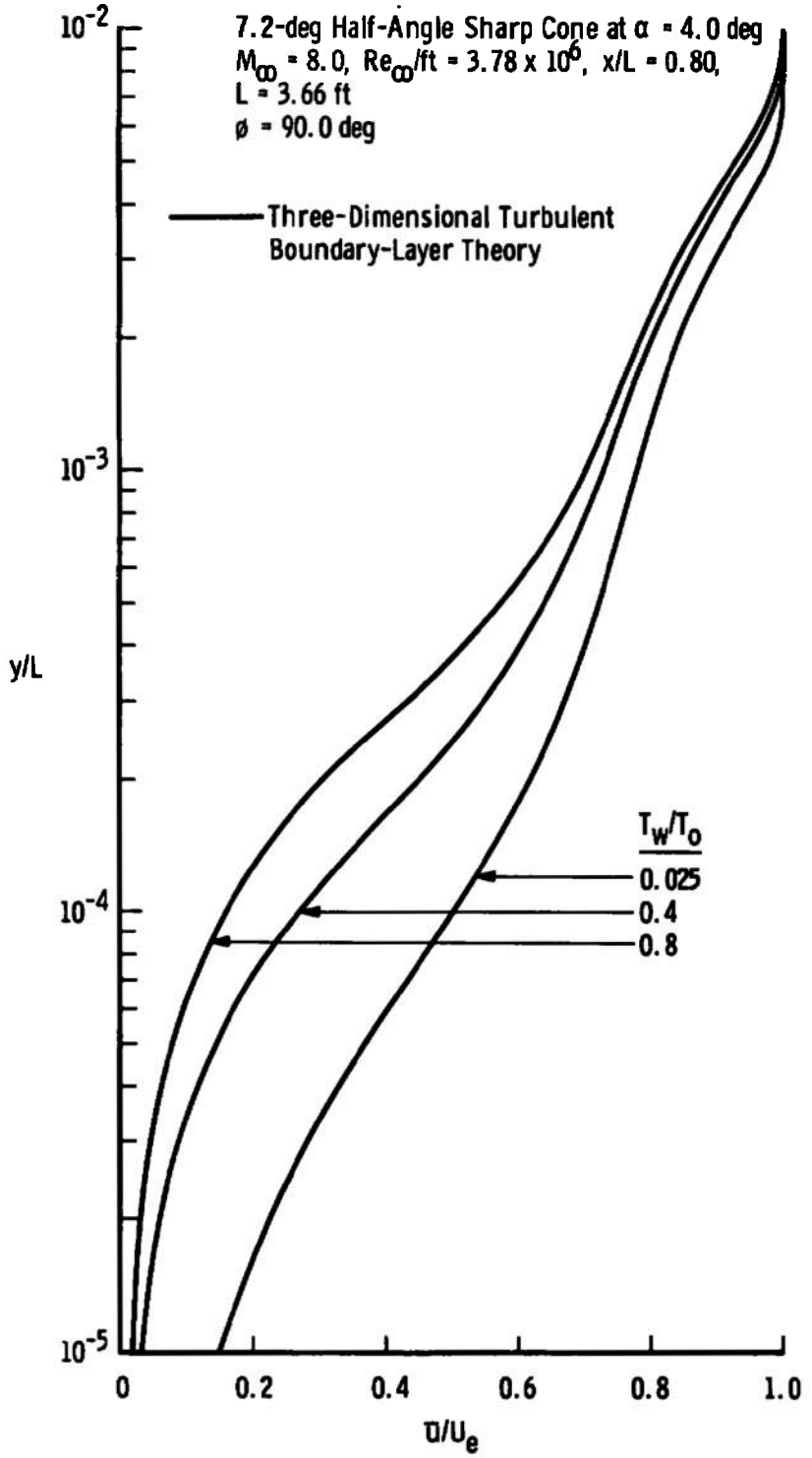

a. Streamwise Velocity Ratio

Fig. 23 Effects of Wall Temperature on Three-Dimensional Turbulent Boundary-Layer Profiles under Hypersonic Conditions

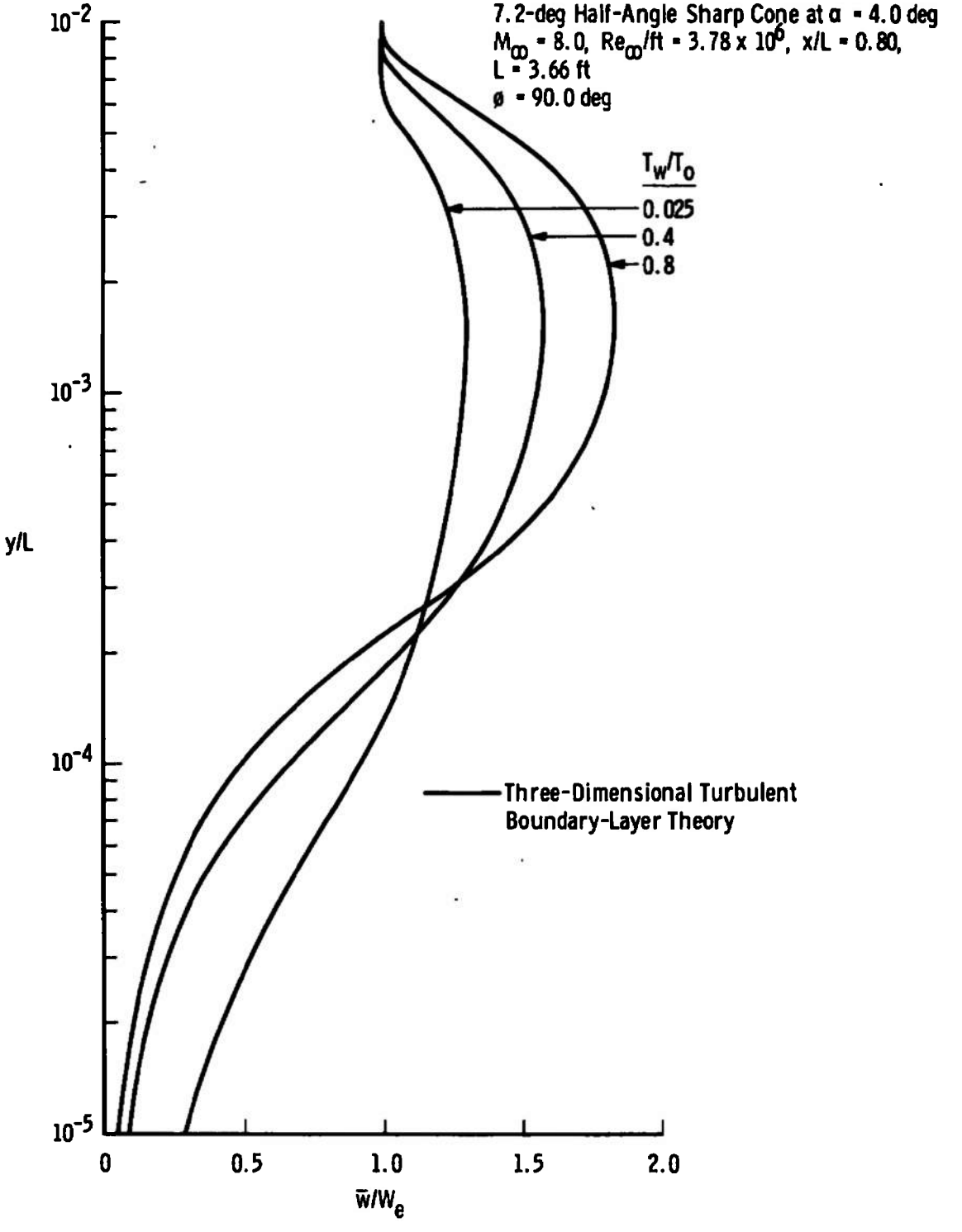

b. Crossflow Velocity Ratio
Fig. 23 Continued

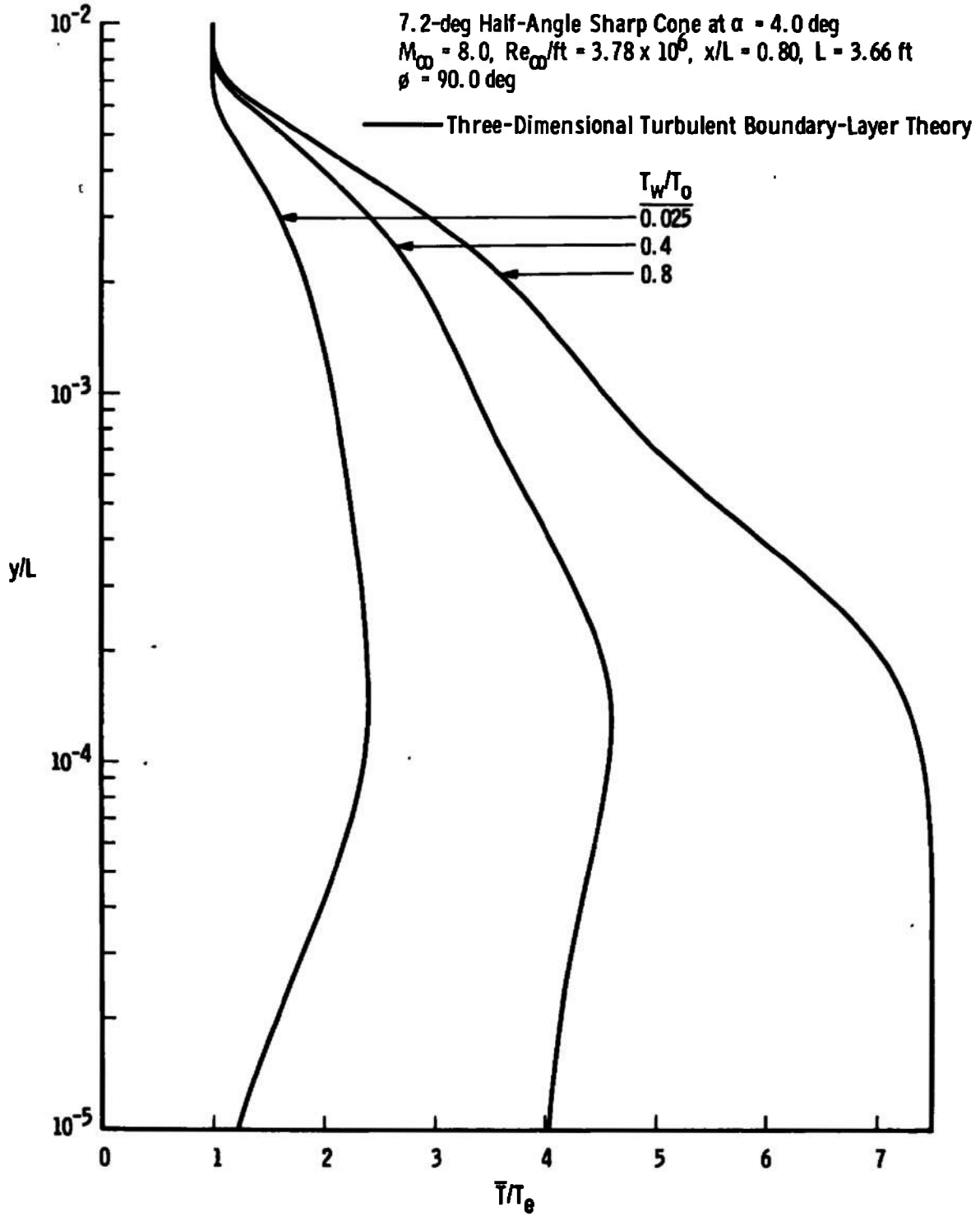

c. Static Temperature Ratio
Fig. 23 Continued

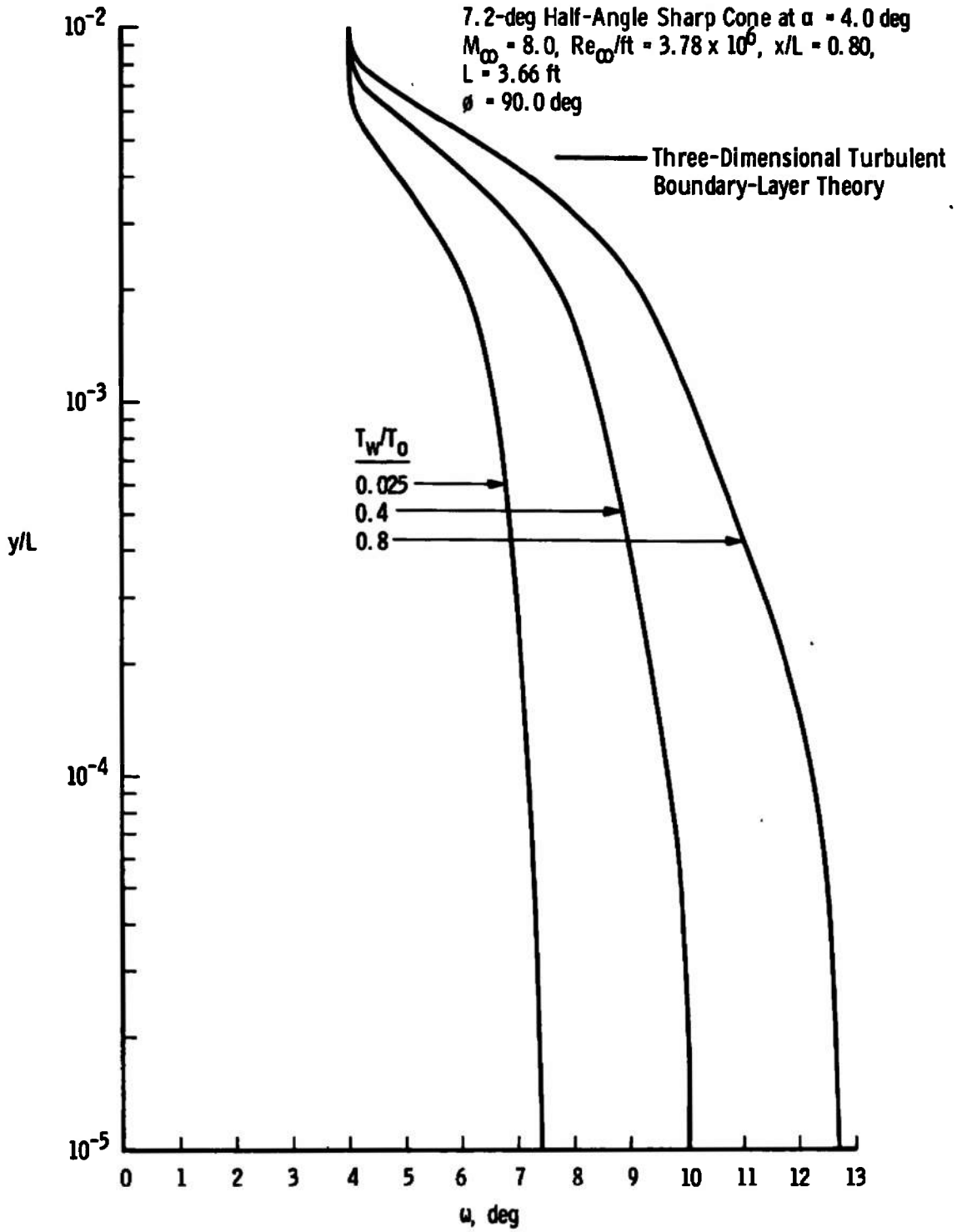

d. Streamline Directions in Boundary Layer
Fig. 23 Continued

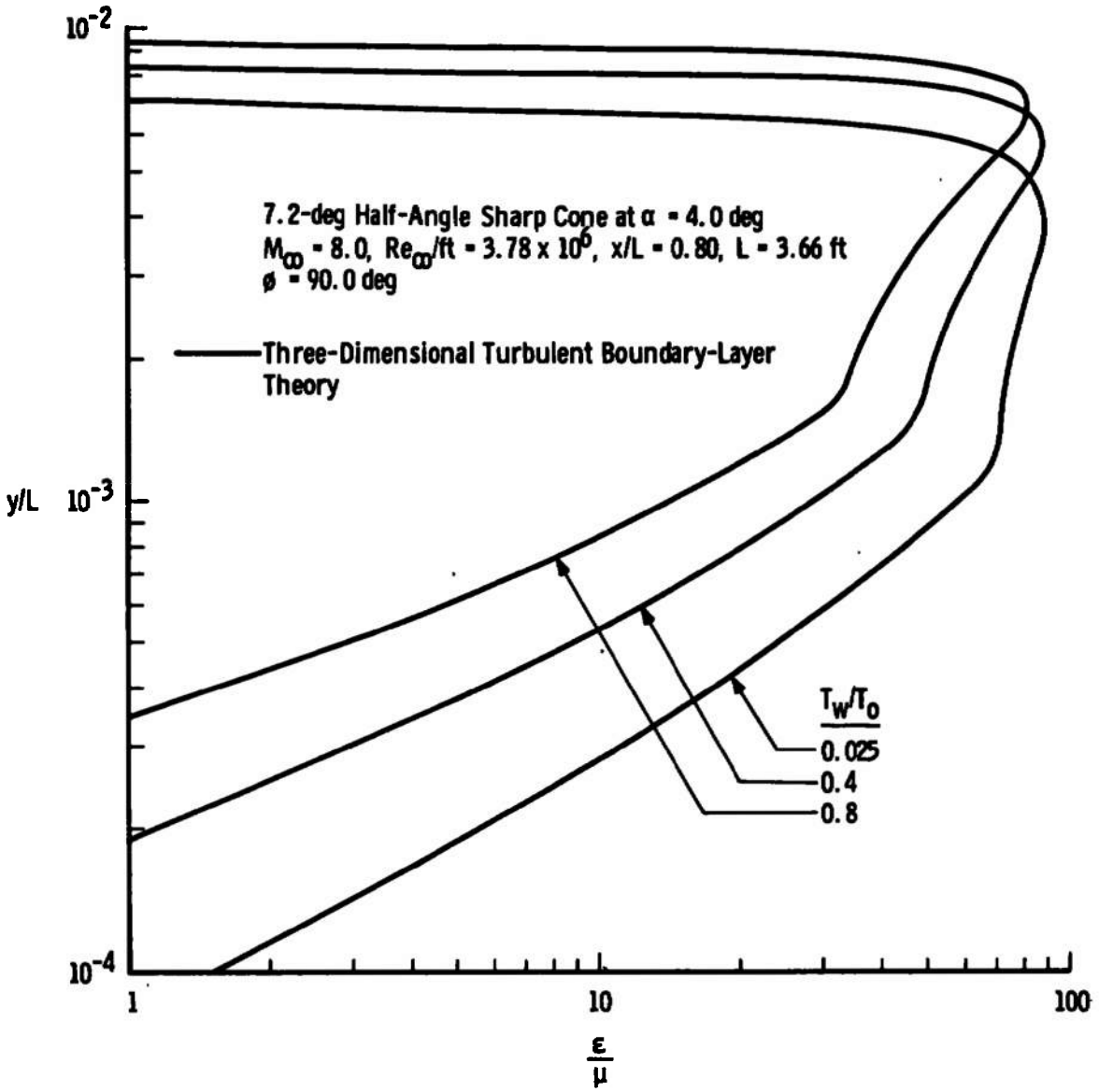

e. Eddy-Viscosity Ratio
Fig. 23 Concluded

TABLE I
COMPARISON OF EXACT RESULTS WITH APPROXIMATE SCALING TECHNIQUE FOR STANTON NUMBER DISTRIBUTIONS ON A SHARP CONE AT INCIDENCE UNDER COLD WALL HYPERSONIC CONDITIONS

x/L	$St_\infty \times 10^3$									
	ϕ = 0 deg		ϕ = 45 deg		ϕ = 90 deg		ϕ = 135 deg		ϕ = 180 deg	
	Exact	Eq. (49)	Exact	Eq. (49)	Exact	Eq. (49)	Exact	Eq. (49)	Exact	Eq. (49)
0.50	1.959	1.981	1.710	1.726	1.204	1.214	0.824	0.833	0.642	0.655
0.65	1.867	1.879	1.629	1.638	1.149	1.152	0.786	0.790	0.616	0.621
0.80	1.803	1.803	1.571	1.571	1.105	1.105	0.758	0.758	0.596	0.596
0.95	1.748	1.742	1.526	1.518	1.074	1.068	0.735	0.732	0.580	0.576

7.2-deg Half-Angle Sharp Cone at α = 4.0 deg

M_∞ = 8.0, Re_∞/ft = 3.78×10^6

T_w/T_o = 0.40, L = 3.66 ft

Note: In the above table, "exact" denotes the present three-dimensional turbulent boundary-layer theory.

UNCLASSIFIED
Security Classification

DOCUMENT CONTROL DATA - R & D

(Security classification of title, body of abstract and indexing annotation must be entered when the overall report is classified)

1 ORIGINATING ACTIVITY (Corporate author) Arnold Engineering Development Center Arnold Air Force Station, Tennessee	2a. REPORT SECURITY CLASSIFICATION UNCLASSIFIED 2b. GROUP N/A

3 REPORT TITLE

ANALYSIS OF THE THREE-DIMENSIONAL COMPRESSIBLE TURBULENT BOUNDARY LAYER ON A SHARP CONE AT INCIDENCE IN SUPERSONIC AND HYPERSONIC FLOW

4 DESCRIPTIVE NOTES (Type of report and inclusive dates)

Final Report - July 1971 to February 1972

5 AUTHOR(S) (First name, middle initial, last name)

John C. Adams, Jr., ARO, Inc.

6. REPORT DATE	7a. TOTAL NO. OF PAGES	7b. NO. OF REFS
June 1972	92	54

8a. CONTRACT OR GRANT NO.	9a. ORIGINATOR'S REPORT NUMBER(S)
b. PROJECT NO.	AEDC-TR-72-66
c. Program Element 65802F	9b. OTHER REPORT NO(S) (Any other numbers that may be assigned this report) ARO-VKF-TR-72-37
d.	

10 DISTRIBUTION STATEMENT

Approved for public release; distribution unlimited.

11. SUPPLEMENTARY NOTES	12. SPONSORING MILITARY ACTIVITY
Available in DDC	Arnold Engineering Development Center, Air Force Systems Command, Arnold AF Station, Tenn. 37389

13. ABSTRACT

An analytical approach toward numerical calculation of the three-dimensional turbulent boundary layer on a sharp cone at incidence under supersonic and hypersonic flow conditions is presented. The theoretical model is based on implicit finite-difference integration of the governing three-dimensional turbulent boundary-layer equations in conjunction with a three-dimensional scalar eddy-viscosity model of turbulence. Comparison of the present theory with detailed experimental measurements of the three-dimensional turbulent boundary-layer structure (velocity and temperature profiles), as well as surface streamline direction (obtained via an oil-flow technique) and surface heat-transfer rate, reveals good agreement. Effects of wall temperature on the three-dimensional turbulent boundary-layer profiles under hypersonic conditions are considered relative to interpretation of hot wall, hypersonic wind tunnel, force testing as it relates to cold wall, atmospheric re-entry. The calculated surface upwash angle is found to be fairly sensitive to wall temperature effects with the larger values of the angle occurring with the hotter wall.

DD FORM 1 NOV 65 1473

UNCLASSIFIED
Security Classification

14. KEY WORDS	LINK A		LINK B		LINK C	
	ROLE	WT	ROLE	WT	ROLE	WT
turbulent boundary layer						
compressible flow						
supersonic flow						
hypersonic flow						
three dimensional flow						
conical bodies						